Technical Report Documentation Page

1. Report No.	2. Government Accession No.	3. Recipient's Catalog No.
FHWA/TX-15/0-5722-2		

4. Title and Subtitle	5. Report Date
PERFORMANCE OF LAP SPLICES IN LARGE-SCALE COLUMN SPECIMENS AFFECTED BY ASR AND/OR DEF—EXTENSION PHASE	Published: March 2015
	6. Performing Organization Code

7. Author(s)	8. Performing Organization Report No.
Joseph M. Bracci	Report 0-5722-2

9. Performing Organization Name and Address	10. Work Unit No. (TRAIS)
Texas A&M Transportation Institute College Station, Texas 77843-3135	11. Contract or Grant No. Project 0-5722

12. Sponsoring Agency Name and Address	13. Type of Report and Period Covered
Texas Department of Transportation Research and Technology Implementation Office 125 E. 11th Street Austin, Texas 78701-2483	Technical Report: September 2011–August 2014
	14. Sponsoring Agency Code

15. Supplementary Notes

Project performed in cooperation with the Texas Department of Transportation and the Federal Highway Administration.

Project Title: Lap Splice and Development Length Performance in ASR and/or DEF Damaged Concrete Elements

URL: http://tti.tamu.edu/documents/0-5722-2.pdf

16. Abstract

A large experimental program, consisting of the design, construction, curing, exposure, and structural load testing of 16 large-scale column specimens with a critical lap splice region that were influenced by varying stages of alkali-silica reaction (ASR) and at least early-stage delayed ettringite formation (DEF), was conducted. This report details the developing expansion from late-stage ASR and at least early-stage DEF in the remaining eight specimens since September 2011 and the structural testing of two of these specimens during the three-year project extension phase. In comparison with the response of the control specimens, specimens exhibiting primarily ASR (and at least early-stage DEF) had similar initial stiffness and behavior up to first cracking, had about a 25 to 35 percent increase in post-cracking stiffness up to yielding, had about a 5 to 15 percent increase in yield strength, and showed no overall detrimental effects on the structural response. The increase in stiffness and strength can be explained by the resulting volumetric expansion of the concrete due to the ASR that engaged the transverse reinforcement for better confinement of the core concrete, and engaged the supplemental post-tensioning reinforcement and the column longitudinal reinforcement to generate additional axial compression load. Although the structural performance of column splice regions with varying levels of ASR and up to some DEF showed no detrimental effects, the vulnerability of the column splices with increased levels of DEF and other developing deterioration mechanisms, such as corrosion, could not be evaluated to date.

17. Key Words	18. Distribution Statement
Alkali-Silica Reaction, ASR, Delayed Ettringite Formation, DEF, Lap Splice, Reinforced Concrete, Bridge Column	No restrictions. This document is available to the public through NTIS: National Technical Information Service Alexandria, Virginia 22312 http://www.ntis.gov

19. Security Classif. (of this report)	20. Security Classif. (of this page)	21. No. of Pages	22. Price
Unclassified	Unclassified	106	

PERFORMANCE OF LAP SPLICES IN LARGE-SCALE COLUMN SPECIMENS AFFECTED BY ASR AND/OR DEF—EXTENSION PHASE

by

Joseph M. Bracci
Research Engineer
Zachry Department of Civil Engineering and
Texas A&M Transportation Institute

Report 0-5722-2
Project 0-5722
Project Title: Lap Splice and Development Length Performance in ASR and/or DEF Damaged Concrete Elements

Performed in cooperation with the
Texas Department of Transportation
and the
Federal Highway Administration

Published: March 2015

TEXAS A&M TRANSPORTATION INSTITUTE
College Station, Texas 77843-3135

DISCLAIMER

This research was performed in cooperation with the Texas Department of Transportation (TxDOT) and the Federal Highway Administration (FHWA). The contents of this report reflect the views of the author, who is responsible for the facts and the accuracy of the data presented herein. The contents do not necessarily reflect the official view or policies of the FHWA or TxDOT. This report does not constitute a standard, specification, or regulation.

This report is not intended for construction, bidding, or permit purposes. The engineer in charge of the project was Joseph M. Bracci, P.E. #79855.

ACKNOWLEDGMENTS

This project was conducted at Texas A&M University and was supported by the Texas Department of Transportation and the Federal Highway Administration through the Texas Transportation Institute. The author acknowledges the efforts and contributions of the TxDOT project director, Ricardo Gonzalez, and the members of the Project Monitoring Committee, including Wade Odell, Keith Ramsay, and John Vogel. The author acknowledges the participation and contribution of Drs. David Trejo and Paolo Gardoni in this research program. The author is grateful and is especially proud of the many graduate and undergraduate student researchers involved in the research program. The author thanks Dr. Peter Keating and Mr. Matt Potter of the Civil Engineering High-Bay Structural and Materials Laboratory at Texas A&M University for their technical and logistical assistance during in the construction and structural testing of the large-scale specimens. The author acknowledges the donation of the reinforcing steel for the large-scale specimens from CMC Inc., in particular Paul Fredrickson.

TABLE OF CONTENTS

LIST OF FIGURES

Page

LIST OF TABLES

Page

CHAPTER 1. INTRODUCTION

1.1. PROBLEM STATEMENT

Over the past 25 years or so, the Texas Department of Transportation (TxDOT) has had an aggressive construction program in place to accommodate the expanding population growth within Texas, especially in major metropolitan areas. Because of constrained conditions in metropolitan areas in terms of access space and the raw scale of transportation systems needed to satisfy the increasing traffic demands, the size of transportation structures, both at the member and system levels, have become significantly larger than past construction. Unlike nominal size concrete placements, large concrete placements can experience elevated temperatures during hydration, which can later cause cracking and deterioration of these concrete structures.

Contractors have taken aggressive approaches in building such structures to meet the construction demands in these metropolitan areas. In addition to taking aggressive approaches in scheduling and in resource allocations, some contractors are believed to have proportioned concrete mixtures with early set cement (Type III) to achieve high early strengths. By doing so, contractors can remove forms more quickly, allowing the construction to be completed in an expedited fashion. Although this practice is advantageous in minimizing construction costs and build time, it may have contributed to the early cracking of many structures (termed *premature concrete deterioration*).

In addition, the chemical constituents in the cement and aggregates play a key role in the durability of concrete structures. Professor Folliard's research group at The University of Texas at Austin (Bauer et al. 2006; Folliard et al. 2006) has documented that high alkali contents in cement, especially in Type III cement, when used with reactive siliceous aggregates (which are prominent in Texas) in concrete in the presence of moisture can result in alkali-silica reaction (ASR). ASR can lead to the formation of expansive by-products, which in turn can lead to cracking of the concrete. Folliard et al. (2006) and Burgher et al. (2008) also found that concrete cracking from ASR could lead to other deterioration processes, such as delayed ettringite formation (DEF) and corrosion, which can further reduce the capacity of the structure.

1.2. RESEARCH PROGRAM OBJECTIVES

The major objectives of the research program were to:

- Evaluate the experimental behavior of critical column lap splice regions using large-scale specimens under varying levels of premature concrete deterioration due to ASR and/or DEF.
- Develop an analytical model that describes the behavior of a splice region under varying levels of concrete deterioration based on calibration with the experimental behavior.

1.3. RESEARCH METHODOLOGY

The methodology for this research program was to:

- Conduct a large experimental program, which consisted of the design, construction, curing, exposure, and structural load testing of 16 large-scale column specimens with a critical lap splice region.
- Compare and calibrate models developed in the analytical program with the experimental behavior.

Specimens were carefully instrumented both internally and externally to monitor the strain behavior of the concrete and reinforcing steel from specimen construction, curing, exposure, and final structural load testing. The analytical program consisted of developing a model of the critical splice region of the specimens that captured the overall force-deformation characteristics of the specimen during structural load testing.

1.4. SCOPE

Bracci et al. (2012) documented the details of the research program from project initiation until August 2011. In addition, two technical journal publications were developed based on this research (Eck Olave et al. 2014a and 2014b). In September 2011, TxDOT extended the research project for an additional three years in anticipation of further concrete expansion and developing cracks due to ASR and potentially to DEF in the remaining specimens at the exposure site. This

report documents the research findings during the project extension phase from September 2011–August 2014.

The scope of this report consists of the following:

- Chapter 1 (current chapter) includes the problem statement and project background information.
- Chapter 2 summarizes the relative details of the large-scale specimens including the concrete materials, reinforcing, and instrumentation that were previously reported in Bracci et al. (2012).
- Chapter 3 summarizes the exposure program for the large-scale specimens from Bracci et al. (2012) and presents the internal and external surface expansions of the remaining specimens throughout the entire exposure phase.
- Chapter 4 presents the experimental measured response of two specimens tested during the project extension phase and compares the results with the other specimens tested in Bracci et al. (2012) with varying levels of primarily ASR.
- Chapter 5 presents the summary, conclusion, and recommendation from this research.

The author strongly encourages interested readers to review the project report by Bracci et al. (2012) and technical journal papers by Eck Olave et al. (2014a, 2014b) for additional project details and further explanations.

CHAPTER 2. SPECIMEN DETAILS

2.1. LARGE-SCALE COLUMN SPECIMENS

This research focused on the performance of the splice region of a typical reinforced concrete bridge column in Texas primarily under axial compression loading and subject to ASR and/or DEF. Because in-service bridge columns can vary considerably in size and geometry, the large-scale column (LSC) specimens were designed to utilize a common splice found in the field at the column/foundation connection, which is typical in non-seismic regions. In an effort to reduce costs and maximize the specimen size based on the constraints of the testing laboratory, the research team used 16 LSC specimens in the experimental research program. Specimens were 2 ft × 4 ft (0.6 m × 1.2 m) in cross section with six #11 bars spliced in the 9 ft (2.7 m) splice region, which is the same splice length TxDOT used in the field structures examined.

Figure 2-1 and Figure 2-2 show the LSC specimen dimensions and reinforcement details. Bracci et al. (2012) presents additional information about the LSC specimens.

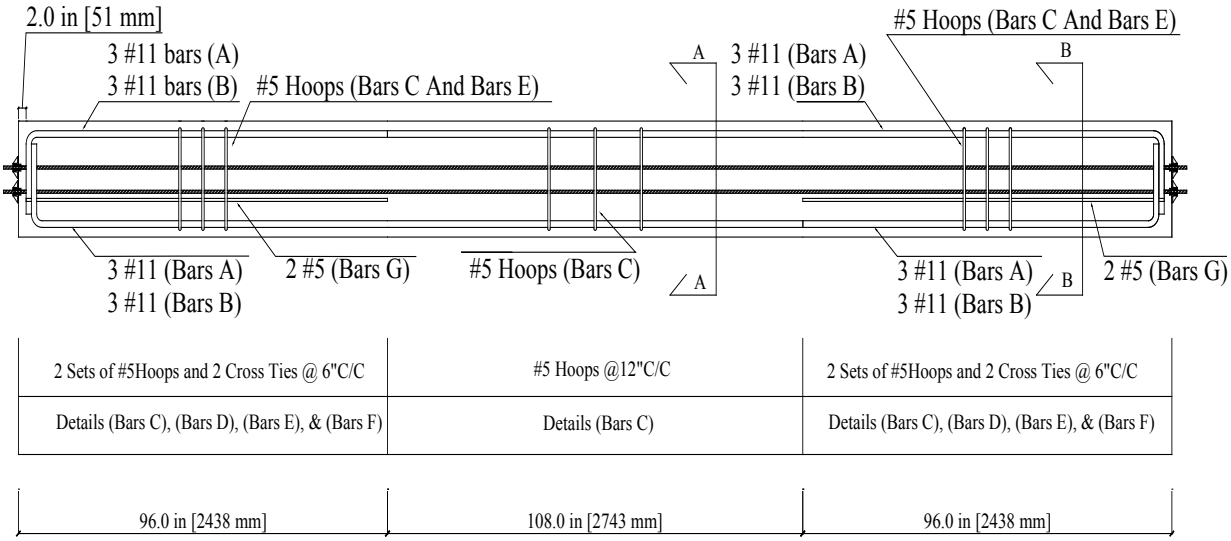

Figure 2-1. Specimen and Reinforcement Layout.

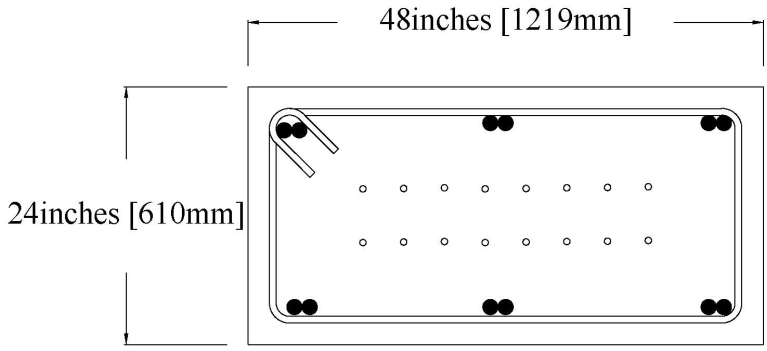

(a) Section A-A Splice Region

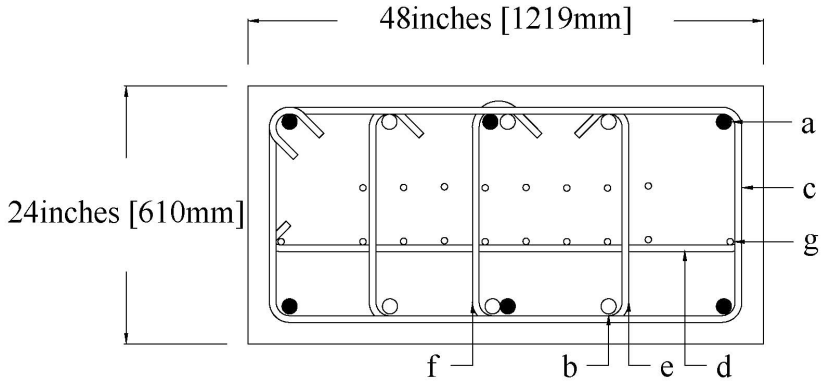

(b) Section B-B End Region

Section B-B Parts	
a	6 #11 Bars A [marked with fill]
b	6 #11 Bars B [marked without fill]
c	#5 Hoops @ 6" C/C (Bars C)
d	#5 Cross Ties @ 6" C/C (Bars D)
e	#5 Hoops @ 6" C/C (Bars E)
f	#5 Cross Ties @ 6" C/C (Bars F)
g	2 #5 Bars (Bars G)

Figure 2-2. Cross Section and Reinforcement Details.

In publications by the American Concrete Institute (ACI 318, 2008) and American Association of State and Highway Transportation Officials (AASHTO, 2004), the required splice length is a function of the required development length of the bar (l_d) and various factors. According to

ACI 318 (2008) for #11 bars with f'_c = 5000 psi (34.5 MPa), the required development length is 46.7 inches (1.2 m). Therefore, the provided splice length of 9 ft (2.7 m) in the LSC specimens corresponds to 2.3 × l_d. A Class B splice length (when the area of reinforcement provided is not at least twice what the analysis required over the entire length of the splice and when the splice is staggered) is required to have 1.3 × l_d, which means that the provided splice length is overdesigned by 78 percent. According to AASHTO (2004), the required development length for a #11 bar is 52 inches (1.3 m). Therefore, the provided splice length in the LSC specimens corresponds to 2.08 × l_d. In AASHTO (2004), this splice is required to have a Class C splice, which requires the splice length to be 1.7 × l_d, implying that the splice is overdesigned by 22 percent. Both ACI 318 (2008) and AASHTO (2004) show this splice to be conservatively designed. The question is whether the effects of ASR and/or DEF will deteriorate the bond of the column reinforcing steel in the splice region enough to overcome the conservative design.

To simulate in-service gravity loading on the bridge column dominated by axial load, the specimens had 16 0.6 inches (15 mm) diameter, unbonded, post-tensioning (PT) strands. The PT strands were centered throughout the specimen cross section and connected at the specimen ends (see Figure 2-3 and Figure 2-4, respectively). The strands were hydraulically jacked to 0.7 f_{pu}, ultimate tensile stress, according to AASHTO (2007), which resulted in 36.3 kips (161.47 kN) per strand and a total of 580.5 kips (2582.19 kN) of compression on the column specimen. This level of axial load corresponded to about 10 percent of the axial compression strength of the column, which is commonly found in columns under service loading.

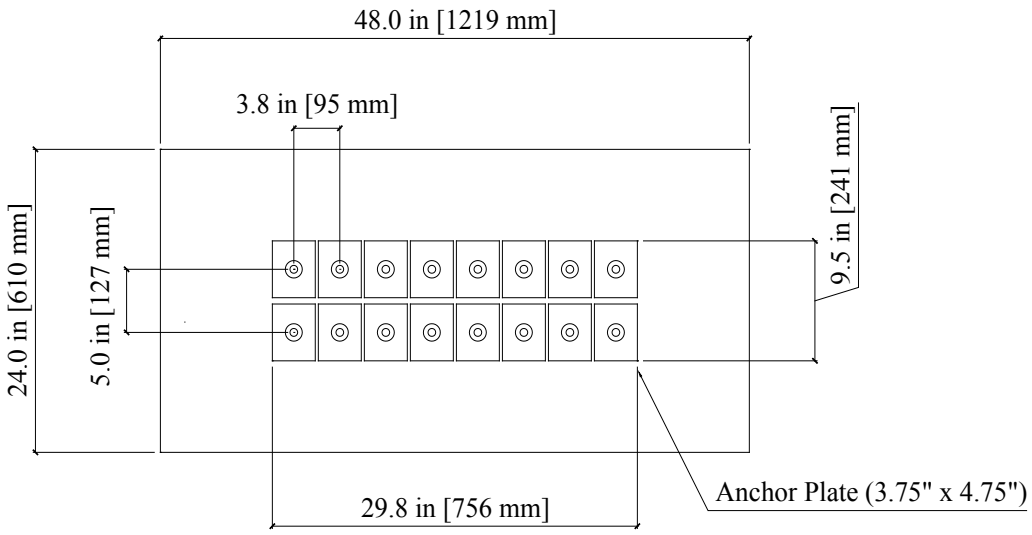

Figure 2-3. Strand Layout (End View).

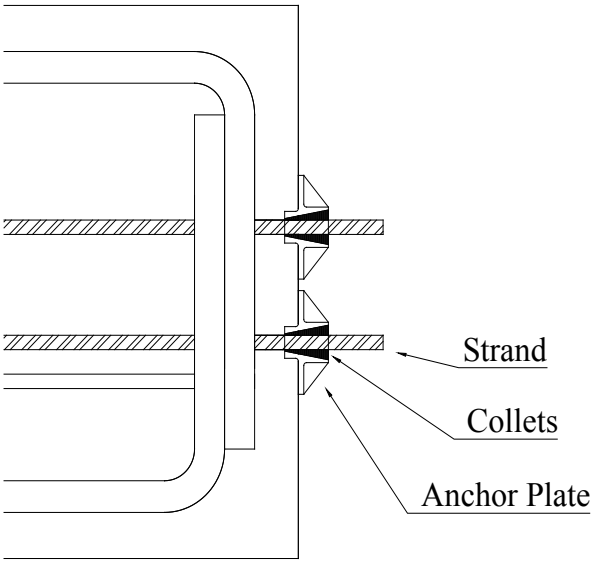

Figure 2-4. Strand End Termination.

In a report, Bracci et al. (2012) documented in detail the concrete materials of construction, which are only briefly summarized here for completeness. Note that although the objective of this research was to accelerate both ASR and DEF, priority was given to accelerating ASR as structures in the field exhibited predominantly ASR and only some exhibited DEF (Folliard et al. 2006). Due to the limited time of the research program, the concrete materials of construction and the curing conditions for the specimens were carefully designed to aggressively promote and

accelerate ASR. The coarse and fine aggregates were selected based on reactivity to promote ASR in the concrete. Type III cement from Lehigh Cement in Evansville, Pennsylvania, was used because of the high alkali content to promote ASR in the LSC specimens. To further increase the alkalis in the concrete mixture, sodium hydroxide (NaOH) was added to the mix. The cement contributed 6.6 lb/cy (3.9 kg/m^3) of alkalis, and the added sodium hydroxide contributed an additional 3.3 lb/cy (2.0 kg/m^3), resulting in a total alkali content of 9.9 lb/cy (5.9 kg/m^3). The mixture proportions used for the LSC specimens were determined based on a target concrete compressive strength of 5,000 psi (34.5 MPa).

The research team used Grade 60 reinforcing steel meeting American Society for Testing and Materials (ASTM) A615 specifications to fabricate the LSC specimens. From tension coupon testing, the yield strength of the reinforcement was about 65 ksi, and significant deformability beyond yielding was achieved.

To promote DEF, the LSC specimens were supplemented with heat during the curing of the concrete by electrical resistive wiring (ERW) to ensure that the concrete temperature throughout the critical splice region was above 160°F (71°C) (Bracci et al. 2012). Researchers preinstalled the ERW in the bottom and top forms, and then used stainless steel covers and insulation. In addition, ERW was required in the mid-depth of the LSC specimens by one-dimensional heat-flow analysis. The ERW was pushed through cross-linked polyethylene tubing that was strung through the vertical center of the cross section of the LSC specimens at four points and passed through the end of the form. The ERW solution consisted of three controllable sections to apply heat, which allowed for a more uniform temperature distribution in the concrete throughout the specimen. Shortly after the concrete was poured into the formwork, the ERW control system was activated such that the concrete temperatures at varying depths would be at least 160°F (71°C) for about 48 hours. After about 48 hours, the ERW control system was turned off and the specimen was allowed to gradually cool to reduce thermal cracking.

2.2. SUMMARY

Bracci et al. (2012) documented the design, construction, and curing of 14 specimens that were transported to the Riverside Campus for the aggressive exposure program, and of two control specimens that remained in the climate controlled structural laboratory without supplemental water/moisture required for premature concrete deterioration. In this section, relevant specimen design, construction, and curing details were summarized with the intent of being helpful to the readers of this report.

CHAPTER 3. EXPOSURE OF LARGE-SCALE SPECIMENS

3.1. INTRODUCTION

This section documents the exposure conditions and behavior, including the measured concrete surface expansions and developing cracks, in the remaining eight LSC specimens during the exposure phase of the project extension. The monitoring of the specimen expansions during this potential deterioration process is extremely important since there is only limited capability of measuring the effects of ASR/DEF in field structures. A further assessment of the effects of both ASR and DEF on the specimens is summarized from the petrography analysis that TxDOT personnel had independently performed on concrete cores taken from specimens following their structural load testing and on concrete cylinders in different exposure environments.

3.2. SPECIMEN EXPOSURE CONDITIONS

Shortly after the construction of LSC specimens and application of the preload to simulate gravity loading from in-service conditions, the specimens were placed outside at the Texas A&M University Riverside Campus in Bryan, Texas, where they were exposed to the environmental weather conditions of the area and supplemental water to accelerate the ASR and DEF deterioration mechanisms. A sprinkler system activated four times a day and for 15 minutes each time provided the supplemental water.

From initial measured expansion data on the specimens, researchers found that the largest surface expansions resulted on the top or sunny side of the specimen (Bracci et al. 2012). To provide more uniform expansion throughout the specimens, the LSC specimens were rotated twice during the entire exposure phase. Figure 3-1 shows the three orientations and the labels for each face. The length of the specimens is 25 ft (7.62 m), which is not shown to scale in the figure. Since Small Face 2 had not experienced any direct sunlight or water in the first orientation, the first rotation positioned this face on top. The second rotation was 90°, which positioned Large Face 2 on top. This face was the critical tension side in the subsequent structural load testing. Figure 3-2 shows the specimens during the third orientation, which was the orientation for the remaining eight specimens during the three-year project extension.

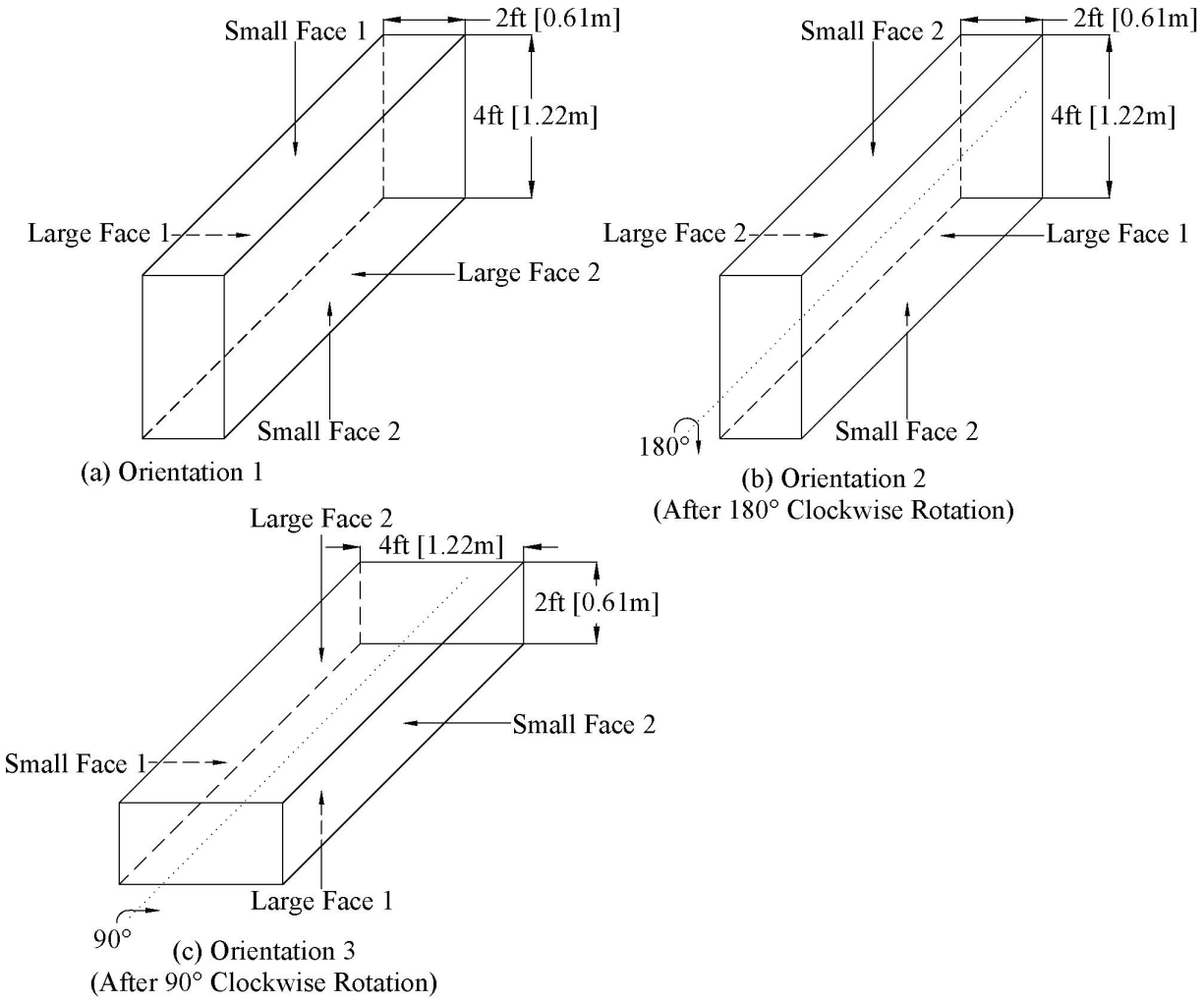

Figure 3-1. Orientations of the LSC Specimens.

Figure 3-2. LSC Specimens at the Riverside Campus during the 3rd Orientation.

Table 3-1 lists the month and year of the specimen casting, first exposure to the environmental conditions with supplemental water, 180° rotation, 90° rotation, and structural load test. LSC1 through LSC4 were transported to the Riverside Campus before May 2008. However, the sprinkler system providing supplemental water was not installed until May. Therefore, these specimens had some time without supplemental water from the sprinkler system. Since water is a necessary component for ASR (Folliard et al. 2006), the researchers defined the initial exposure as the time when the specimens were first exposed to the supplemental water. Table 3-1 highlights the eight remaining specimens during the project extension phase. Note that only specimens LSC4 and LSC12 were structurally tested in the extension phase and their experimental results are reported later in this report. The remaining six specimens will remain at the Riverside Campus site indefinitely without supplemental watering and periodically monitored for changes in the state of concrete cracking.

Table 3-1. Dates of Exposure, Rotations, and Structural Load Testing.

LSC Specimen #	Date of Casting	Date of Initial Exposure	Date of 180° Clockwise Rotation	Date of 90° Clockwise Rotation	Date of Structural Load Test
1	1/2008	5/2008	7/2009	N/A	8/2010
2	**2/2008**	**5/2008**	**7/2009**	**7/2010**	**TBD**
3	2/2008	5/2008	7/2009	N/A	8/2010
4	**3/2008**	**5/2008**	**7/2009**	**7/2010**	**6/2014**
5	4/2008	5/2008	7/2009	7/2010	7/2011
6	**4/2008**	**5/2008**	**7/2009**	**7/2010**	**TBD**
7	**4/2008**	**7/2008**	**7/2009**	**7/2010**	**TBD**
8	5/2008	7/2008	7/2009	7/2010	7/2011
9	6/2008	7/2008	7/2009	N/A	2/2010
10	6/2008	7/2008	7/2009	N/A	2/2010
11	**6/2008**	**9/2008**	**2/2010**	**7/2010**	**TBD**
12	**7/2008**	**9/2008**	**2/2010**	**7/2010**	**6/2014**
13	**7/2008**	**9/2008**	**2/2010**	**7/2010**	**TBD**
14	**8/2008**	**9/2008**	**2/2010**	**7/2010**	**TBD**

3.3. SPECIMEN BEHAVIOR DURING EXPOSURE PHASE

The behavior of the eight remaining LSC specimens during the exposure phase was monitored with external surface strain measuring devices and crack width card indicators during the project extension. Demountable mechanical (DEMEC) points were mounted on the surface of the specimens prior to the exposure phase and provided a way to measure the external surface expansion due to ASR/DEF during the exposure phase. Researchers used crack width card indicators to measure crack widths between select DEMEC points and to compare the strains measured from the DEMEC points. Internally, electronic strain gages were placed on the reinforcing steel and concrete embedment gages within the concrete specimen to measure the internal deformations during the exposure phase. With large expansions from ASR/DEF during the project extension phase and resulting strains beyond the measureable range of the internal instrumentation, the internal instrumentation data are not reported here. However, Bracci et al. (2012) reported the initial measurements up to the project extension phase.

3.3.1. Surface Strains between DEMEC Points

After the LSC specimens were rotated 90° for the third and final orientation, Large Face 1 was placed on the bottom (Figure 3-1). Figure 3-2 shows the LSC specimens during the third orientation with Large Face 2 on top. The distance between each specimen in this orientation was approximately 1 ft. Since Small Face 1 and Small Face 2 were now mostly in the shaded and in tight conditions, no surface data were measured on these faces during the third orientation. Figure 3-3 shows the DEMECs on Large Face 2 in a 5 × 5 grid, resulting in four transverse (TS1, TS2, TS3, and TS4) and five longitudinal (LS1, LS2, LS3, LS4, and LS5) averaged strains measured along the splice length of the LSC specimens.

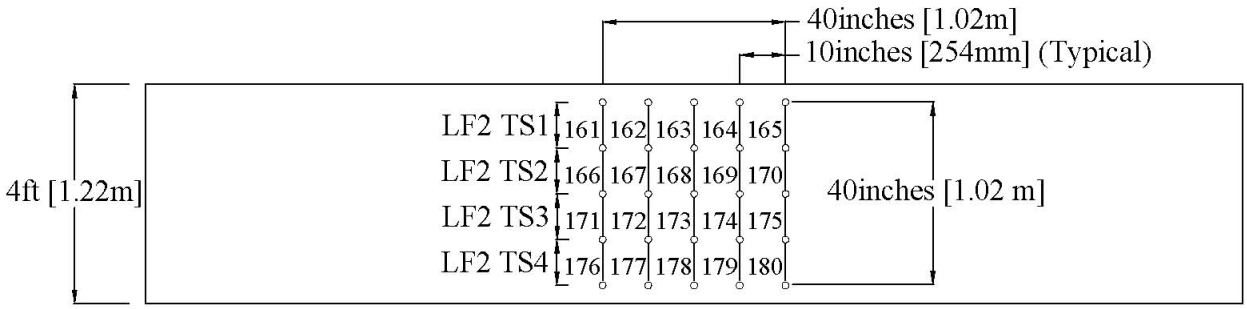

(a) Transverse Strain Locations on Large Face 2

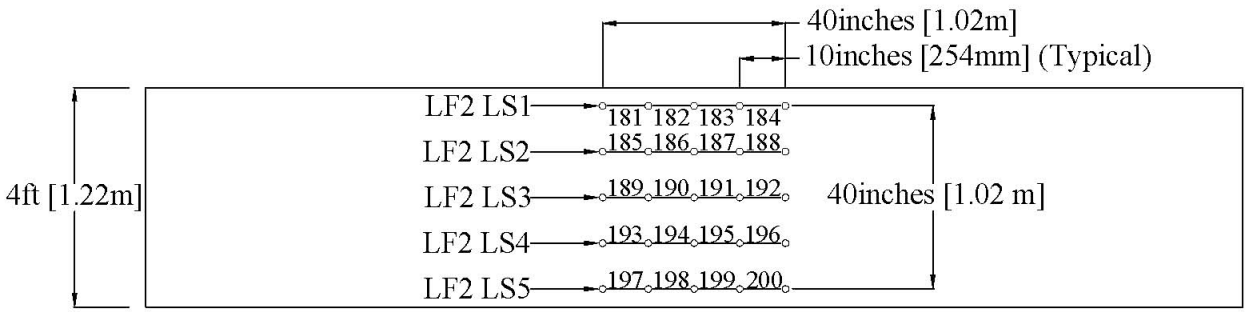

(b) Longitudinal Strain Locations on Large Face 2

Figure 3-3. Transverse and Longitudinal Strain Locations on the LSC Specimens' Large Face 2 during the 3rd Orientation.

Figure 3-4 and Figure 3-5 show the average transverse surface strains on Large Face 2 in the four sections of the face (TS1, TS2, TS3, and TS4) in the remaining eight LSC specimens during the entire exposure period. Figure 3-4 is for specimens LSC2, LSC4, LSC6, and LSC7; and Figure 3-5 is for specimens LSC11, LSC12, LSC13, and LSC14. Note that since DEMEC

measurements were taken only on Large Face 1 and not on Large Face 2 during the first and second orientations of the exposure phase, the strain measurements on Large Face 2 during the two initial orientations were assumed to be identical to that measured on Large Face 1. This was considered realistic since the physical orientations of both faces were exposed to similar environmental conditions of supplied water and sunlight. The figures show that the developing transverse expansion due to ASR/DEF rapidly increased during the first two years of exposure, and then had expansions at lesser rates to eventually leveling out. Over the past three years of exposure (since August 2011), the amount of surface expansion did increase, but at a lesser rate than occurred during the first two years of exposure. Most specimens had measured transverse expansions in the first quarter of the specimen width that were significantly larger than those measured in the middle half of the specimen. When researchers compared the transverse expansion amongst the remaining specimens in the exposure phase, they noted that LSC4 and LSC12 had the largest developing expansions due to ASR/DEF and were thus identified for structural testing to be reported in a later section. Specifically for LSC4, the figure shows that that quarter strain measurements were about 0.023 and 0.018, and the middle strain measurements were about 0.014. Similarly for LSC12, the figure shows that that quarter strain measurements were about 0.018 and 0.012, and the middle strain measurements were about 0.010. It is important to recognize that the transverse hoop reinforcement in the specimens some 2–3 inches (51–76 mm) below the surface will presumably resist the expansions in the transverse direction of the specimen and that these expansions will thus develop associated strains and stresses. Noting that ASTM grade 60 steel typical yields at a strain of about 0.002, the measured transverse surface strains were five to 10 times larger than this yield strain of the steel. In addition, Bracci et al. (2012) reported that strain gages attached to the transverse hoop steel had yielded during the initial phases of the exposure program, but the reported strains were approximately half of that occurring at the concrete surface. Unfortunately, the strain gages did not work properly throughout the duration of the exposure phase due to the expansive environment of the concrete that ASR/DEF influenced and also due to limitations on the maximum measureable strain of the gage.

Figure 3-6 and Figure 3-7 show the longitudinal surface strains on Large Face 2 in the five sections of the face (LS1, LS2, LS3, LS4, and LS5) in the remaining eight LSC specimens during the entire exposure period. Figure 3-6 is for specimens LSC2, LSC4, LSC6, and LSC7,

and Figure 3-7 is for specimens LSC11, LSC12, LSC13, and LSC14. Similarly, note that the DEMEC measurements during the first and second orientations of the exposure phase were taken from strain measurements on Large Face 1. Figure 3-6 and Figure 3-7 show a significant amount of variability in the strain readings over time. This variability is due to a variety of reasons including the relatively smaller expansion in the longitudinal direction, user errors since over time different researchers were used to take the DEMEC measurement strains, and possible measuring equipment errors. However, the figures show a common trend in the expansion data that levels out at a longitudinal strain of about 0.001, which is about half of the yield strain of column longitudinal reinforcing steel.

When researchers compared Figure 3-4 through Figure 3-7, they noted that the transverse surface strains are approximately 10 times larger than the longitudinal surface strains that were also observed in the previously tested specimens (Bracci et al. 2012). The axial post-tensioning strands along the LSC specimen length simulating the service bridge column axial load and the column longitudinal reinforcement (6#11 bars) most likely provided the restraint for the expansion due to ASR/DEF in the longitudinal direction. In comparison, the transverse reinforcement in the specimens (#5 hoops spaced at 12 inches [0.3 m] centers) was significantly less than the longitudinal reinforcement.

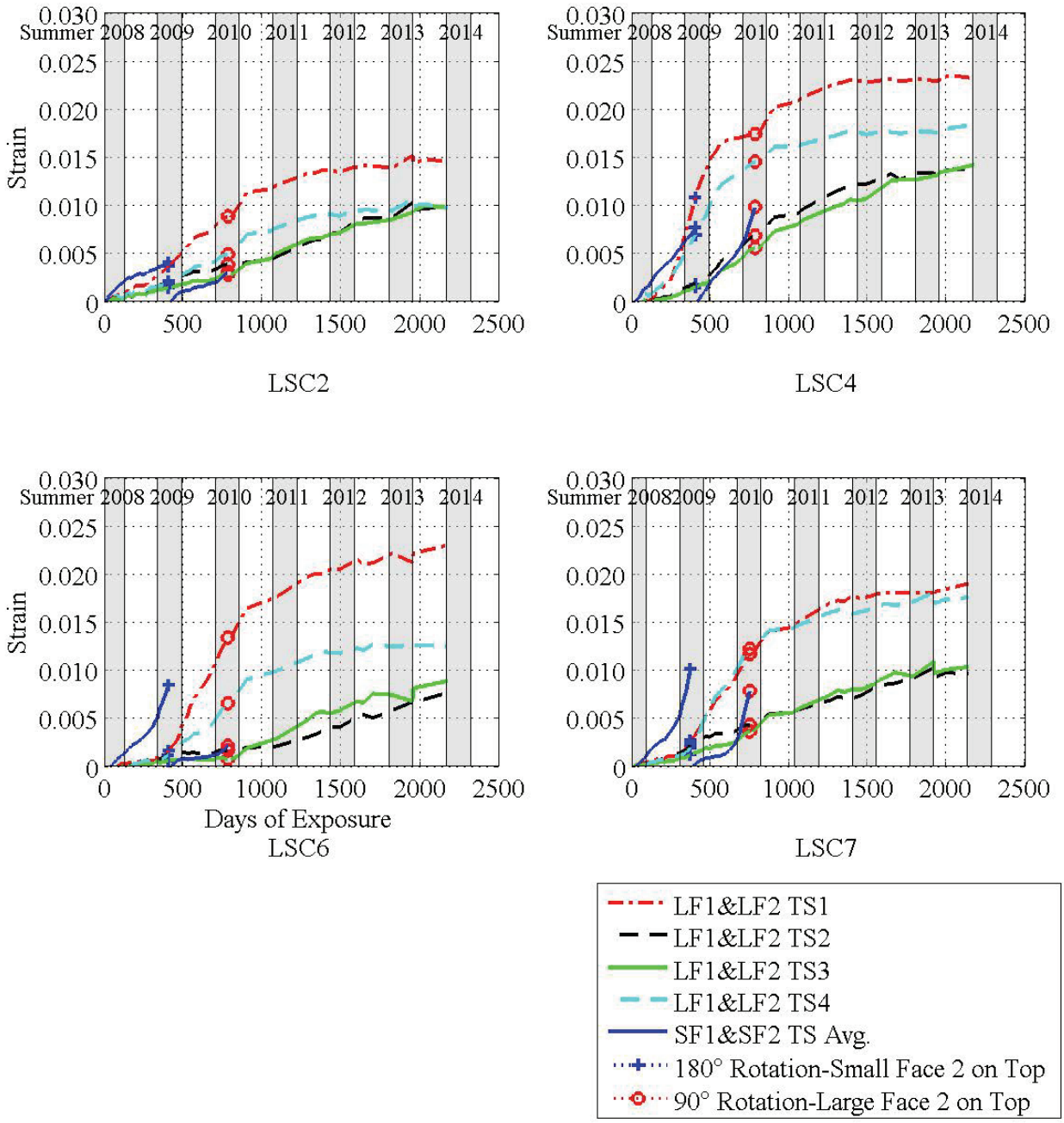

Figure 3-4. Transverse DEMEC Strain Measurements on Large Face 2 for LSC2, LSC4, LSC6, and LSC7.

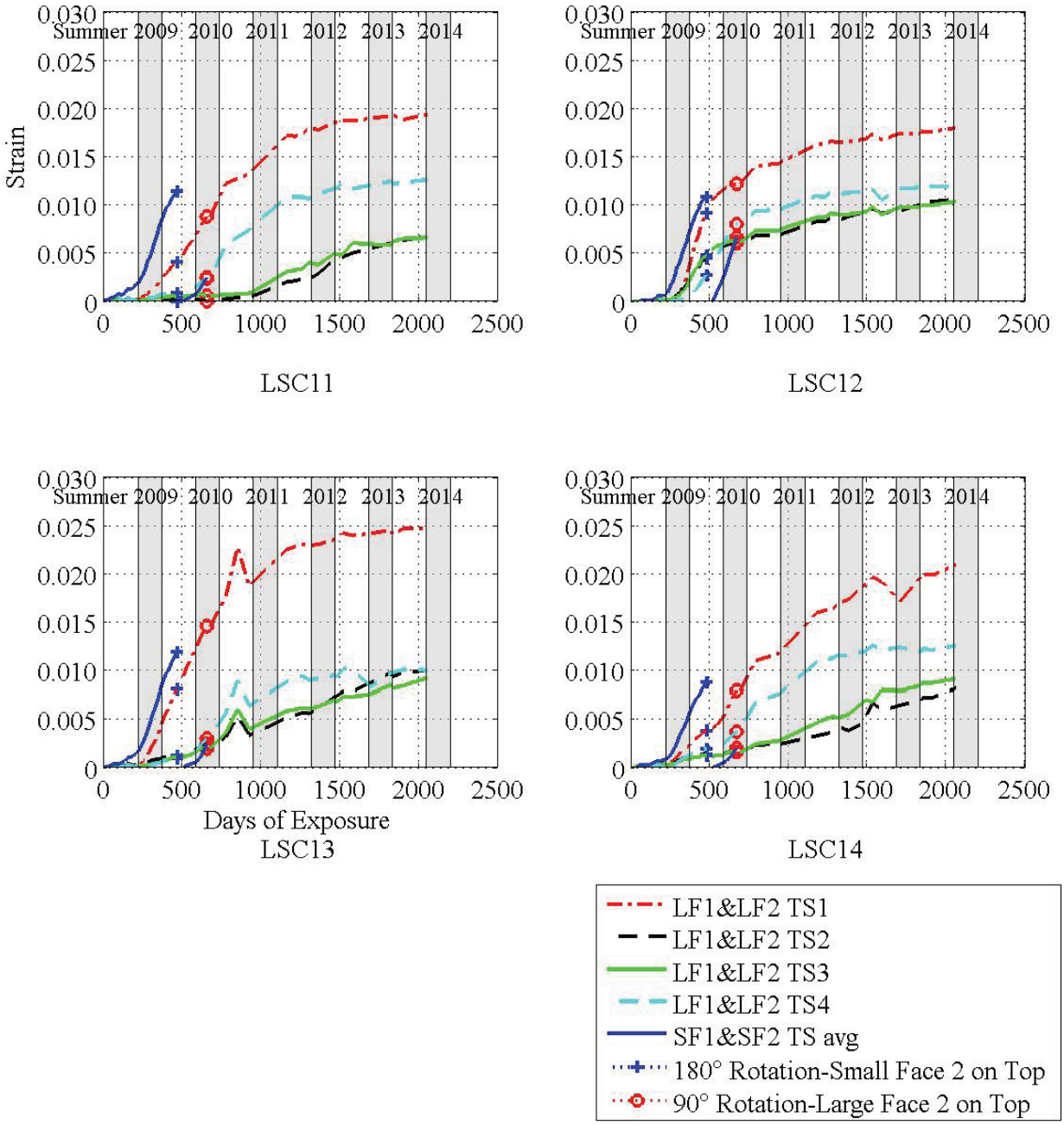

Figure 3-5. Transverse DEMEC Strain Measurements on Large Face 2 for LSC11, LSC12, LSC13, and LSC14.

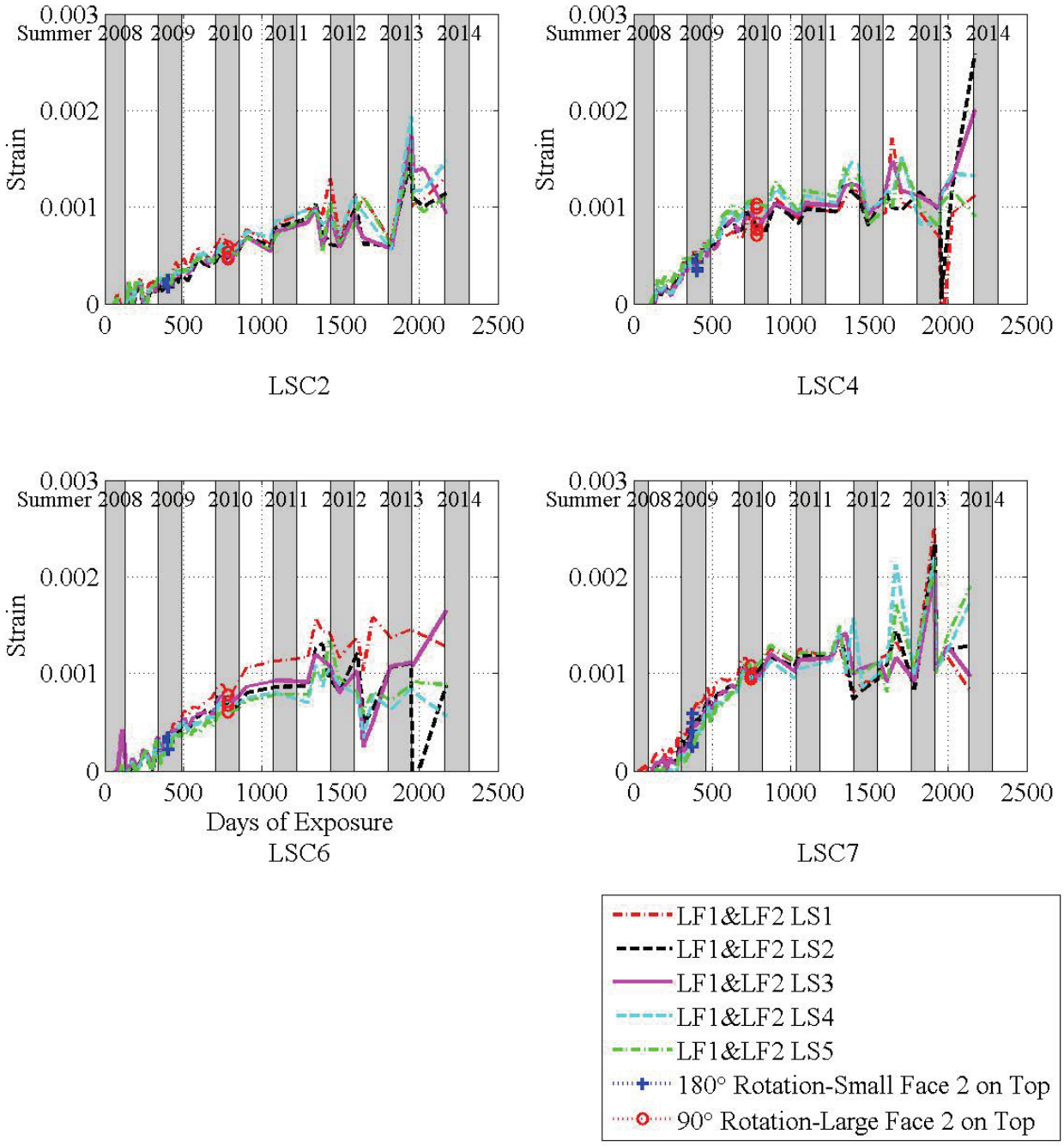

Figure 3-6. Longitudinal DEMEC Strain Measurements on Large Face 2 for LSC2, LSC4, LSC6, and LSC7.

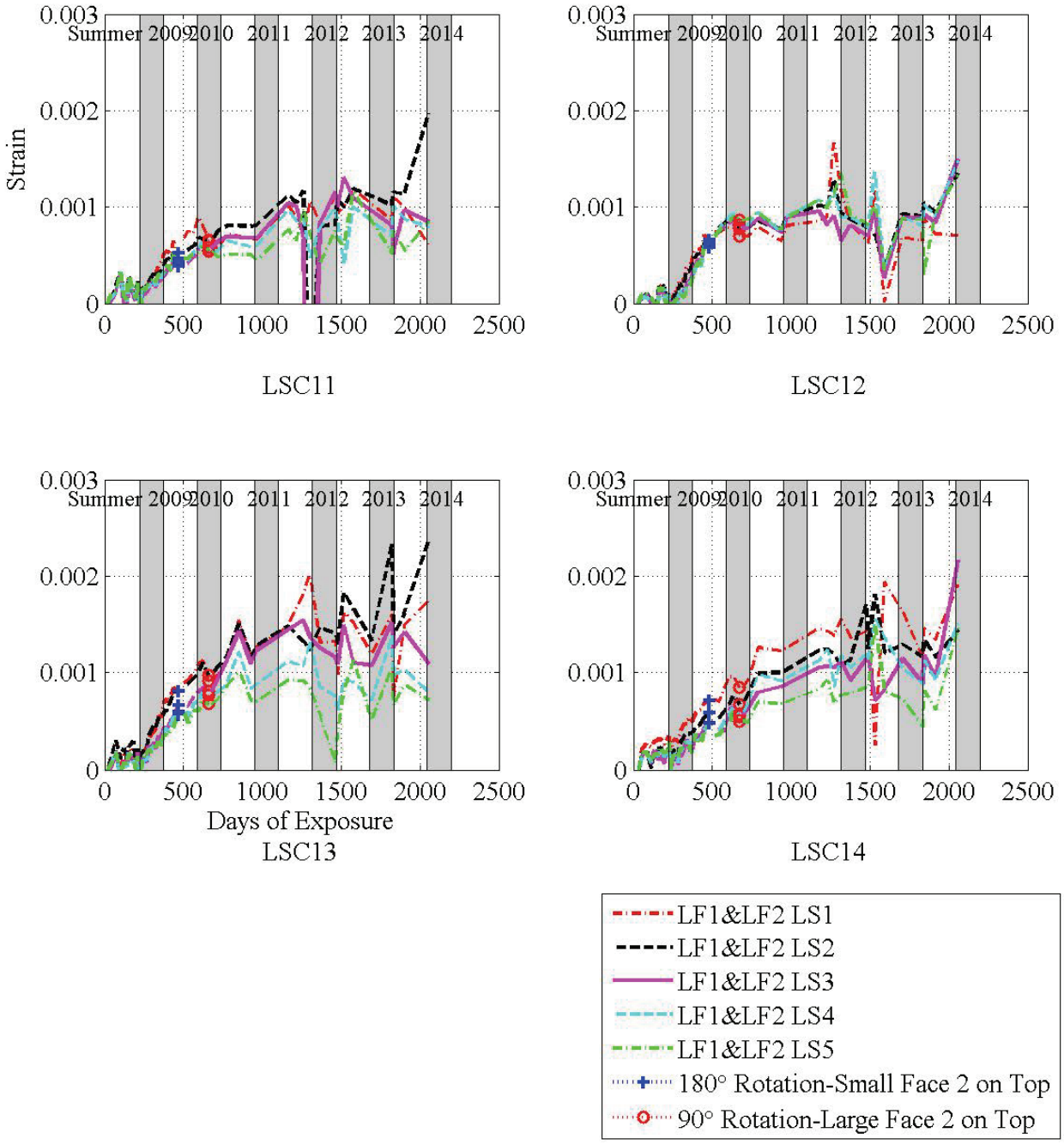

Figure 3-7. Longitudinal DEMEC Strain Measurements on Large Face 2 for LSC11, LSC12, LSC13, and LSC14.

3.3.2. Crack Width Measurements

In existing bridge columns, cracks can be measured quite easily using crack width card indicators or crack width measuring devices, while other strain data are more difficult to obtain since instrumentation was not installed prior to bridge construction. However, in this research, the surface strains calculated using the DEMEC points more accurately represent the total surface expansion, since crack width card indicators cannot measure small cracks and concrete expansion between the cracks due to ASR/DEF. Therefore, the strains from crack width measurements in the large-scale specimens were compared to the strains computed using the DEMECs. Figure 3-8 shows that typical surface cracks develop primarily in the longitudinal direction of the LSC specimens, noting that the DEMEC points shown are approximately 10 inches (0.25 m) apart. Therefore, only longitudinal crack widths were measured in this research using a crack width card indicator. This card can be used to measure crack widths as small as 0.004 inches (0.1 mm) to as large as 0.06 inches (1.5 mm). Figure 3-9 shows a larger longitudinal crack on specimen LSC4 with a crack width of about 0.04 inches (1.0 mm). For specimens LSC4 and LSC12, the largest crack width measured was about 0.12 inches (3.0 mm) and 0.06 inches (1.5 mm), respectively.

Figure 3-8. Typical Longitudinal Crack in Specimens.

Figure 3-9. Larger Longitudinal Crack Width on Specimen LSC4.

To estimate expansive surface strains, the width of the cracks along the transverse direction between DEMEC points were added and then divided by the original distance between the same DEMEC points, $l_d(0)$ taken to be 40 inches (1 m), to give a strain value shown below.

$$\varepsilon_{crack} = \frac{\sum \text{crack width}}{l_d(0)} \qquad \text{(Eq. 3-1)}$$

In the third specimen orientation during the project extension phase, the longitudinal crack widths were measured along a line of DEMEC points on the outer edge of the DEMEC point grid in the transverse direction.

The transverse surface strains on Large Face 2 were calculated by summing the longitudinal crack widths along a line of DEMEC points according to Eq. 3-1. Figure 3-10 shows these strains for specimens LSC2, LSC4, LSC6, and LSC7 and Figure 3-11 shows these strains for specimens LSC11, LSC12, LSC13, and LSC14. The figure shows that strains by summing the crack widths across the specimen section ranged from about 0.005 to about 0.010. By comparing Figure 3-10 and Figure 3-11 with Figure 3-4 and Figure 3-5, the researchers found the strain values by summing the crack widths along one line of DEMEC points are smaller than the

average surface strains, which are calculated from the average of the measured distance between DEMECs along the five lines in the transverse directly. The transverse expansion strain by summing the crack widths generally are about 50 percent of the average surface strain using the DEMEC point measurements, consistent with measurements prior to the extension phase (Bracci et al. 2012). This reduced strain from the sum of the crack widths can be explained by the expansion of the concrete between cracks that was not accounted for and other cracks that were too small to measure with the crack width card indicator.

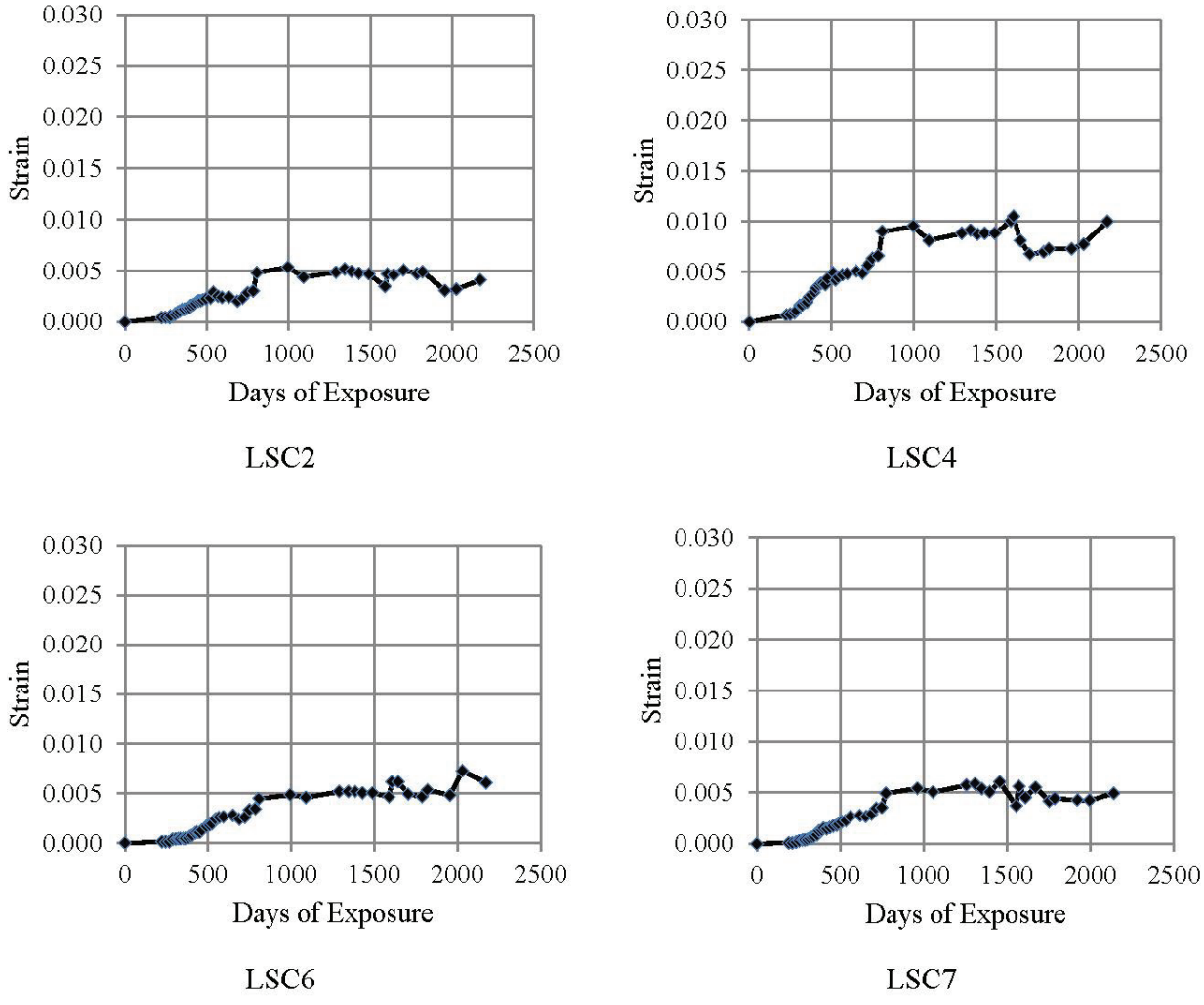

Figure 3-10. Transverse Strain Measurements by Summing Crack Widths on Large Face 2 for LSC2, LSC4, LSC6, and LSC7.

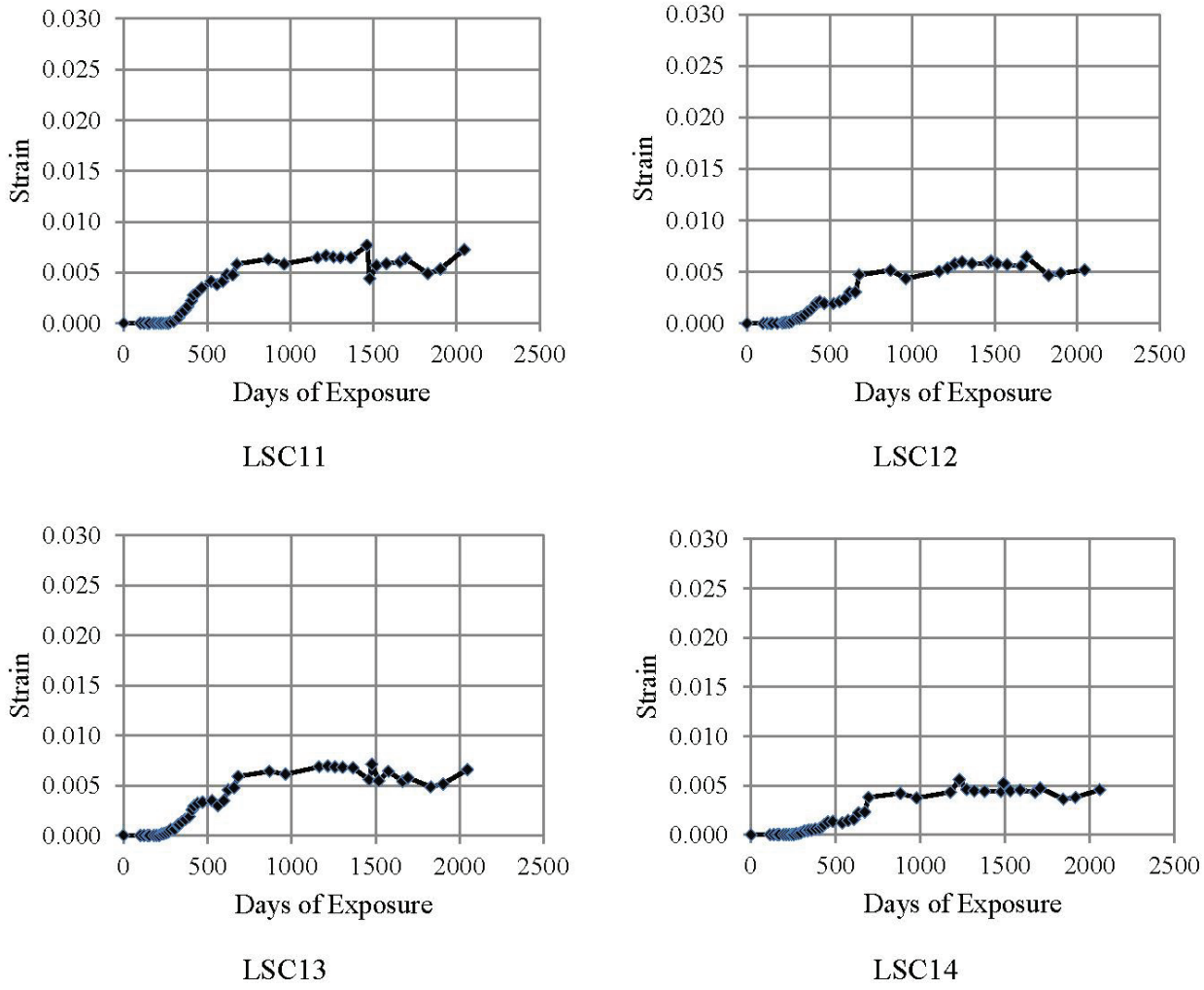

Figure 3-11. Transverse Strain Measurements by Summing Crack Widths on Large Face 2 for LSC11, LSC12, LSC13, and LSC14.

3.4. PETROGRAPHIC ANALYSIS RESULTS

To determine if ASR and/or DEF was evident in the LSC specimens, researchers took a series of concrete cores from the specimens LSC4 and LSC12 following their structural testing. Figure 3-12 shows some sample cores and clearly shows that extensive cracking has developed at the concrete surface and internally within the cores. In particular, note the evidence of ASR reaction particles (ASR gel) that has accumulated in voids and at the boundary of the transverse reinforcing steel and surrounding concrete. The accumulation of ASR gel at the steel-concrete interface was a concern for TxDOT in that it may have a negative effect on the bond strength of column-spliced bars. This research documents the development of ASR and the formation of ASR gel throughout the

concrete and at the steel column interfaces. The structural testing as presented in the next chapter highlights the structural performance of these specimens.

(a) Side Face Core from LSC4 **(b) End Core from LSC4**

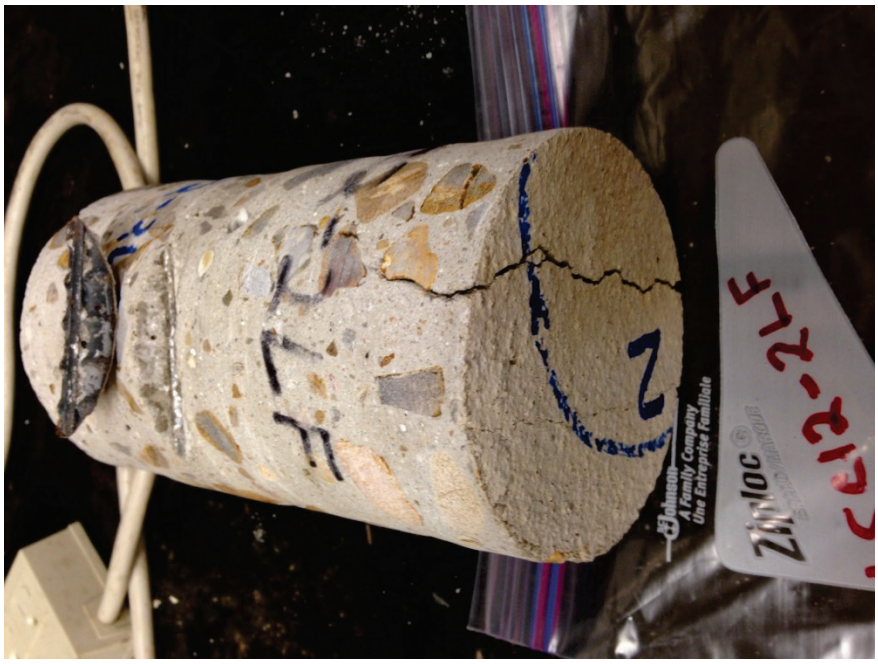

(c) Large Face Core from LSC12

Figure 3-12. Sample Concrete Cores.

Figure 3-13 shows sample concrete cylinders that were cast with the same concrete used to construct specimens LSC4 and LSC12, and were exposed to different environmental conditions. Some cylinders were stored on top of the LSC specimens at the exposure site in the presence of weather and supplemental watering, while the others were stored in a humidity-controlled wet

room. The figure clearly shows that the extent and width of concrete surface cracking was greater on cylinders stored at the field exposure site as compared to the wet room (maximum widths of about 0.01 and 0.006, respectively). However, the extent of this map cracking and the width of surface cracking in all cylinders were significantly less than what developed in the LSC specimens (see Figure 3-8, Figure 3-9, and Figure 3-13).

(a) LSC4—Exposure Site Storage **(b) LSC4—Wet Room Storage**

(c) LSC12—Exposure Site and Wet Room Storage, Respectively

Figure 3-13. Sample Concrete Cylinders.

Researchers sent TxDOT personnel four items so they could independently perform a petrographic analysis:

- A drilled 4-inch (102 mm) concrete core from tested specimens LSC4 and LSC12.
- Two 4-inch (102 mm) concrete cylinders from the concrete batch of specimen LSC4 (one stored on the top of specimen LSC4 at the exposure site and the other in a laboratory humidity-controlled wet room).

Specifically, the identification, severity, and progression of the ASR and DEF damage were desired, as well as visual documentation of any distress due to ASR/DEF. Appendix A shows the full petrographic analysis report from TxDOT. Below, the researchers summarized the key findings from the petrographic analysis.

The general visual observations were, "All of the cores had obvious distress cracks on the surface and sides of the core. The cores also had obvious coarse aggregate distress/dissolution and abundant reactions products. The cylinders primarily had fine cracking on the sides of the cylinders."

In relation to summarizing the deleterious reaction mechanism, the research team noted that "The primary distress mechanism in all the cores is attributed to ASR. ASR gel was observed in air voids, within distress aggregate and as exudation from reactive particles. Ettringite was noted in air voids, within micro cracks and gaps around aggregates. The two cores had much more severe level of reactivity compared to the cylinders."

Cores taken from LSC4 and LSC12 has surface crack widths of about 0.04 inches (1 mm) that extended up to 2.75 inches (70 mm) into the concrete core, which is the approximate location of the transverse and longitudinal reinforcement. Figure 3-12 shows that ASR gel had accumulated at the interface of the transverse reinforcing and surrounding concrete. In addition, Appendix A includes microscopic documentation that provides evidence of primarily ASR-caused micro damage and distress, and recent evidence of some DEF distress in the concrete cores.

The concluding comments state: "Based on this analysis, the cores exhibited (sic) high levels of ASR degradation (late-stage ASR). Both the fine and coarse aggregates are experiencing ASR attack in the cores. The two cylinders also had evidence of ASR activity; however, it was in the

early-stages compared to the cores. The aggregate and paste distress level associated with ASR in the cylinder is mild. The extent that DEF has played (sic) a role in the overall distress is inconclusive; however, there is evidence as seen in the scanning electron microscope (SEM) (sic) and optical microscopy images that DEF has contributed to some of the distress primarily in the cores. Ettringite formation in the cylinders was very low compared to the cores which had extensive development of ettringite formation (primarily redistribution of the ettringite into voids, cracks and gaps)."

3.5. SUMMARY AND CONCLUSIONS

In summary, the remaining eight LSC specimens stored at the Riverside Campus during the project extension phase were exposed to outdoor weather conditions in Bryan, Texas, and to wet-dry cycles using supplemental water to accelerate the ASR/DEF deterioration mechanisms. External surface measurements were continually recorded for all specimens throughout the exposure phase. These measurements provided significant information about the expansion mechanism in the LSC specimens. Most of the internal instrumentation was not functioning, likely as a result of the large expansion concrete strains due to ASR/DEF.

From the information that Bracci et al. (2012) provided, it was concluded that all specimens successfully developed significant premature concrete deterioration due to primarily ASR and minimal DEF in terms of concrete expansion and surface cracking that is representative of observations in in-service bridges. In addition, the deterioration mechanism was continuing. Therefore, TxDOT extended the project for three years to develop more severe damage states. This report documents the measured concrete expansion and surface cracking during the exposure phase in the project extension phase.

Table 3-2 shows the dates of specimen casting, initial environmental exposure, structural load testing, and the estimated degree of deterioration from ASR and DEF at the time of structural testing. For specimens LSC4 and LSC12, the estimated degrees of ASR and DEF deterioration were based on the external strains and surface cracking measured, and the petrography analysis report. For ASR, both specimens were categorized as having late-stage ASR. Since DEF was observed in the petrography analysis of the concrete cores, but the overall impact of the distress was inconclusive, researchers have categorized that at least early-stages of DEF has developed.

Table 3-3 shows the last average transverse surface strains of all faces before the LSC specimen was tested and the maximum crack width measured on each face. Specimen LSC4 had a higher level of transverse expansion and slightly larger cracks than specimens LSC5 and LSC8 that Bracci et al. (2012) had previously tested, and had the highest levels of expansion and cracking in specimens tested previously. Specimen LSC12 had a lower level of transverse expansion as compared to LSC4, but had a comparable level of transverse expansion in specimens LSC5 and LSC8 that were previously tested. In addition, the largest crack width in LSC12 was similar to LSC4 and slightly larger than those tested previously. Note that in Table 3-2 and Table 3-3 the test specimens documented in this report are highlighted.

Table 3-2. Specimen Age and Degree of Deterioration.

LSC Specimen #	Date of Casting	Date of Initial Exposure	Date of Structural Load Test	Degree ASR	Degree DEF
1	1/2008	5/2008	8/2010	M/L	N/E
3	2/2008	5/2008	8/2010	M/L	N/E
4	**3/2008**	**5/2008**	**6/2014**	**L**	**E***
5	4/2008	5/2008	7/2011	M/L	N/E
8	5/2008	7/2008	7/2011	M/L	N/E
9	6/2008	7/2008	2/2010	M/L	N/E
10	6/2008	7/2008	2/2010	M/L	N/E
12	**7/2008**	**9/2008**	**6/2014**	**L**	**E***
15	8/2008	N/A	2/2009	N	N
16	8/2008	N/A	2/2009	N	N

NOTE: N/A = specimen was not exposed to environmental exposure conditions; N = none; E = early-stage; M = middle-stage; L = late-stage. These stages were established based on the petrography analysis of concrete cores taken from specimens after structural testing and from the surface and internal expansion measurements and cracking throughout the specimen prior to testing.

E* Results of the petrography analysis of the concrete cores were not conclusive in identifying the extent that DEF had on the overall distress of the specimens. However, there was evidence in SEM and optical microscopy images that DEF has contributed to some of the distress. Therefore, researchers have categorized that at least early-stages of DEF have developed.

Table 3-3. Specimen Surface Expansions.

LSC #	Average Transverse Surface Strain at Time of Load Test (strain)				Maximum Crack Width at Time of Load Test (inch [mm])			
	Small Face 1	Small Face 2	Large Face 1	Large Face 2	Small Face 1	Small Face 2	Large Face 1	Large Face 2
1	0.0064	0.0024	0.0070	NT	0.03 (0.8)	0.04 (1.0)	0.04 (1.0)	NT
3	0.0067	0.0026	0.0054	NT	0.04 (0.9)	0.03 (0.6)	0.03 (0.6)	NT
4	*	*	*	**0.0172**	**0.06 (1.3)**	**0.06 (1.3)**	**0.12 (2.5)**	**0.06 (1.3)**
5	0.0080	0.0087	0.0090	0.0123	0.03 (0.6)	0.03 (0.6)	0.03 (0.6)	0.04 (1.0)
8	0.0082	0.0092	0.0088	0.0112	0.01 (0.3)	0.03 (0.8)	0.03 (0.8)	0.03 (0.6)
9	0.0051	0.0009	0.0026	NT	0.01 (0.2)	0.01 (0.2)	0.01 (0.2)	NT
10	0.0052	0.0013	0.0038	NT	0.01 (0.2)	0.02 (0.4)	0.02 (0.4)	NT
12	*	*	*	**0.0125**	**0.06 (1.3)**	**0.06 (1.3)**	**0.06 (1.3)**	**0.05 (1.2)**
15	N/A	N/A	N/A	N/A	N/A	N/A	N/A	N/A
16	N/A	N/A	N/A	N/A	N/A	N/A	N/A	N/A

NOTE: N/A = data not taken but presumed to be minimal; NT = data not taken but presumed similar to that on Large Face 1.

* Data not taken during project extension phase.

The following highlights some of the findings derived from the exposure program during the three-year project extension:

- The remaining eight specimens showed comparable levels of developing specimen surface expansion and cracking. Specimens LSC4 and LSC12 had the largest levels of expansion and cracking, and were selected as the specimens to be structurally testing. The remaining six specimens were repositioned at the Riverside Campus site and the sprinkler system was removed since they are designated for long-term exposure.
- The transverse surface strains were about 10 times larger than the longitudinal surface strains due to the longitudinal restraint from the axial post-tensioning steel and longitudinal column reinforcement, and the transverse tension field that Poisson's effect had induced under post-tensioning.

- The average strains calculated from measuring the sum of the crack widths between DEMEC points were about 50 percent of the surface strains calculated from measuring the distance between DEMEC points.
- The amount of expansion in the remaining eight LSC specimens during the project extension phase did increase, but at a lesser rate than what occurred during the first two years of exposure. In addition, the overall amount of expansion and cracking in the specimens were characterized as being slightly larger than specimens that were last tested prior to the project extension phase.
- Concrete cores taken from the tested specimens in the project extension phase had extensive cracking on the concrete surface and internally within the cores. ASR reaction particles (ASR gel) had accumulated in voids and at the boundary of the transverse reinforcing steel and surrounding concrete.
- Concrete cylinders made with the concrete used to construct Specimens LSC4 and LSC12 showed that the extent and width of concrete surface cracking was greater on cylinders stored at the field exposure site as compared to the humidity-controlled wet room. However, the extent of this map cracking and the width of surface cracking in all cylinders were significantly less than what developed in the LSC specimens.
- Petrography analysis identified ASR as the primary distress mechanism in all cores. ASR gel was observed in air voids, within distress aggregates, and as exudation from reactive particles. Ettringite was noted in air voids, within micro cracks, and gaps around aggregates. There was evidence of distress in the concrete cores as a result of DEF; however, the extent of the distress was inconclusive. The two core examples had more severe levels of reactivity to ASR and DEF as compared to the concrete cylinders.
- Using measured external concrete surface expansion data throughout the deterioration program, measured crack widths and patterns throughout the deterioration program, and from petrography analysis of concrete cores taken from the specimens after they were structural tested, the researchers categorized the two tested specimens during the project extension phase as being primarily influenced by late-stage ASR and also by at least early-stage DEF. However, the extent that DEF had on the overall distress of the specimens was inconclusive.

CHAPTER 4. EXPERIMENTAL TESTING PROGRAM

4.1. INTRODUCTION

This chapter discusses the experimental test setup, specimen instrumentation, and structural behavior of two of the remaining eight LSC specimens during structural load testing. The remaining eight LSC specimens showed comparable levels of developing specimen expansion and cracking during the exposure phase. In addition, the expansion and developing cracks over the three-year project extension were not significantly larger than that in specimens previously testing with the largest levels of expansion and cracking (Bracci et al. 2012). Therefore, the researchers and the TxDOT research advisory team decided to only structurally test two of the remaining eight specimens. As such, specimens LSC 4 and LSC12 were chosen since they had the most extensive surface expansion and cracking.

Figure 4-1, Figure 4-2, Figure 4-3, and Figure 4-4 show sample cracking that developed throughout the exposure phase for Specimens #1, #8, and #12, with about 2.3, 3.0, and 5.8 years of exposure, respectively. The figures show that substantial cracking resulted and the cracking pattern was similar between the specimens, even though the exposure periods of the specimens varied. Specimens #1 and #8 had similar crack widths; however, Specimen #12 had much larger crack widths (about twice that in Specimens #1 and #8, as reported in Table 3-3). Note that the specimen cracking as shown in Figure 4-5, Figure 4-6, Figure 4-7, Figure 4-8, and Figure 4-9 is comparable to the cracking in actual field structures affected by ASR (see Bracci et al. 2012).

Figure 4-1. Cracking of Specimen #1 prior to Structural Load Testing.

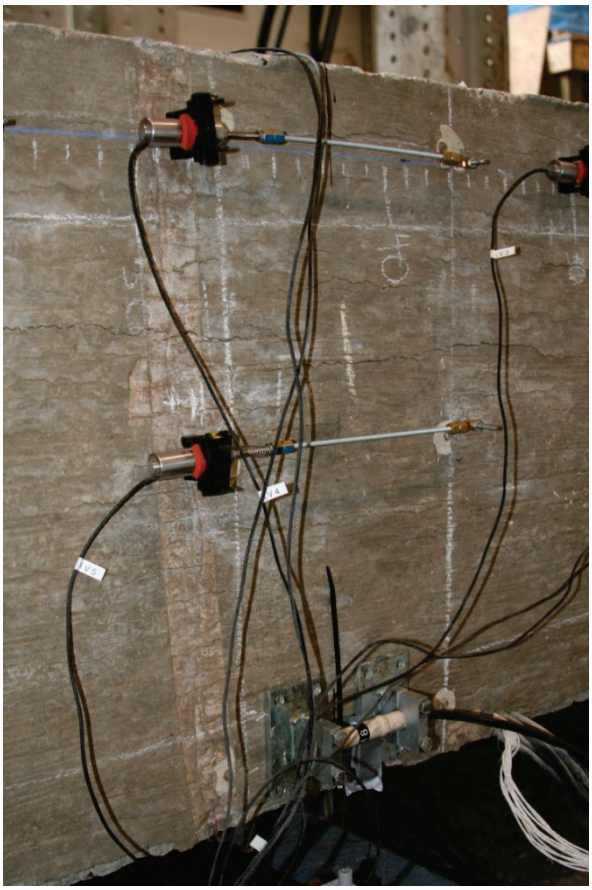

Figure 4-2. Cracking of Specimen #8 prior to Structural Load Testing.

Figure 4-3. Cracking of Specimen #12 prior to Structural Load Testing.

4.2. FOUR-POINT FLEXURAL LOAD SETUP

The design of the LSC specimens was based on the four-point load test setup, which applies a constant moment demand and no shear demand across the entire splice region. The objective of this testing is to identify the structural behavior and ultimate capacity of the splice region due to flexure demands, and determine the mode of failure in the cases of varying levels of ASR and DEF deteriorations. If the bars in the splice are sufficiently anchored, then the failure mechanism should develop at the splice ends, which would mean that the provided splice length was sufficient to satisfy ultimate demand loading. However, if the longitudinal reinforcing bars undergo bond slip (either as a result of cracking due to ASR/DEF or of ASR/DEF reaction particles affecting the interface of the reinforcing bars and adjacent concrete) and are not developed sufficiently to attain its yield strength during ultimate demand loading, then the provided splice length is not adequate. The structural load testing of specimens with varying levels of premature concrete deterioration will help determine the capability of column splice regions in TxDOT field structures with similar ASR/DEF deterioration and structural detailing in

resisting ultimate demand loads to ensure safety design requirements. Bracci et al. (2012) provided a comprehensive description of the test setup and some of the relevant material for this reporting is duplicated below.

4.2.1. Experimental Design and Specimen Layout

Figure 4-4 shows a typical LSC specimen positioned on two "pinned" supports 6 inches (152 mm) from either end of the specimen. This distance was chosen to prevent the concrete cover at the specimen ends from crushing. The pinned supports were attached to the strong floor of the Structures and Materials Testing Laboratory, and a thin layer of neoprene was placed between the bottom of the LSC specimens and the upper plate of the support (see Figure 4-5) to help prevent a concentration of stresses in the concrete due to imperfections on the concrete surface. However, the neoprene also easily compressed and resulted in slight vertical deflections during loading, which was taken into account by proper placement of the instrumentation. Similar supports were positioned under the load actuators at 8 ft (2.4 m) from each end of the LSC specimens (at the splice end). To ascertain a stable system, the researchers reinforced the top plates of the supports on each side by installing three 2-inch (51 mm) round bar stock to fix the support at the actuator end (see Figure 4-6) and then braced the actuator in the out-of-plane direction to ensure that it moved only vertically during testing. Neoprene pads were also placed between the concrete and the support to create a better interface for the transfer of forces.

Figure 4-4 shows the shear and moment demands from the four-point load setup. The maximum shear force is the force from each actuator, F_{act}, which is constant between the support and the actuator loading. Between the two actuator loading points (splice region) there is no shear force. The maximum moment (constant in splice region) is the actuator force F_{act} times the distance from the support to the loading point, L_{supp}.

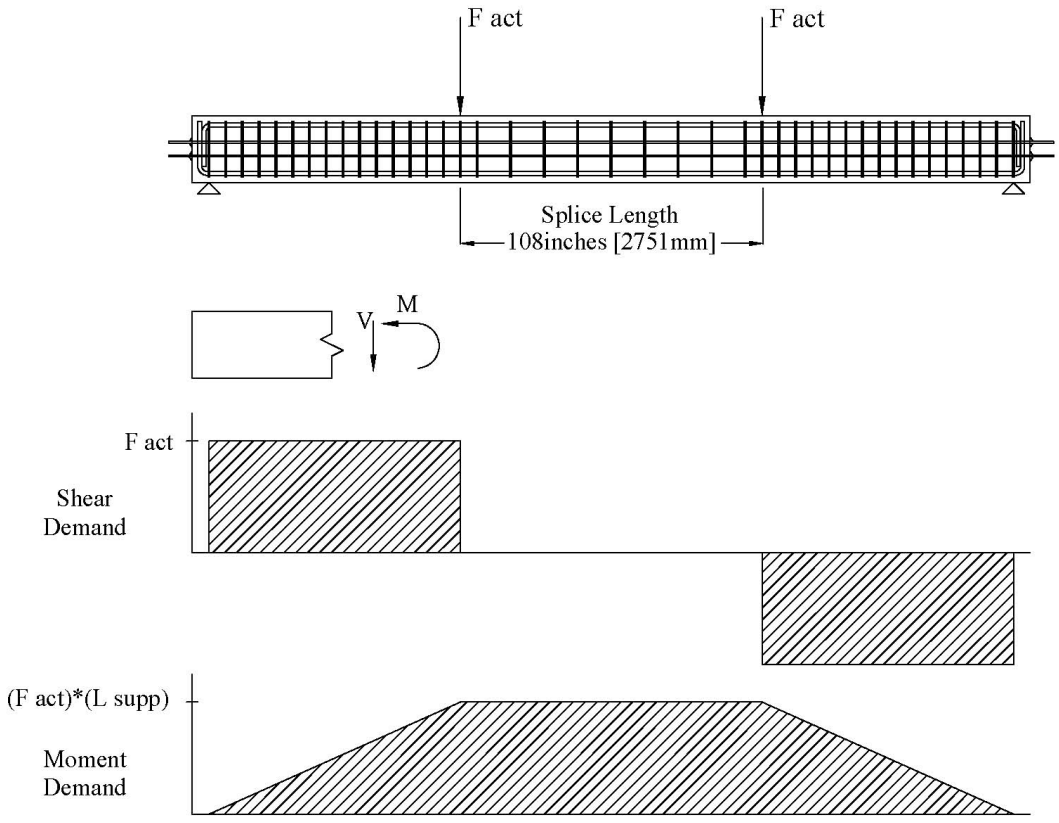

Figure 4-4. Four-Point Load Test Setup and Demand Loading.

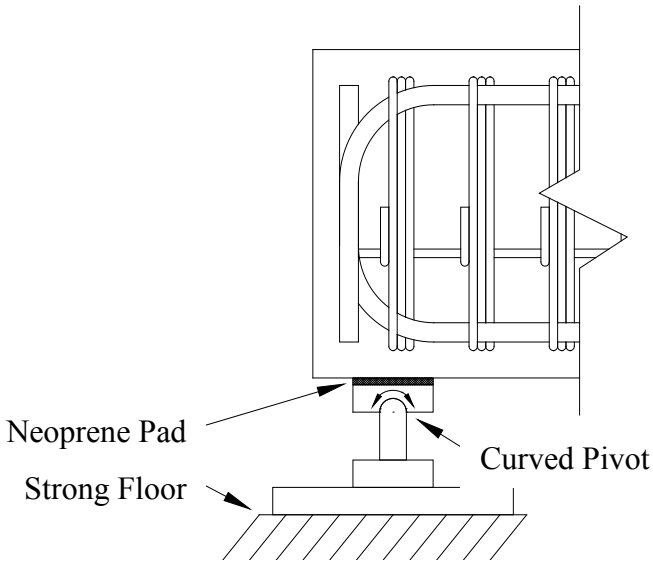

Figure 4-5. Pinned Support Setup.

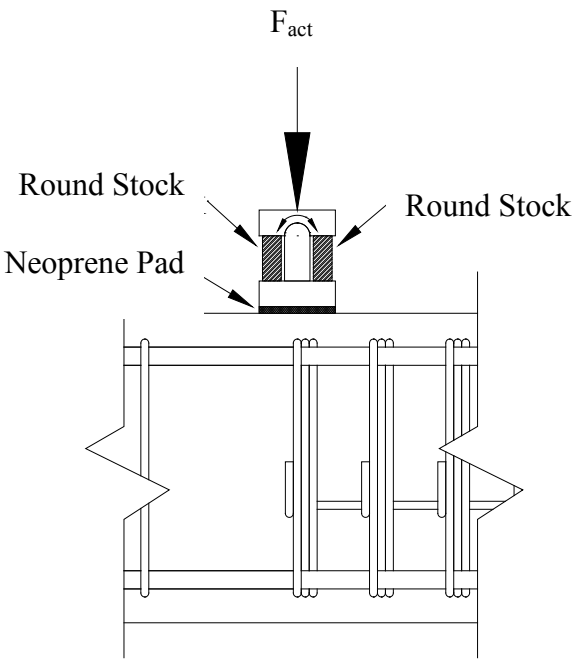

Figure 4-6. Fixed Support Setup.

Two 220 kips (979 kN) actuators attached to an overhead steel frame were used to load the specimen in displacement control loading. The steel frame was anchored to the strong floor in the Structure and Materials Testing Laboratory. Figure 4-7 shows the actuators positioned over one of the LSC specimens.

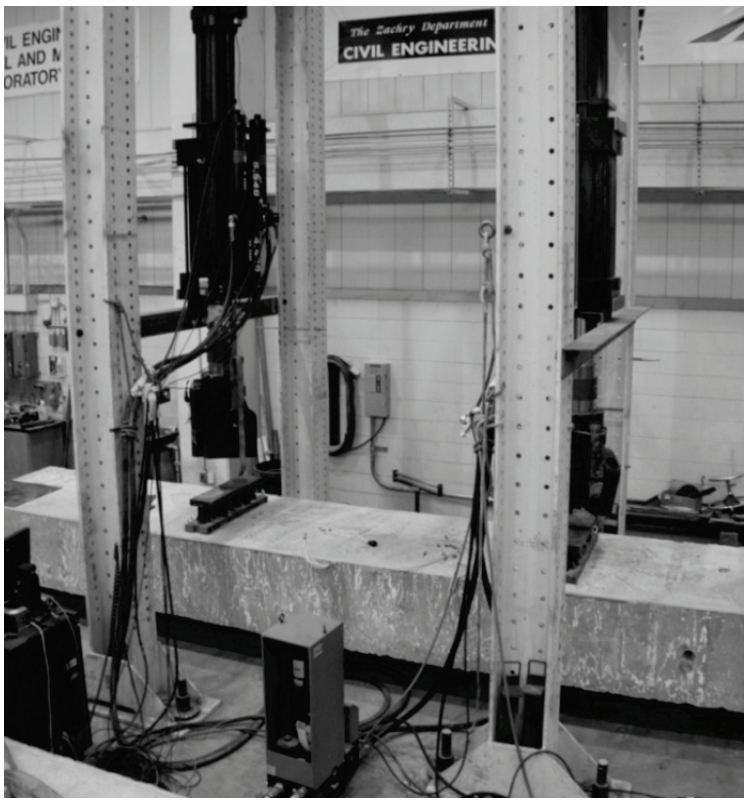

Figure 4-7. Specimen in the Four-Point Test Setup.

4.2.2. Instrumentation

The researchers attached external instrumentation to the LSC specimens to measure the deflections and external surface strains during the structural load testing. String potentiometers (STR) with a 4-inch (102 mm) stroke were used to measure the specimen deflections at various points. Figure 4-8 shows a typical STR connected to the bottom of the LSC specimen to measure vertical deformations. Figure 4-9 shows the position of the STRs on the LSC specimen to measure critical deformations during testing.

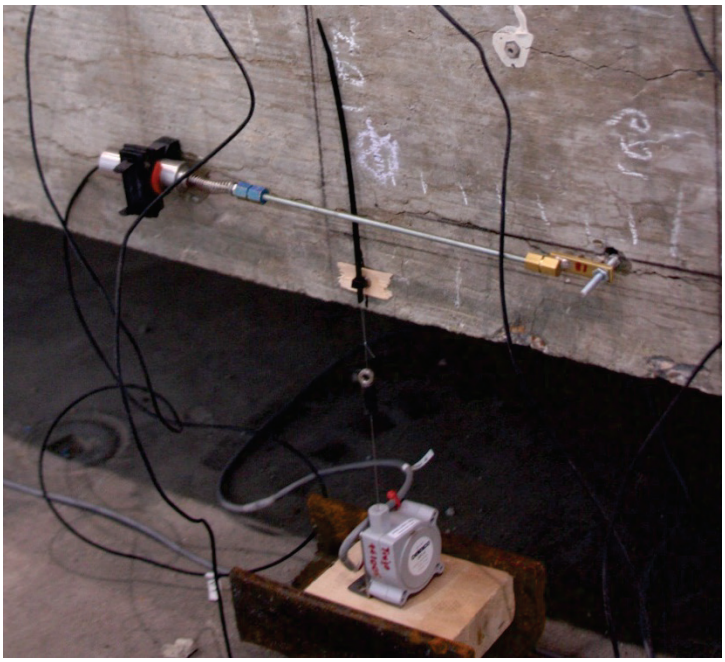

Figure 4-8. STR Installation prior to Testing.

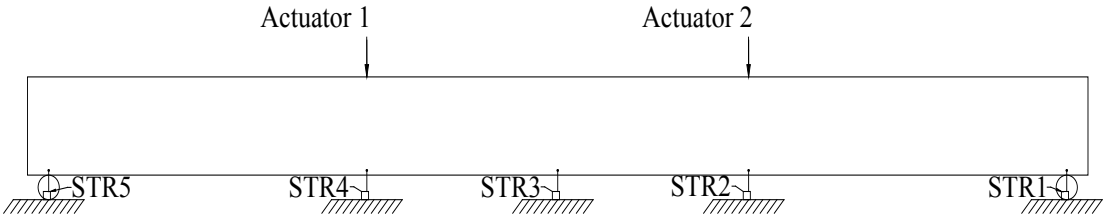

Figure 4-9. STR Locations for the Four-Point Test.

The relative specimen deflections under Actuator 1 and Actuator 2 were calculated using STR readings. The deflection under Actuator 1 and Actuator 2 ($\Delta_{\text{act 1,4pt}}$ and $\Delta_{\text{act 2,4pt}}$) was calculated by subtracting the deflection at the ends (Δ_{STR5} and Δ_{STR1}), which accounted for the flexibility in the test setup and neoprene support conditions from the original deflection under the actuators (Δ_{STR4} and Δ_{STR2}).

$$\Delta_{\text{act 1,4pt}} = \Delta_{\text{STR4}} - \Delta_{\text{STR5}} \quad \text{(Eq. 4-1)}$$

$$\Delta_{\text{act 2,4pt}} = \Delta_{\text{STR2}} - \Delta_{\text{STR1}} \quad \text{(Eq. 4-2)}$$

Linear variable differential transformers (LVDT) and concrete embedment gages (type KM) were also used to measure the tension and compression strains of the specimen in various locations during the load testing. LVDTs were securely attached to the concrete specimen separated by a gage length of 4 inches (102 mm) or 12 inches (305 mm). Researchers drilled 0.25-inch (6 mm) diameter holes into the specimen face, placed 0.25-inch (6 mm) stainless steel threaded couplers into the holes, and then secured these using adhesive epoxy. These couplers provided an anchor to screw the threaded rods into the specimen. The threaded rods were then attached to the LVDT using metal and plastic brackets. Figure 4-8 and Figure 4-10 show sample LVDTs on the LSC specimens. The final positioning of the LVDTs on the specimens and the LVDT gage lengths are discussed in the forthcoming paragraphs.

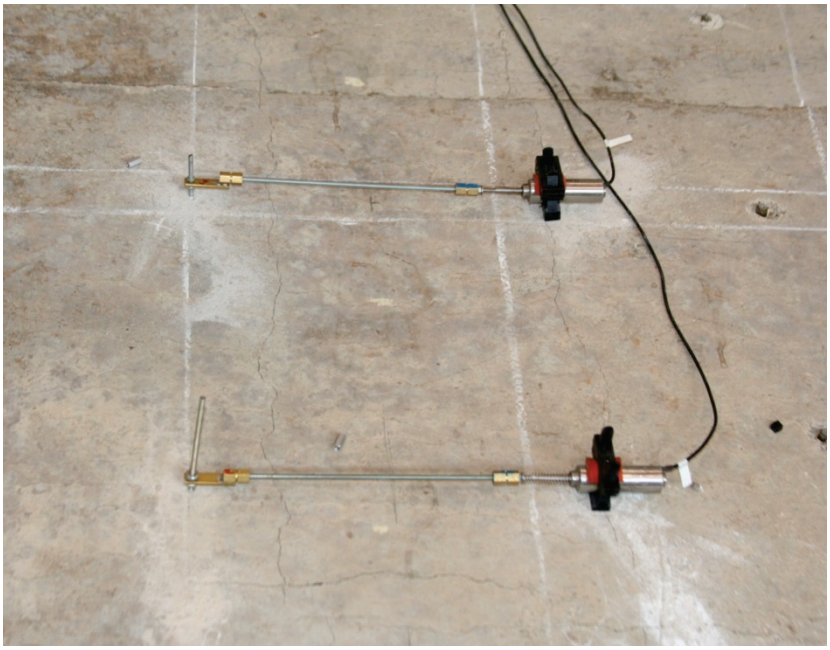

Figure 4-10. LVDT Installation prior to Testing.

KM gages were attached to the surface of the LSC specimens using adhesive epoxy. First, the research team smoothened the surface by sanding across the entire footprint of the KM base plates. A spacing bar was placed between the KM base plates to keep the base plates a proper distance apart (with a 4-inch [102 mm] gage length). Before testing, the base plates were epoxied to the concrete surface, the spacing bars were removed, and the KM gages were then attached to the base plates. Figure 4-11 shows a KM gage attached to the LSC specimen.

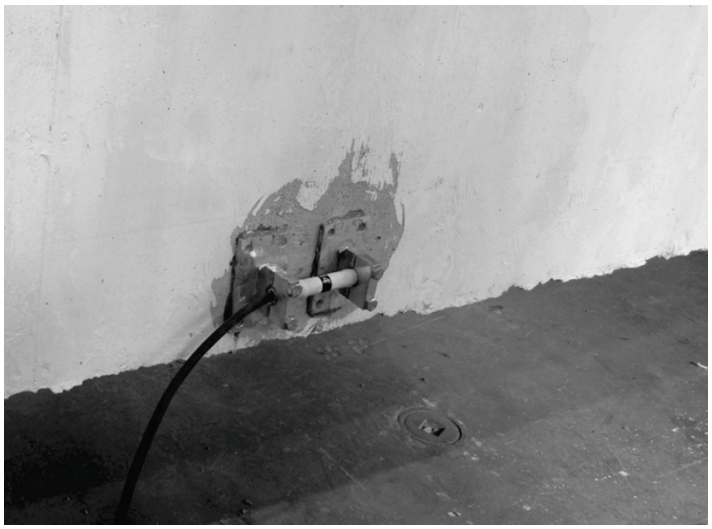

Figure 4-11. KM Gage Installation prior to Testing.

Figure 4-12 shows the STR and KM instrumentation layout for the LSC4 and LSC12 specimens. KM15 was used on the side face to measure the compression strain due to bending. KM6, KM7, KM13, and KM14 were positioned at the splice end. KM8, KM9, KM11, and KM12 were positioned in the center of the LSC specimens on the compression side (the top) and located above the internal strain gages in the specimen and KM10 was placed in the center of the mid-section of the LSC specimens to monitor compression strains in the middle of the splice. KM8 through KM12 were used to validate the strains from the internal strain gages as well as provide a longitudinal strain profile across the length of the splice in the compression region.

Likewise, LV1 through LV7 were spaced along the tension region every 18 inches (457 mm) to monitor the longitudinal strains along the length of the splice. The purpose of this was twofold:

- To validate the strain measurements from the internal strain gages.
- To create a strain profile for the splice from one end to the other.

Additionally, LV8 and KM15 were used in conjunction with LV7 to produce a strain distribution across the critical region of the splice end as in the first test. Finally, LV9 and LV10 were placed on the bottom in the critical region to measure the strain in the outermost fiber of the tension region. All LVs had a 12-inch (305 mm) gage length.

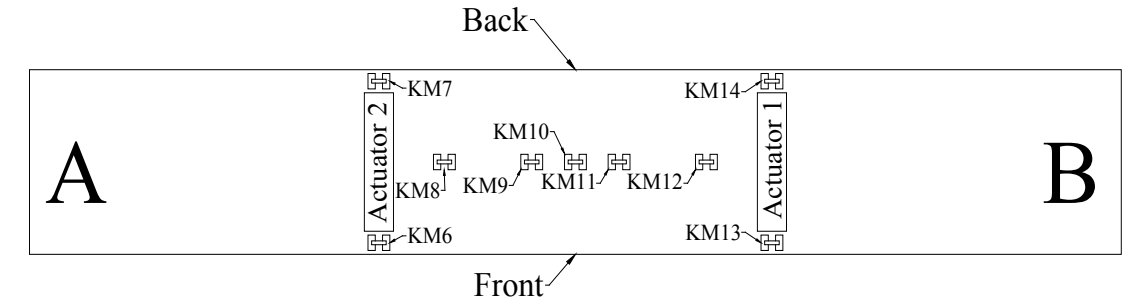

Top View

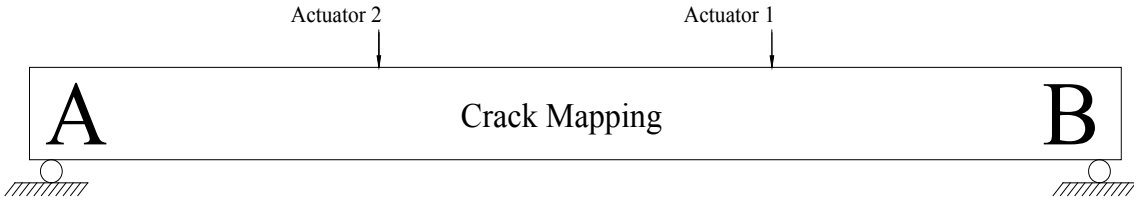

Front View

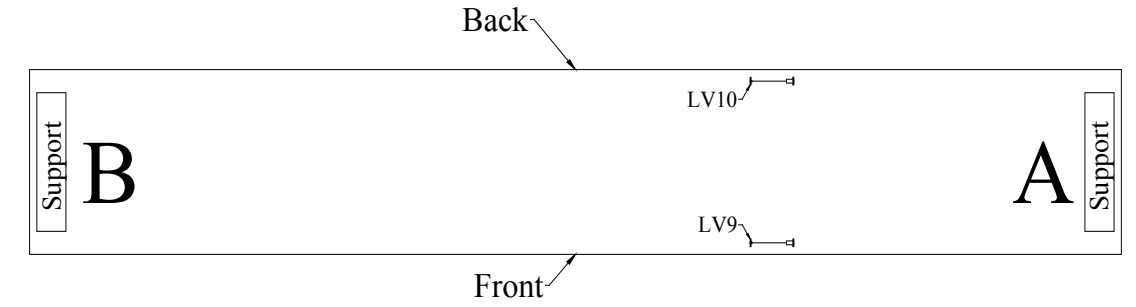

Bottom View

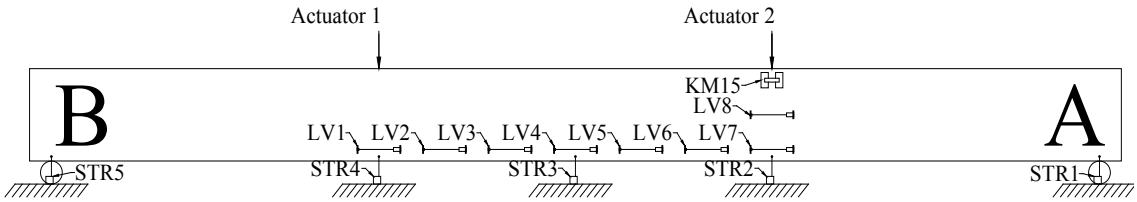

Back View

Figure 4-12. External Instrumentation Layout for the Four-Point Tests.

4.2.3. Test Procedures

Prior to beginning the test, the researchers set the actuators onto the loading supports, then placed these in displacement control at 0.001 inches/sec (25 μm/sec) until cracks initiated in the specimen. The research team then increased the rate to 0.002 inches/sec (51 μm/sec) until near failure of the specimen. In addition, the actuators were stopped and held periodically so the researchers could map cracks and take pictures of the LSC specimens. During the loading, the instrumentation was carefully monitored to identify possible failure conditions such as crushing of the concrete and bond slip. Displacement control loading allowed for small differences in the actuator loads exerted on the LSC specimens, but provided increased control over the specimen response beyond the post-cracking behavior region up to specimen failure. The load testing in the four-point setup lasted about 30 to 45 minutes.

4.3. EXPERIMENTAL RESPONSE

During all tests, the data acquisition system logged measured data for both the internal and external sensors installed in the LSC specimens at a rate of one sample per second.

4.3.1. Material Strength Test Results

During the casting of the LSC specimens, the researchers cast 4-inch × 8-inch (102 mm × 203 mm) cylinders according to ASTM C39 (2014). Some cylinders were stored in a curing room at 73.4°F (23°C) and 100 percent relative humidity as specified in AASHTO T126 (2001). Other cylinders were kept in the field with the LSC specimens where they were exposed to accelerated atmospheric conditions at the Texas A&M University Riverside Campus and supplemental watering. To determine the concrete compressive strength at the time of LSC specimen testing, the research team tested three cylinders from the field and curing room around the same time as the LSC structural tests.

Table 4-1 shows the individual and average compressive strength of the cylinders for all cases as well as the cylinder test date. Note that the field cylinders for LSC15 and LSC16 were not exposed to the same environmental conditions as the others since these were the control specimens. The specimens were all cast separately, therefore with different mixes, even though the same mix design was used throughout. The concrete mix was designed for a compressive strength of 5,000 psi (34 MPa); however, few cylinder tests resulted with this strength. For the specimen LSC4, the average concrete compressive strengths were 7,061 (49 MPa) and 6,090 psi (42 MPa) for the field and wet room cured cylinders, respectively, near the time of structural testing. Note that these strengths are larger than the cylinders from all other specimens, but are still within an acceptable range given the variability of concrete production, especially during summer months. Similarly for LSC12, the concrete compressive strengths were 5,210 psi (36 MPa) for both the field and wet room cured cylinders, which is close to the design strength and similar to the strength from other specimens.

Table 4-1. Concrete Cylinder Compressive Strengths.

	28-Day Strength, psi (MPa)					Strength at Time of Structural Testing, psi (MPa)				
	Test Date	Cured		Field		Test Date	Cured		Field	
		Sample	Avg.	Sample	Avg.		Sample	Avg.	Sample	Avg.
LSC4						**7/2014**	**6470**	**6090**	**7062**	**7061**
							5880	**(42)**	**7060**	**(49)**
							5900			
LSC12						**7/2014**	**5400**	**5210**	**5350**	**5210**
							4780	**(36)**	**5070**	**(36)**
							5450			
LSC1	02/2008	4592	4554	4543	4549	09/2010	4281	5533	5276	5300
		4479	(31)	4682	(31)		6135	(38)	5005	(37)
		4592		4423			6183		5618	
LSC3	03/2008	4740	4813	4626	4449	09/2010	6223	5684	5077	5196
		4854	(33)	4288	(31)		5364	(39)	6613	(36)
		4846		4432			5467		3899	
LSC5	04/2008	4652	4602	4280	4293	08/2011	5913	5637	6101	6046
		4602	(32)	4293	(30)		5432	(39)	6208	(42)
		4551		4307			5566		5828	
LSC8	06/2008	3990	3937	3963	3891	08/2011	5286	5339	5254	5246
		3817	(27)	3767	(27)		5304	(37)	5448	(36)
		4004		3944			5427		5035	
LSC9	07/2008	4679	4869	3789	4111	03/2010	4639	4244	5371	4966
		5016	(34)	4231	(28)		4361	(29)	4082	(34)
		4911		4314			3732		5443	
LSC10	07/2008	4589	4609	4492	4418	03/2010	4647	4886	5053	5024
		4584	(32)	4414	(30)		4735	(34)	5690	(35)
		4655		4349			5276		4329	
LSC15	09/2008	3784	3891	3776	3874	02/2009	3398	3528	3987	3942
		4014	(27)	3802	(27)		3844	(24)	3740	(27)
		3875		4044			3342		4098	
LSC16	09/2008	4017	3964	3899	3744	02/2009	3676	3862	3175	3462
		3919	(27)	3536	(26)		3899	(27)	3509	(24)
		3956		3797			4011		3700	

Figure 4-13 compares cylinders from the batch of specimens LSC4 and LSC12. Some were stored in the humidity controlled wet room and others were stored at the exposure site on top of specimens (see Figure 4-13). The figure shows that very few, small surface cracks developed in the cylinders stored in the wet room. The largest crack width measured on these cylinders was about 0.006 inches (0.15 mm) for LSC4 and LSC12 concretes. Note that some cylinders from all concrete LSC specimens had a white residue that leached from cracks. In comparison, cylinders stored at the exposure site in the same environmental conditions as the LSC specimens (exterior weather conditions and supplemental watering four times a day) had more numerous, larger surface cracking than the cylinders taken from the wet room. The largest crack width on these cylinders was about 0.01 inches (0.25 mm).

Figure 4-13. Cylinders at the Riverside Campus.

4.3.2. Four-Point Flexural Test Results

Figure 4-14 shows the measured force-deformation behavior of the control specimens (LSC15 and LSC16) and those with varying degrees of primarily ASR (and minimal DEF), as identified in Table 3-2 and Table 3-3 during the four-point test setup prior to the project extension phase, and as Bracci et al. (2012) had originally reported. Figure 4-15 and Figure 4-16 show the measured force-deformation behavior of LSC12 and LSC4, respectively, tested during the project extension phase with increasing levels of concrete expansion and cracking due to

primarily ASR and some level of DEF, as identified in Table 3-3, during the four-point test setup. The figures show that the structural behaviors of Specimens #12 and #4 are comparable to those specimens tested early in the research project that were influenced primarily by ASR. In particular, the structural testing of Specimen #4 was taken to significantly larger deformations (terminated close to when the researchers deemed structural failure was eminent) in order to get an indication of structural ductility capability of the spliced region. In addition, the structural response of the specimen at around 1-inch (25 mm) displacement seemed to have unloaded at one actuator point and further loaded at the other actuator point. This response developed when the physical supports at the specimen ends had shifted slightly because of the elongation of the specimen at the bottom. Once the supports stabilized, the actuator loadings continued as expected for the test setup under displacement control loading.

When the researchers compared Figure 4-14, Figure 4-15, and Figure 4-16, they noted the following in specimens with varying degrees of ASR and some DEF:

- Showed no evidence of bond deterioration within the splice.
- Had similar initial stiffness and behavior up to the first cracking.
- Had a 25 to 35 percent increase in post-cracking stiffness up to yielding.
- Had a 5 to 15 percent increase in yield strength.
- Showed no overall detrimental effects on the structural response when compared to control specimens without ASR deterioration.

This improved behavior can be explained by the resulting volumetric expansion of the concrete due to ASR that engaged the longitudinal and transverse reinforcement. The activation of the reinforcement is believed to have resulted in increased axial loading and better confinement of the core concrete.

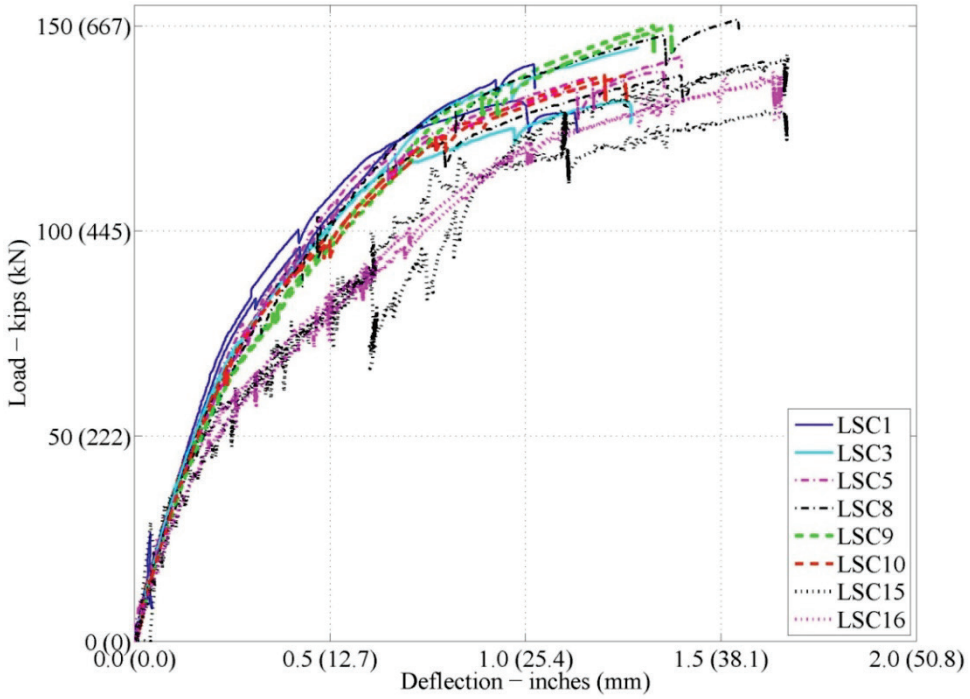

Figure 4-14. Experimental Load vs. Deflection during the Four-Point Test: Specimen Behavior at the Actuator Load Point (Splice End) (Bracci et al. 2012).

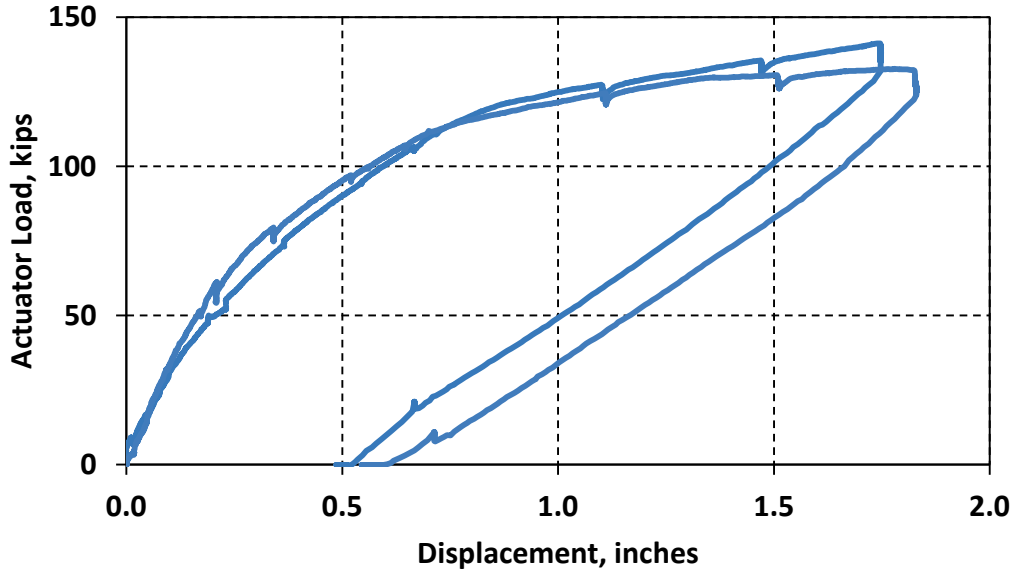

Figure 4-15. Experimental Load vs. Deflection during the Four-Point Test: Specimen LSC12 Behavior at the Actuator Load Point (Splice End).

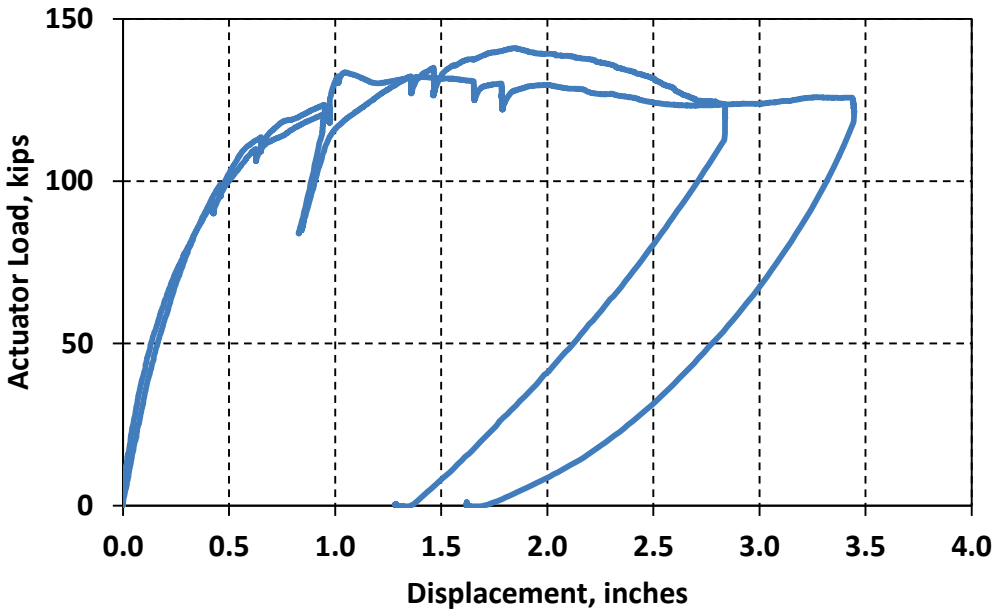

Figure 4-16. Experimental Load vs. Deflection during the Four-Point Test: Specimen LSC4 Behavior at the Actuator Load Point (Splice End).

Figure 4-17 shows the measured side-face concrete surface strains at the depth of the longitudinal reinforcement throughout the splice region for specimens LSC4 and LSC12. The figure clearly shows that most of the tension strains are occurring at the points directly under the actuator loading points or at the ends of the splice region (LV1 and LV7; see Figure 4-12). The tensile strains developing between the splice region end points using LV2, LV3, LV4, LV5, and LV6 had minimal developing strains. Therefore, the provided lap splice length in the specimens was sufficient to provide full bending moment strength throughout the splice region, implying that the splice length provided was sufficient to overcome the current stage premature concrete deterioration primarily due to late-stage ASR and at least some early-stage DEF.

Figure 4-18 shows the measured side-face concrete surface strains at varying depths of the section and the top and bottom surface strains at the splice end (refer to Figure 4-12). The figure shows that large tensile strains developed along the bottom of the section, lesser tensile strains developed at mid-depth of the section, and compressive strains developed near the top of the section approaching concrete crushing, which is typical of bending deformations. Note that KM13 for LSC4 went beyond the measureable range of the sensor at a strain of about −0.004.

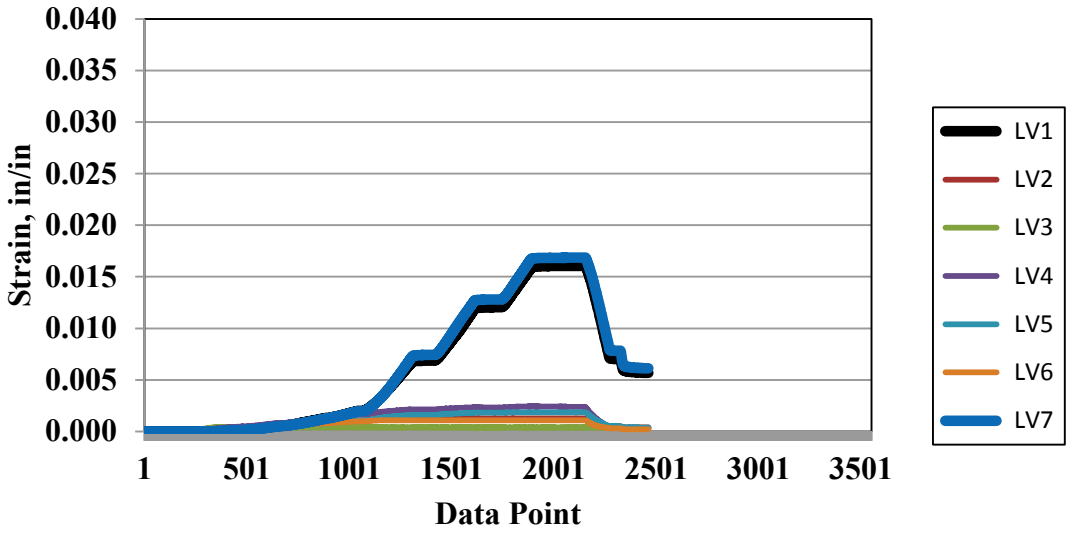

(a) Specimen LSC12

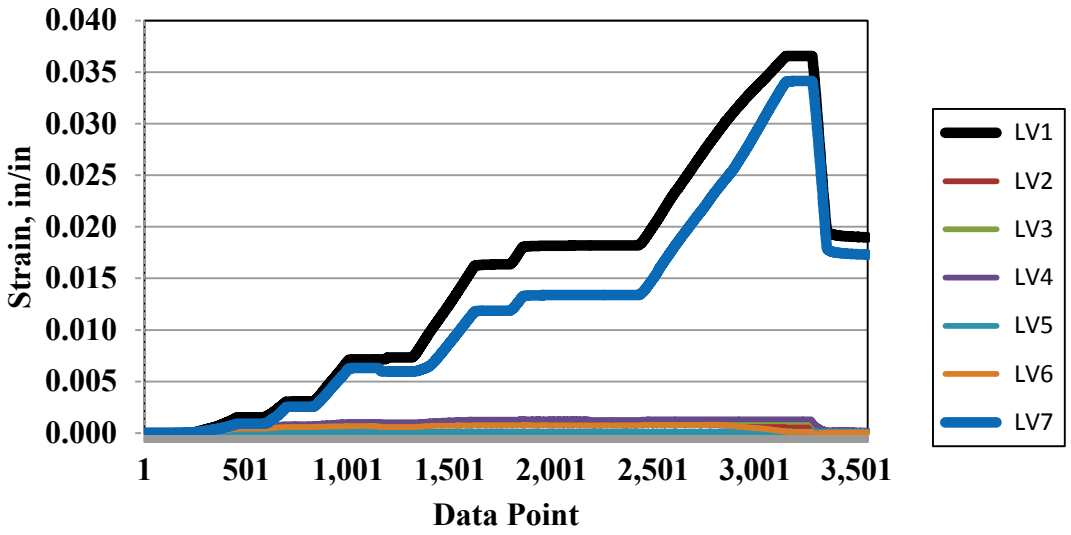

(b) Specimen LSC4

Figure 4-17. Strain Readings from LVDTs (12-Inch Gage Length) in the Tension Region.

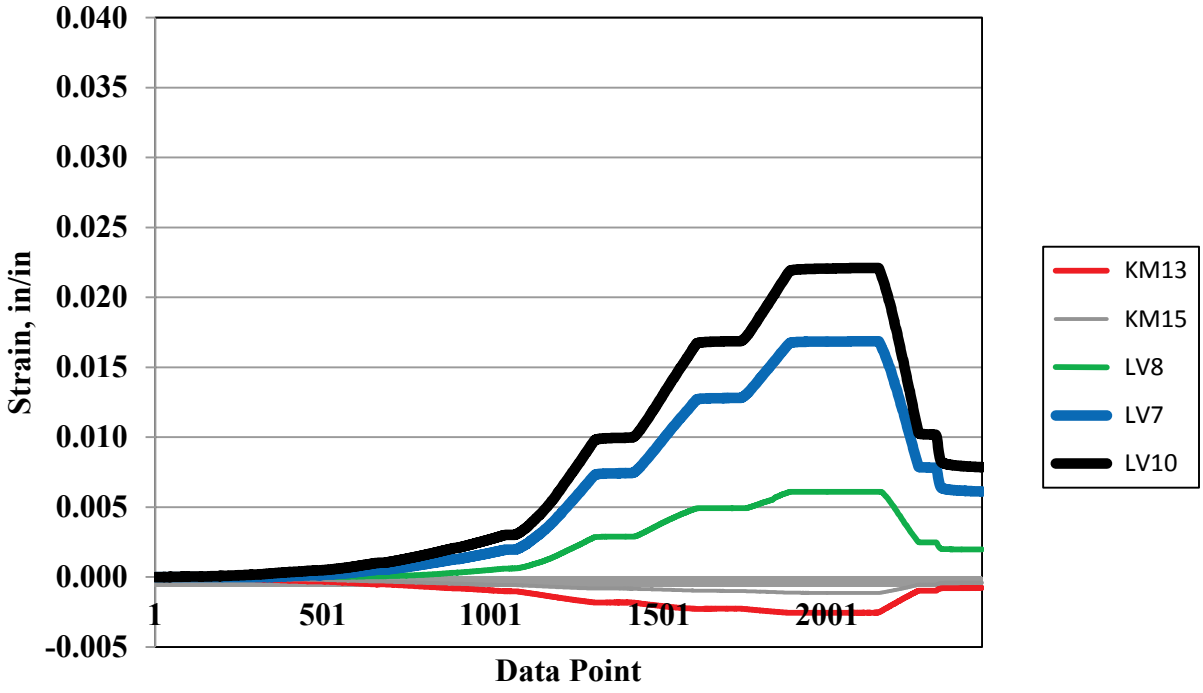

(a) Specimen LSC12

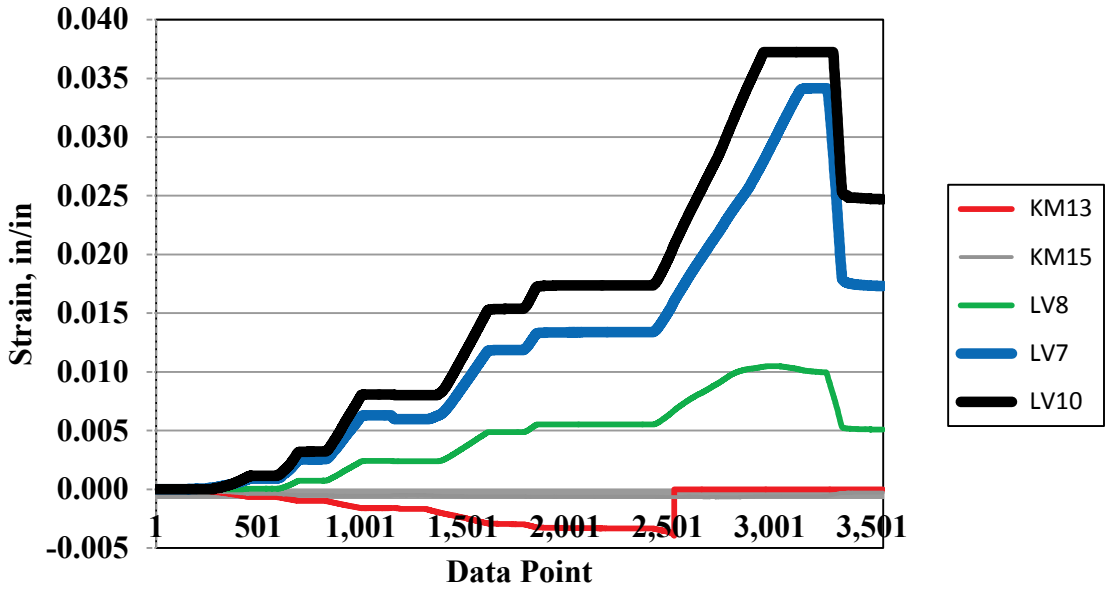

(b) Specimen LSC4

Figure 4-18. Section Strain Readings at Splice End (at Actuator).

4.4. SUMMARY AND KEY FINDINGS

The experimental testing program in this research consisted of the design, construction, curing, exposure, and structural load testing of 16 LSC specimens with a critical lap splice region under varying degrees of premature concrete deterioration due to primarily ASR and at least some (early-stage) DEF. Of these specimens, two control specimens without any ASR/DEF deterioration and four groups of two specimens with varying levels of ASR and up to at least early-stage DEF (the last two specimens tested during the project duration) were structurally load tested in both the four-point and three-point load test setups (except for the last two specimens). The remaining six specimens were repositioned at the Riverside Campus site and the sprinkler system was removed since these specimens are designated for long-term exposure.

The following are the key findings from the experimentally measured structural force-deformation response, internal and external strain measurements, and developing failure mechanisms on the specimens tested:

- In comparison with the response of the control specimens, specimens exhibiting primarily ASR (and up to some DEF) had similar initial stiffness and behavior up to first cracking, had about a 25 to 35 percent increase in post-cracking stiffness up to yielding, had about a 5 to 15 percent increase in yield strength, and showed no overall detrimental effects on the structural response.
- The increase in stiffness and strength can be explained by the resulting volumetric expansion of the concrete due to the ASR that engaged the transverse reinforcement for better confinement of the core concrete, and engaged the supplemental post-tensioning reinforcement and the column longitudinal reinforcement to generate additional axial compression load.

Although the structural performance of column splice regions with varying levels of ASR and at least early-stage DEF showed no detrimental effects, the vulnerability of the column splices with increased levels of DEF deterioration could not be evaluated to date. In spite of the research team's best efforts to accelerate deterioration resulting from DEF, more time and possibly different exposure conditions are needed to allow the remaining six specimens to further deteriorate.

CHAPTER 5. SUMMARY, CONCLUSIONS, AND RECOMMENDATIONS

5.1. SUMMARY

Over the past 25 years or so, the Texas Department of Transportation has had an aggressive construction program in place to accommodate the expanding population growth within Texas. However, there is a significant amount of the reinforced concrete construction that has developed early cracking, termed *premature concrete deterioration*. Most of this deterioration has been identified or at least suspected to be primarily from ASR and in some cases, DEF. Both deterioration mechanisms lead to volumetric expansion of the concrete due to ASR gel and/or the reformation of ettringite within the concrete, respectively. As such, the initial development of cracking from these mechanisms typically occurs in the tension field of the concrete member due to gravity loading during service conditions. An area of concern for TxDOT is the performance of column splice regions when varying levels of premature concrete deterioration (due to ASR and/or DEF) adversely affect it.

Therefore, the major objectives of this research program were to:

- Evaluate the experimental behavior of critical column lap splice regions using large-scale specimens under varying levels of premature concrete deterioration due to ASR and/or DEF.
- Develop an analytical model that can evaluate the behavior of a splice region under varying levels of concrete deterioration based on calibration with the experimental behavior.

In summary, the experimental testing program in this research consisted of the design, construction, curing, exposure, and structural load testing of 16 large-scale column specimens with a critical lap splice region under varying degrees of premature concrete deterioration due to ASR/DEF. Two of these specimens were constructed, preloaded to simulate gravity load conditions, and stored in the climate-controlled structural laboratory without supplemental water, which basically eliminated the development of ASR and DEF. The experimental behaviors of these two specimens were considered as the undamaged control behavior. The other 14 large-scale specimens were constructed, preloaded to simulate gravity load conditions, and then stored

in an open field at the Texas A&M University Riverside Campus where they were exposed to wet-dry cycles. Data were recorded for surface expansions measurements in all specimens throughout the exposure program. All specimens have successfully developed ASR/DEF deterioration (described as up to late-stage ASR and at least early-stage DEF from the measured instrumentation, crack width data, and petrography analysis) in terms of internal concrete and reinforcing steel expansions, external surface expansions, and surface cracking that is representative of observations in in-service bridges.

Of the 16 specimens, two control specimens without any ASR/DEF deterioration and four groups of two specimens with varying stages of ASR and up to at least early-stage DEF were structurally load tested in both the four-point and three-point load test setups (except for the last two specimens tested in the project extension phase). Six additional specimens are being stored at the exposure site indefinitely under outdoor exposure conditions (the sprinkler system for wet/dry exposure had to be removed) and the researchers will periodically inspect these specimens on an unfunded basis.

To complement the experimental program, the researchers developed analytical models (reported in Bracci et al. 2012) based on the flexure theory to characterize the force-deformation behavior and internal strains of the LSC specimens in both the four-point and three-point load test setups. In both the critical splice region and the specimen end regions, the longitudinal reinforcing steel was assumed to develop tensile resistance linearly from zero resistance at the end of the bar to the yield strength at the code calculated development length of the bar. The research team compared results from these models with the experimental response of undamaged LSC specimens, and then adjusted these for the increased axial load due to the longitudinal expansion from ASR and minimal DEF.

5.2. CONCLUSIONS

The conclusions and key findings from each phase of the research program are presented in this section.

5.2.1. Deterioration Program

In summary, the 14 large-scale specimens stored at the Riverside Campus were exposed to the outdoor weather conditions of Bryan, Texas, and to wet-dry cycles using supplemental water. Internal instrumentation and external surface measurements were continually recorded for all specimens throughout the deterioration program. It can be concluded that all specimens have successfully developed significant premature concrete deterioration due to ASR and/or DEF in terms of concrete expansion and surface cracking that is representative of observations in in-service bridges. In addition, the deterioration mechanism is continuing.

The following highlights some of the findings derived from the exposure program during the three-year project extension:

- The remaining eight specimens showed comparable levels of developing specimen surface expansion and cracking. Specimens LSC4 and LSC12 had the largest levels of expansion and cracking, and were selected as the specimens to be structurally testing. The remaining six specimens were repositioned at the Riverside Campus site and the sprinkler system was removed since they are designated for long-term exposure.
- The transverse surface strains were about 10 times larger than the longitudinal surface strains due to the longitudinal restraint from the axial post-tensioning steel and longitudinal column reinforcement, and the transverse tension field that Poisson's effect had induced under post-tensioning.
- The average strains calculated from measuring the sum of the crack widths between DEMEC points were about 50 percent of the surface strains calculated from measuring the distance between DEMEC points.
- The amount of expansion in the remaining eight LSC specimens during the project extension phase did increase, but at a lesser rate than what occurred during the first two years of exposure. In addition, the overall amount of expansion and cracking in the specimens were characterized as being slightly larger than the specimens that were last tested prior to the project extension phase.
- Concrete cores taken from the tested specimens in the project extension phase had extensive cracking on the concrete surface and internally within the cores. ASR reaction

particles (ASR gel) had accumulated in voids and at the boundary of the transverse reinforcing steel and surrounding concrete.

- Concrete cylinders made with the concrete used to construct the specimens LSC4 and LSC12 showed that the extent and width of concrete surface cracking was significantly greater on cylinders stored at the field exposure site than at the humidity-controlled wet room. However, the extent of this map cracking and the width of surface cracking in all cylinders were significantly lesser than what developed in the LSC specimens.
- Petrography analysis identified ASR as the primary distress mechanism in all cores. ASR gel was observed in the air voids, within distress aggregates, and as exudation from reactive particles. Ettringite was noted in the air voids, within micro cracks, and gaps around aggregates. There was evidence of distress in the concrete cores as a result of DEF; however, the extent of the distress was inconclusive. The two core samples had more severe levels of reactivity to ASR and DEF than the concrete cylinders.
- Using measured external concrete surface expansion data throughout the deterioration program, measured crack widths and patterns throughout the deterioration program, and from petrography analysis of concrete cores taken from the specimens after they were structurally tested, the researchers then categorized the two tested specimens during the project extension phase as being primarily influenced by late-stage ASR and at least early-stage DEF. However, the extent that DEF had on the overall distress of the specimens was inconclusive.

5.2.2. Experimental Testing Program

The experimental testing program in this research consisted of the design, construction, curing, exposure, and structural load testing of 16 LSC specimens with a critical lap splice region under varying degrees of premature concrete deterioration due to primarily ASR and at least some (early-stage) DEF. Of these specimens, two control specimens without any ASR/DEF deterioration and four groups of two specimens with varying levels of ASR and up to at least early-stage DEF (the last two specimens tested during the project duration) were structurally load tested in both the four-point and three-point load test setups (except for the last two specimens). The remaining six specimens were repositioned at the Riverside Campus site and the sprinkler system was removed since they are designated for long-term exposure.

The following are the key findings from the experimentally measured structural force-deformation response, internal and external strain measurements, and developing failure mechanisms on the specimens tested:

- In comparison with the response of the control specimens, specimens exhibiting primarily ASR (and up to some DEF) had similar initial stiffness and behavior up to first cracking, had about a 25 to 35 percent increase in post-cracking stiffness up to yielding, had about a 5 to 15 percent increase in yield strength, and showed no overall detrimental effects on the structural response.
- The increase in stiffness and strength can be explained by the resulting volumetric expansion of the concrete due to the ASR that engaged the transverse reinforcement for better confinement of the core concrete, and engaged the supplemental post-tensioning reinforcement and the column longitudinal reinforcement to generate additional axial compression load.

Although the structural performance of column splice regions with varying levels of ASR and up to some DEF showed no detrimental effects, the vulnerability of the column splices with increased levels of DEF deterioration could not be evaluated to date. In spite of the research team's best efforts to accelerate deterioration resulting from DEF, more time and possibly different exposure conditions are needed to allow the remaining six specimens to further deteriorate.

5.2.3. Analytical Modeling

Bracci et al. (2012) reported the significant findings from the analytical modeling research. Since the experimental response in specimens tested in the project extension phase were similar to that tested previously, no changes in the modeling were necessary, nor reported here.

5.3. RECOMMENDATIONS

Although results from the experimental program indicate that late-stage ASR and at least some early-stage DEF did not significantly influence the performance of the specimen lap splice regions with concentric axial loading due to service conditions, care should be taken when applying these results and findings to other structural applications. The lap splice length in the

specimens tested was overdesigned per TxDOT standards for the bar size being used, and less conservative designs may exhibit different behavior. The splice region in the specimens tested also had a single full column hoop at a typical 12-inch (0.3 m) spacing that provided sufficient confinement of the concrete core region. In reinforced concrete structural members without proper confining steel or proper longitudinal steel, special monitoring of developing crack patterns and crack widths should take place in assessing the structural capability since this task was beyond the scope of the research performed. In addition, because the ASR process was accelerated and testing was performed at relatively early-stages in the research, longer-term deterioration may result in different specimen performance.

As of the preparation of this report, it appears that most of the expansion and cracking in the specimens primarily occurred due to ASR, but at least some early-stage DEF was also present. DEF and other deterioration mechanisms, such as corrosion, may further develop over time since significant cracking due to ASR will allow for more water and corrosive substances to penetrate the concrete cover and core regions. These deterioration mechanisms were not addressed in this report and will need to be fully studied experimentally for their effects on the structural performance of column splice regions.

In structures suspected to be influenced by ASR and other deterioration mechanisms, close monitoring of developing crack patterns and crack widths should be recorded and carefully studied. When crack widths exceed those typical for in-service structures and when cracking patterns become identifiable, petrography analysis of concrete cores taken from the structure should be performed to identify the developing expansion mechanism in the concrete. In addition, the provided reinforcing steel should be carefully identified and assessed for strength, and for transverse confinement of the concrete core region when the concrete may be exposed to expansive pressures.

In addition, this report documents the developing maximum crack width measurements and the surface strain measurements—via caliper readings using DEMEC points and by summing of cracks measured with a crack width card indicator in a given region—that developed in this experimental program on large-scale column specimens. When measured crack widths and surface strains in actual bridge structures exceed the values of those in this report, special care

should be exercised to assess the structural capability of the splice regions since this task was beyond the scope of the research performed.

REFERENCES

AASHTO, "LRFD Bridge Design Specifications," American Association of State Highway and Transportation Officials, Washington, D.C., 2007.

AASHTO, "LRFD Bridge Design Specifications," American Association of State Highway and Transportation Officials, Washington, D.C., 2004.

AASHTO, *Standard Method of Test for Making and Curing Concrete Test Specimens in the Laboratory*. Publication No. T126. American Association of State Highway and Transportation Officials, Washington, D.C., 2001.

ACI Committee 318, "Building Code Requirements for Structural Concrete (ACI 318-08) and Commentary," American Concrete Institute, Farmington Hills, MI, 2008.

American Society for Testing and Materials. ASTM C39: Standard Test Method for Compressive Strength of Cylindrical Concrete Specimens, Annual Book of ASTM Standards: Volume 04.02, Concrete and Aggregates. West Conshohocken, PA, 2014.

Bauer, S., B. Cornell, D. Figurski, T. Ley, J. Miralles, and K. Folliard. "Alkali-Silica Reaction and Delayed Ettringite Formation in Concrete: A Literature Review," Report No. FHWA/TX-06/0-4085-1. Center for Transportation Research, The University of Texas at Austin, TX, 2006.

Bracci, J.M., P. Gardoni, M.K. Eck, and D. Trejo, "Performance of Lap Splices in Large-Scale Column Specimens Affected by ASR and/or DEF," Texas Transportation Institute, Research Report 0-5722-1, 2012.

Burgher, B., Thibonnier, A., Folliard, K.J., Ley, T., and Thomas, M. "Investigation of the Internal Stresses Caused by Delayed Ettringite Formation in Concrete," Technical Report No. FHWA/TX-09/0-5218-1, The University of Texas at Austin, Center for Transportation Research, 2008.

Eck Olave, M.K, J. Bracci, P. Gardoni, and D. Trejo, "Performance of RC Affected by ASR. I: Accelerated Exposure and Damage," *ASCE, Journal of Bridge Engineering*, 10.1061/(ASCE)BE.1943-5592.0000655, 2014a.

Eck Olave, M.K, J. Bracci, P. Gardoni, and D. Trejo, "Performance of RC Affected by ASR. II: Experiments and Assessment," *ASCE, Journal of Bridge Engineering*, 10.1061/(ASCE)BE.1943-5592.0000657, 2014b.

Folliard, K.J., R. Barborak, T. Drimalas, L. Du, S. Garber, J. Ideker, T. Ley, S. Williams, M. Juenger, M. Thomas, and B. Fournier., "Preventing ASR/DEF in New Concrete : Final Report," Technical Report No. 0-4085-5, The University of Texas at Austin, Center for Transportation Research, 2006.

APPENDIX

Texas Department of Transportation

Petrographic Analysis

09/22/2014

Report:	TTI ASR DEF
Date Received:	07/01/2014
Structure Type:	Unknown
Sample Type:	2Cores & 2Cylinders
Location:	Unknown
Coarse Aggregate Producer:	NA
Coarse Aggregate Type:	Siliceous Gravel
Fine Aggregate Producer:	NA
Fine Aggregate Type:	Siliceous Sand
Cement Producer:	NA
Cement Type:	NA

Comments:

This petrographic analysis was performed in response to a request from Dr. Joseph Bracci to assist the Texas A&M University in an ASR/DEF investigation of six submitted cores. The following objectives were specified by Texas A&M:

- General observations on concrete quality. (Comments on placement, mixture proportions, water-cement ratio).
- Visual documentation of ASR and/or DEF micro structural damage. (Images depicting gel/ettringite locations, cracking and gapping of paste/aggregate interfaces).
- Qualitative study of damage severity in each sample. (Comparison of micro structural damage between all samples).
- Qualitative study of damage progression through the length of the sample. (Comparison of micro structural damage in surface and core concretes of each sample).

General Appearance: Two cores and two cylinders were submitted for analysis and were designated as: LSC12 ISF, LSC4 ISF, LSC4 5F and LSC4 4W. The submitted cores were 3-3/4 inch in diameter and ranged from 5-1/4 to 6-3/4" inches in length. The cylinders were 4" in diameter and 7-3/4" in length. All of the cores had obvious distress cracks on the surface and sides of the core. The cores also had obvious coarse aggregate distress/dissolution and abundant reactions products. The cylinders primarily had fine cracking on the sides of the cylinders.

Water/Cement Ratio: None of the cores had abnormal or elevated w-c ratio. Based on appearance of the paste (color, ferrite distribution and granularity of the hydrates) cores LSC4 ISF and LSC4 5F had similar w/c ratio. Core LSC12 ISF was next highest and Cylinder LSC 4W had the highest.

Proportioning and types of aggregate: Based on microscopic observations the paste volume indicate a high sack mix, low coarse aggregate factor and gap grading was noted in all the cores. Coarse aggregate consist of siliceous gravel comprised of chert, agate, quartzite, volcanic and spares amounts of lightweight aggregate. Fine aggregate consist of quartz, chert, volcanic, and agate.

Paste content and appearance: Paste content is indicative of a high sack mix and appearance is normal except for the numerous fine micro cracking and reaction products. The reaction products consist of ASR gel and ettringite. Core LSC12 ISF has the highest paste volume. No fly ash or other mineral admixtures were present in the mix.

Air Content: Non-Air Entrained.

Degree of Hydration: Normal.

Carbonation: Carbonation was noted at the exterior surface of all the cores and on the sides of the cylinders. The following chart represents the depth of carbonation for each core/cylinder:

Specimen #	Carbonation Depth from Top Surface	Carbonation Depth on sides of Cylinders
LSC12 ISF Core	7mm	NA
LSC4 ISF Core	2mm	NA
LSC4 5F Cylinder	3.5mm	3.5mm
LSC4 4W Cylinder	1.5mm	2.5mm

Deleterious Reaction Mechanism: The primary distress mechanism in all the cores is attributed to ASR. ASR gel was observed in air voids, within distress aggregate and as exudation from reactive particles. Ettringite was noted in air voids, within micro cracks and gaps around aggregates. The two cores had much more severe level of reactivity compared to the cylinders.

The following schematic is a representation of the cracking and orientation observed in the core specimens:

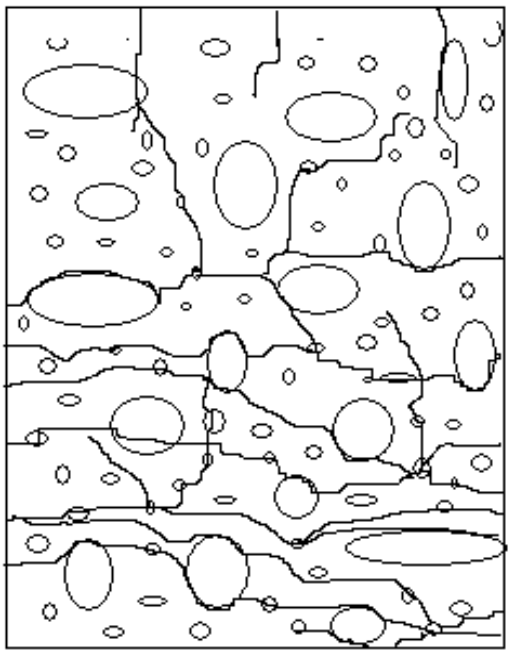

The following table describes the various levels of distress observed in the cores:

Sample #	Surface Distress	Level of ASR Distress	Reactivity Level & Aggregate count/cross-sectional area m=mild md=moderate s=severe	Evidence of DEF
LSC12 ISF	High (multiple surface cracks from 10mm to 2-3/4" deep from the surface)	High with reactive particles noted throughout the core.	16md/s CA reactive and 30md/s FA particles counted in (14.06sqin area)	Ettringite was noted within voids, cracks and at gaps at paste aggregate interfaces.
LSC4 ISF	High (multiple surface cracks from 3mm to 2-1/4" deep from the surface)	High with reactive particles noted throughout the core.	26md/s CA reactive and 64md/s FA particles counted in (23.44 sqin area)	Ettringite was noted within voids, cracks and at paste aggregate interfaces
LSC4 5F	Sparse cracking on the top of the cylinder. Top surface cracks measured from 4 to 11mm deep. Much more cracking apparent on the side of the cylinder.	Low level of ASR activity, reactive particles showed very mild levels of distress	20m CA reactive and 33m FA particles counted in (14.06sqin area)	Ettringite noted within voids, cracks and at paste aggregate interfaces
LSC4 4W	Very few cracks at the top surface. Cracks are more numerous on the side of the cylinder.	Low to moderated ASR activity, reactive particles showed very mild levels of distress	6m CA reactive and 24m FA particles counted in (14.06sqin area)	Ettringite noted within voids, cracks, at paste aggregate interfaces

Concluding Comments: Based on this analysis the cores exhibiting high levels of ASR degradation (late-stage ASR). Both the fine and coarse aggregates are experiencing ASR attack in the cores. The two cylinders also had evidence of ASR activity; however, it was in the early-stages compared to the cores. The aggregate and paste distress level associated with ASR in the cylinder is mild. The extent that DEF has play a role in the overall distress is inconclusive; however, there is evidence as seen in the SEM and optical microscopy images that DEF has contributed to some of the distress primarily in the cores. Ettringite formation in the cylinders was very low compared to the cores which had extensive development of ettringite formation (primarily redistribution of the ettringite into voids, cracks and gaps).

The following images depict the features observed in the above analysis which illustrates various stages of ASR and Ettringite formation:

Large surface crack (approximately 1mm) on top surface of core LSC12 ISF

Large cracks illustrated on top of core LSC4 ISF

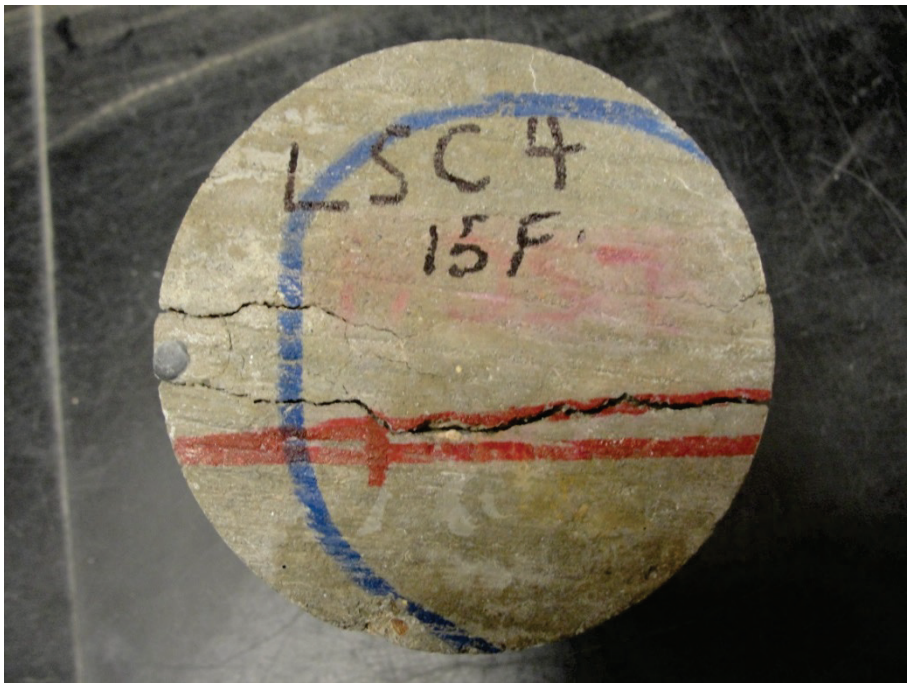

Fine network of cracking on side of cylinder LSC4 5F

No obvious cracking on surface of cylinder LSC4 5F

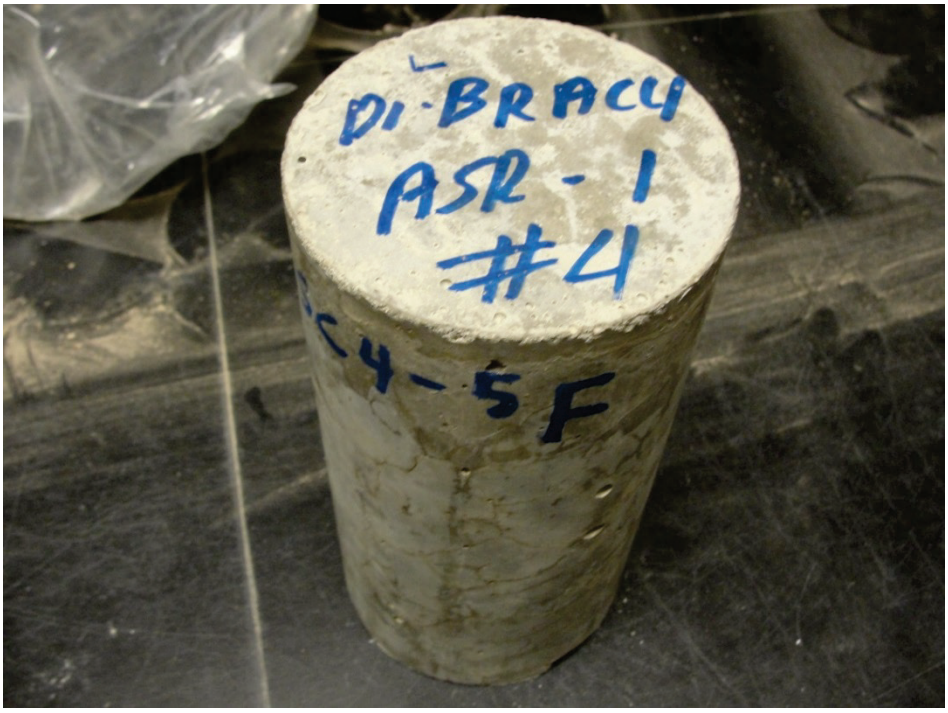

Fine cracking on side of cylinder LSC4 4W

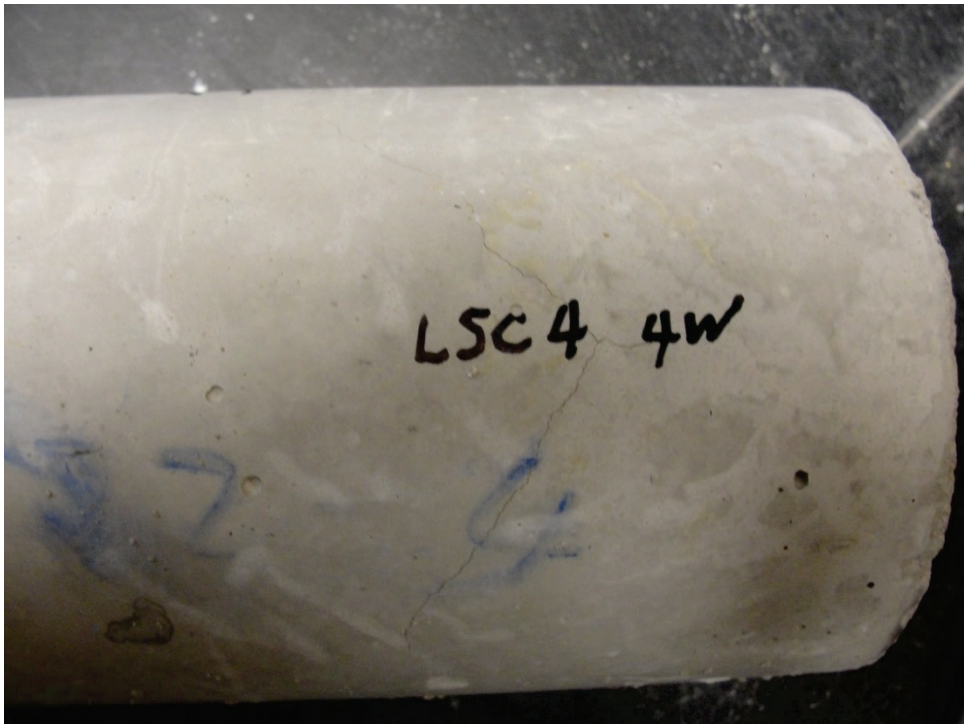

The following digital images and SEM/EDS/Dot Maps illustrate features associated with ASR and potential DEF:

Illustration of ASR Gel filled cracks and associated micro cracking within paste

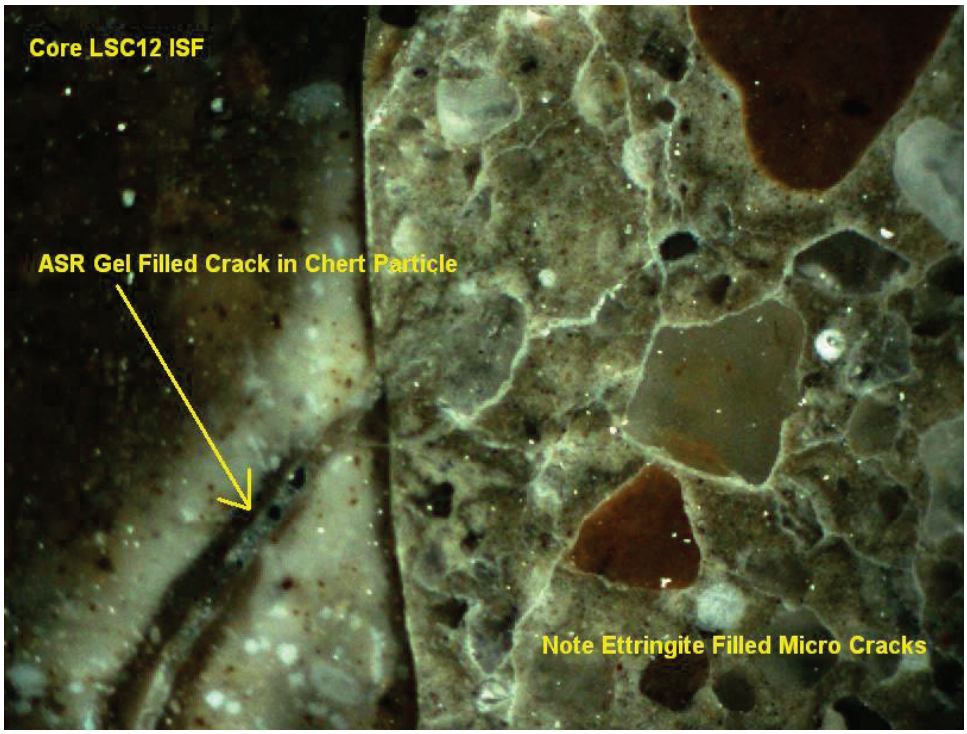

Image illustrated large gel filled crack and various aggregate distress

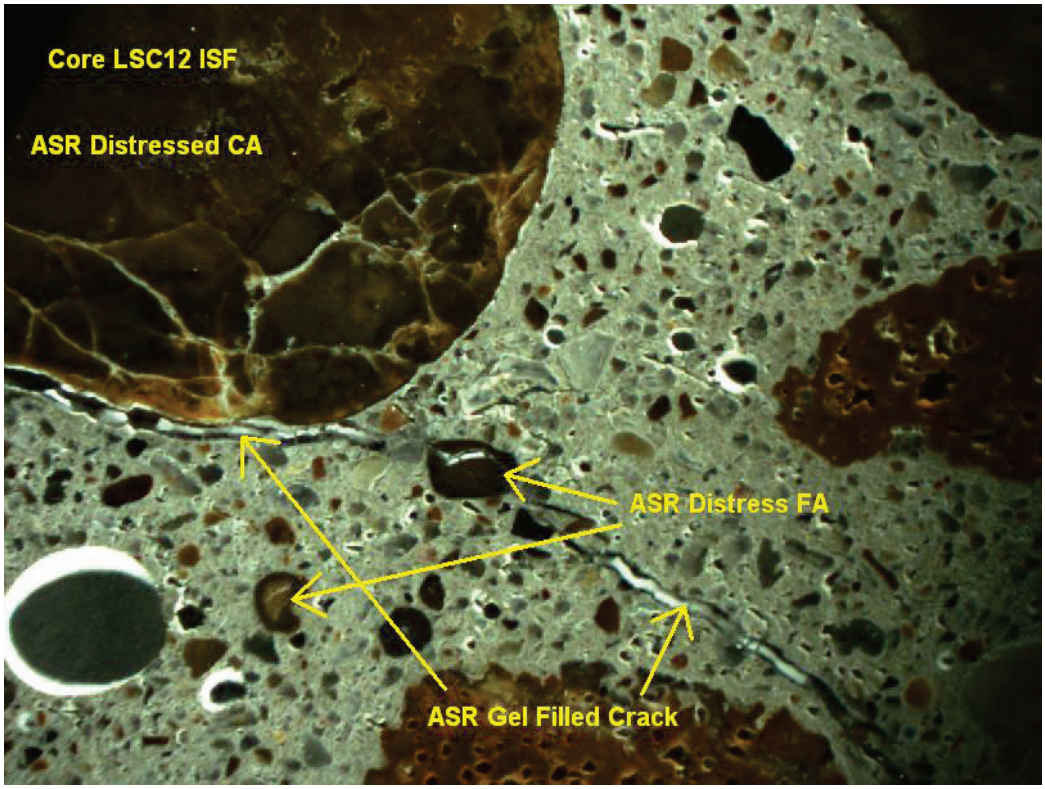

Image illustrating ASR distressed aggregates and gel formation

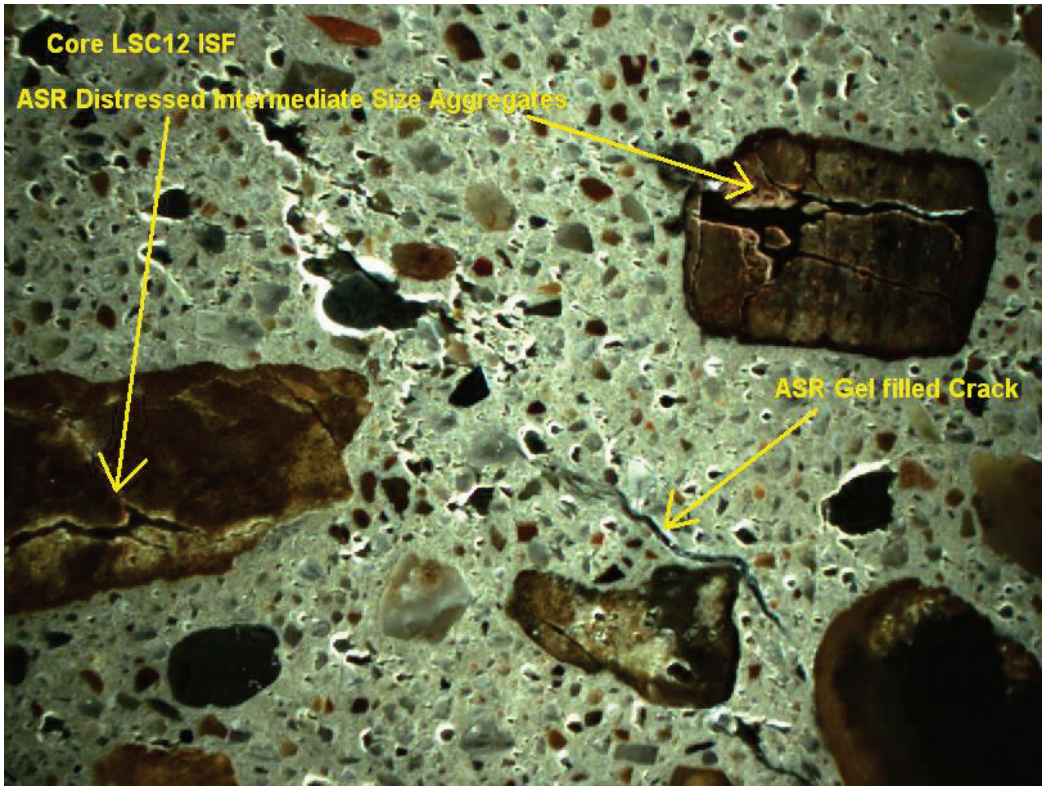

ASR gel formation and associated distress cracking within paste

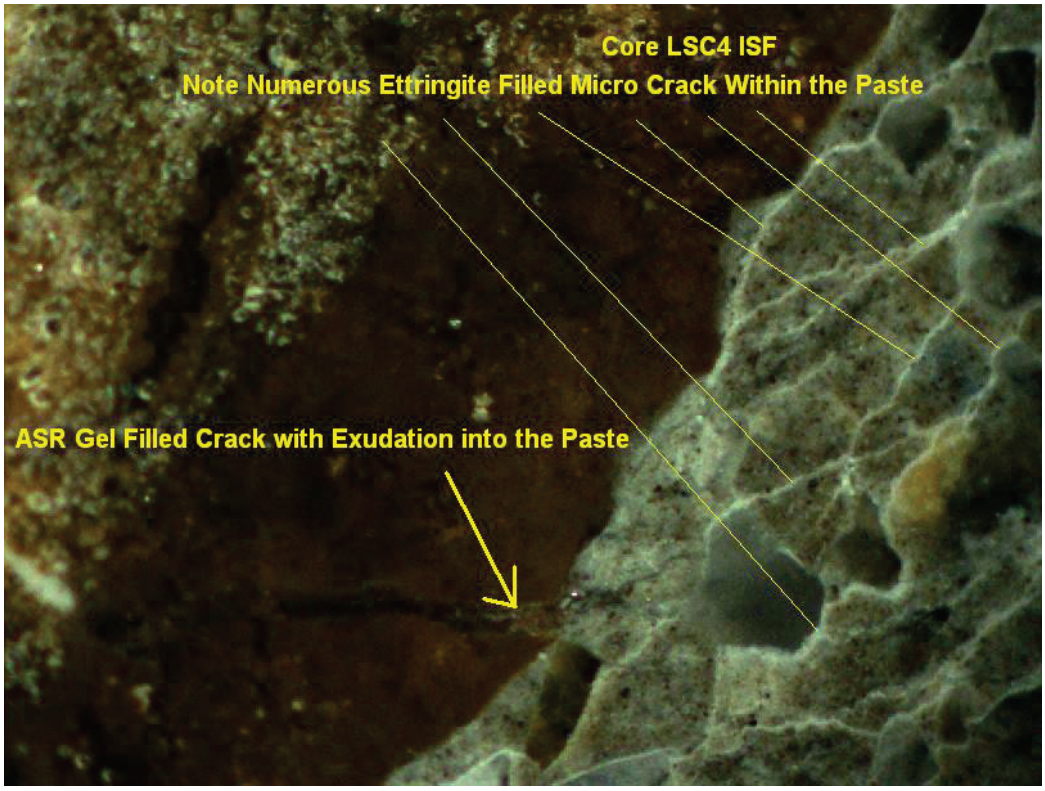

ASR distressed aggregate and gel formation

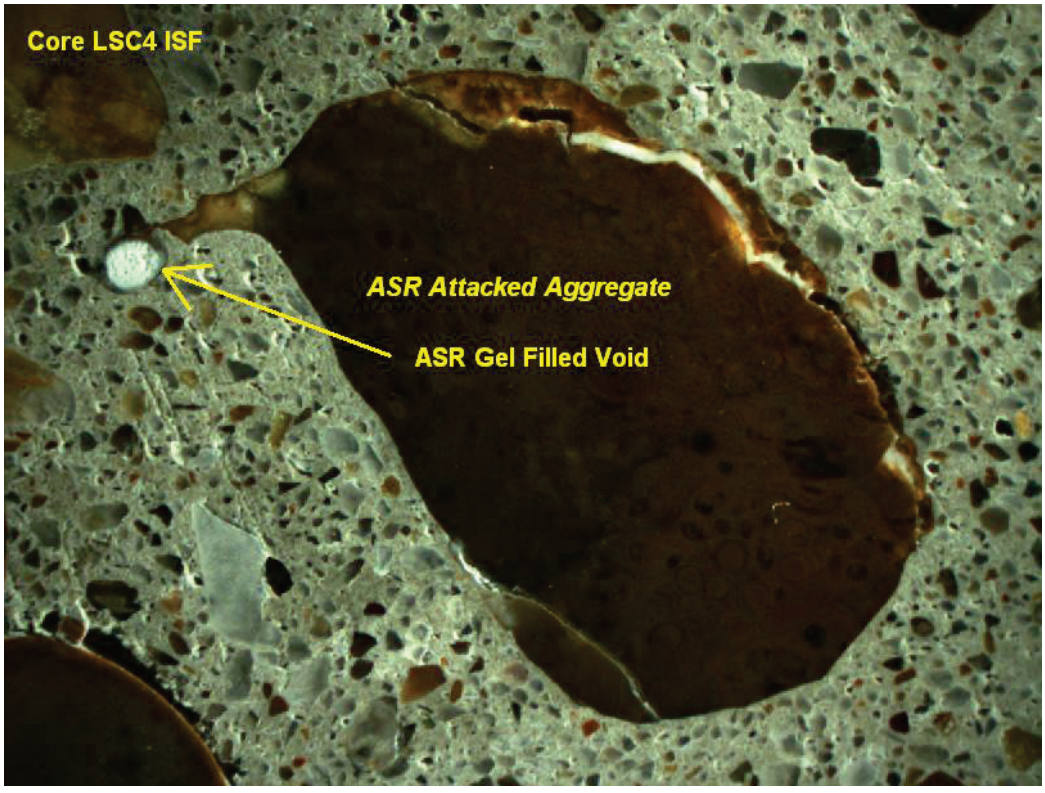

Illustration of ASR activity

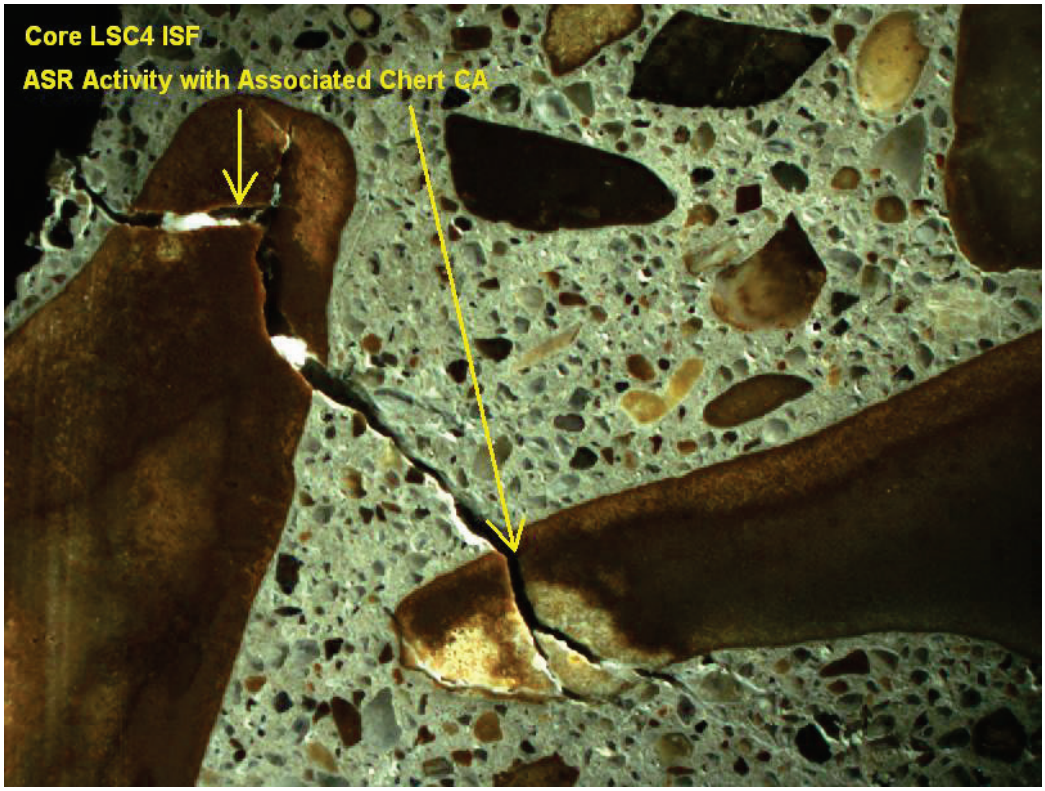

ASR distressed aggregate

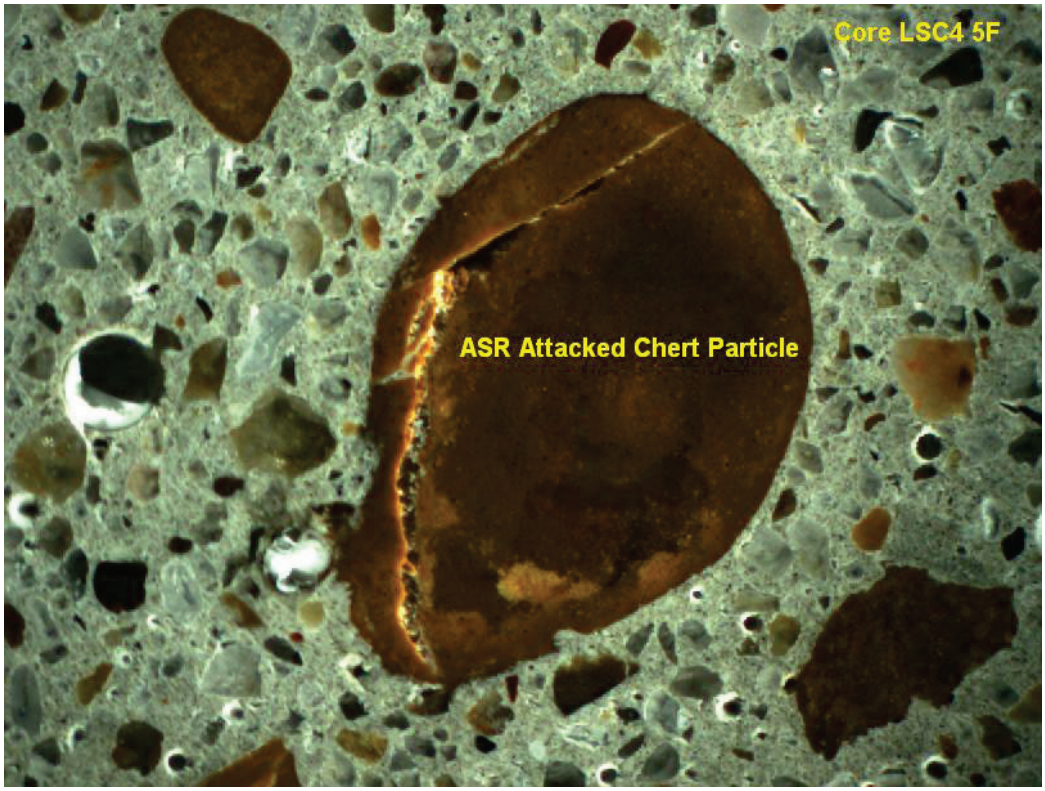

ASR distress aggregate

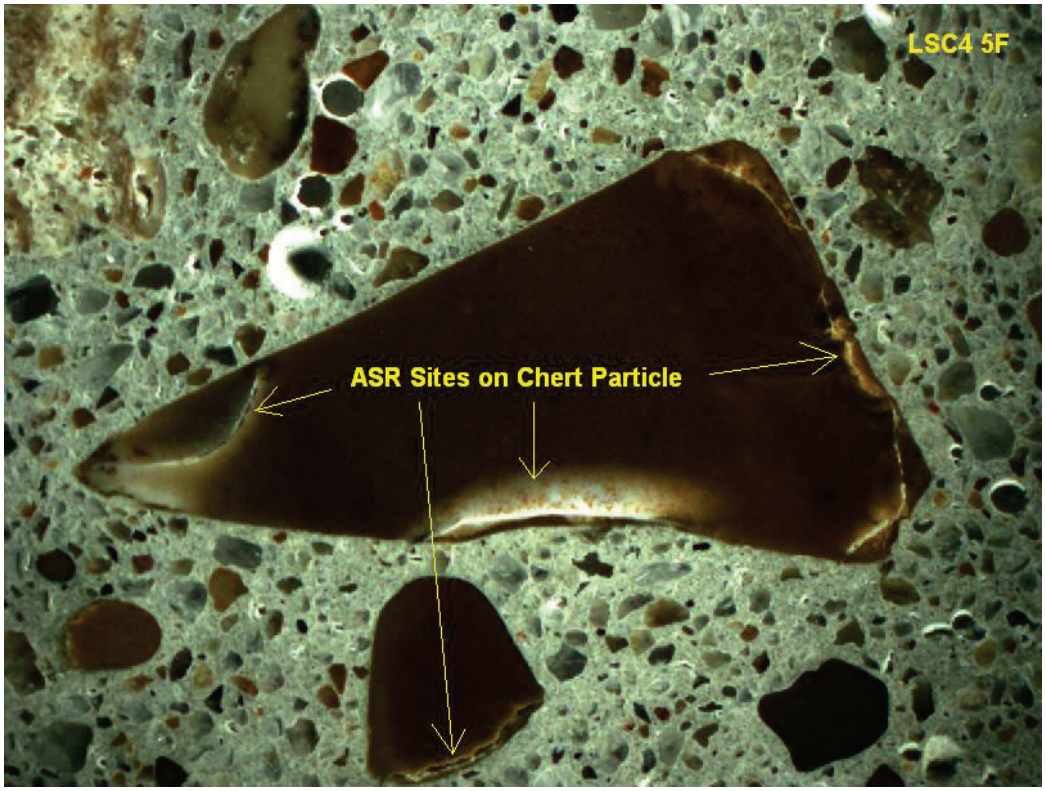

Image illustrating depth of carbonation in cylinder LSC4 5F (3.18 mm)

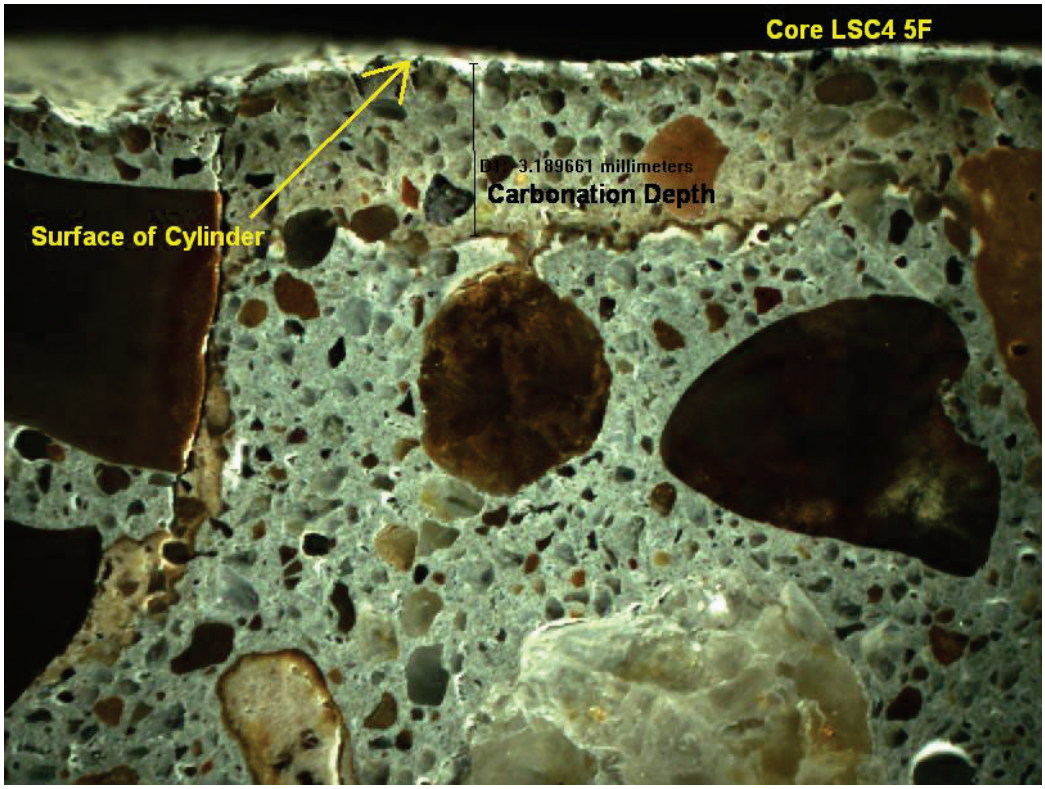

Image illustrating carbonation depth on side of cylinder (1.84 mm)

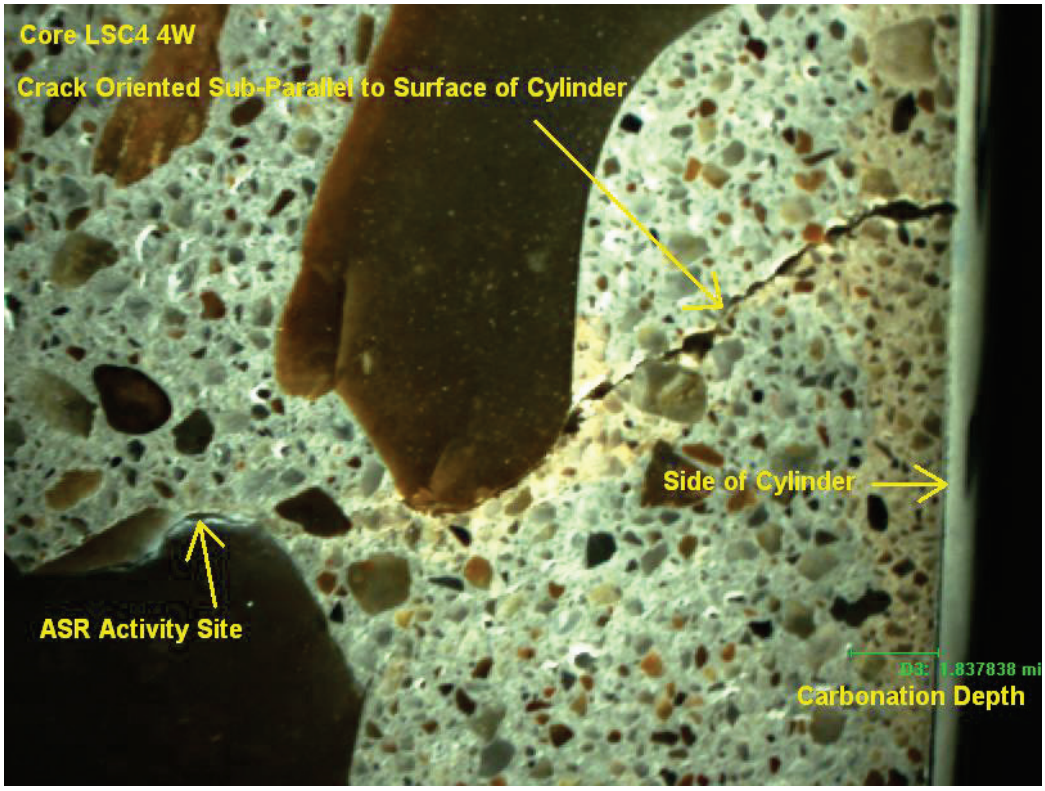

Mild ASR distressed aggregate

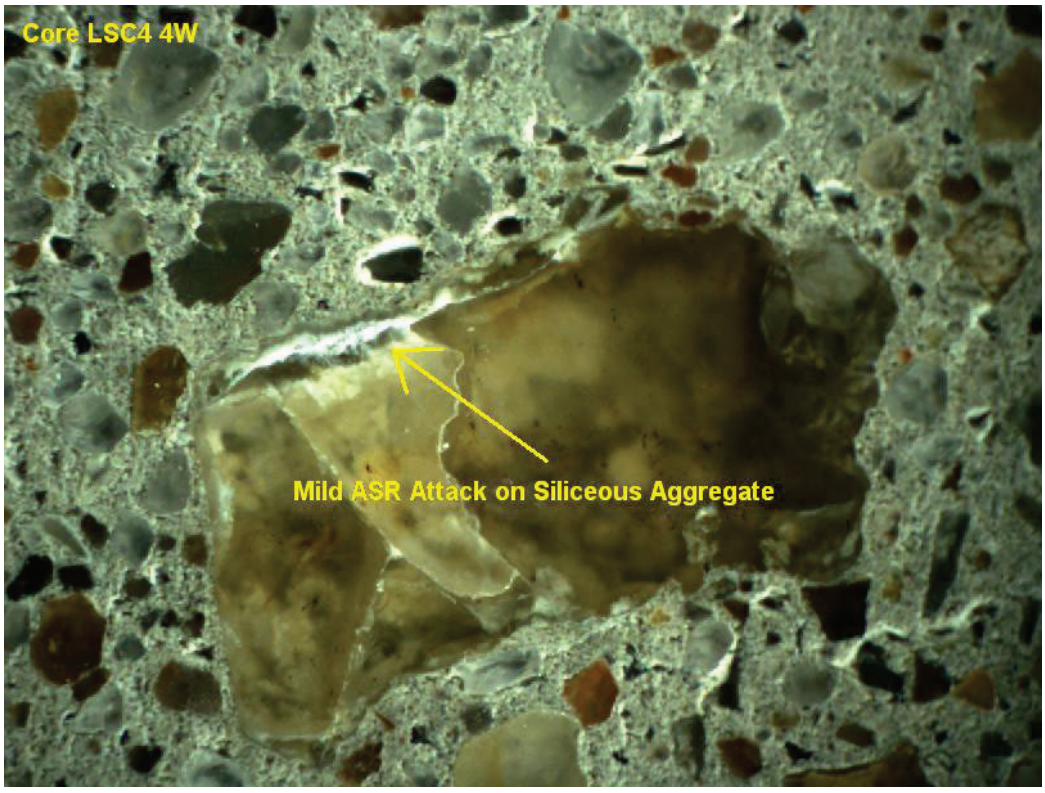

Optical image illustrating ASR activity

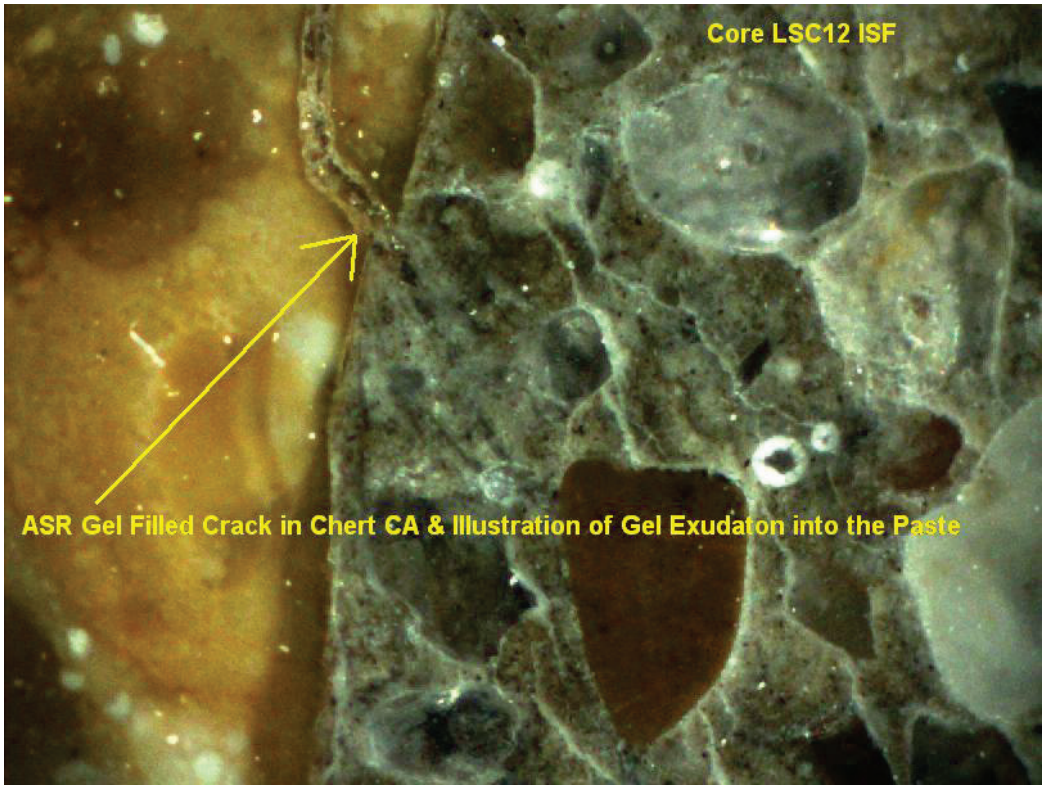

BSE image of previous optical image illustrating ASR distress

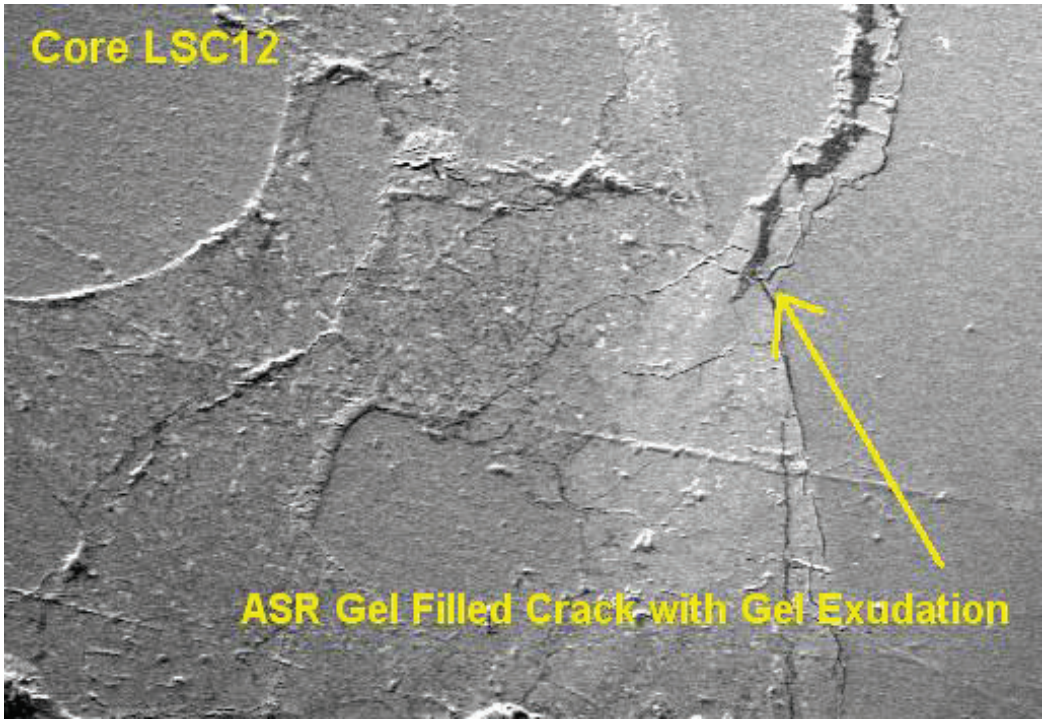

Calcium DOT map showing calcareous rich paste

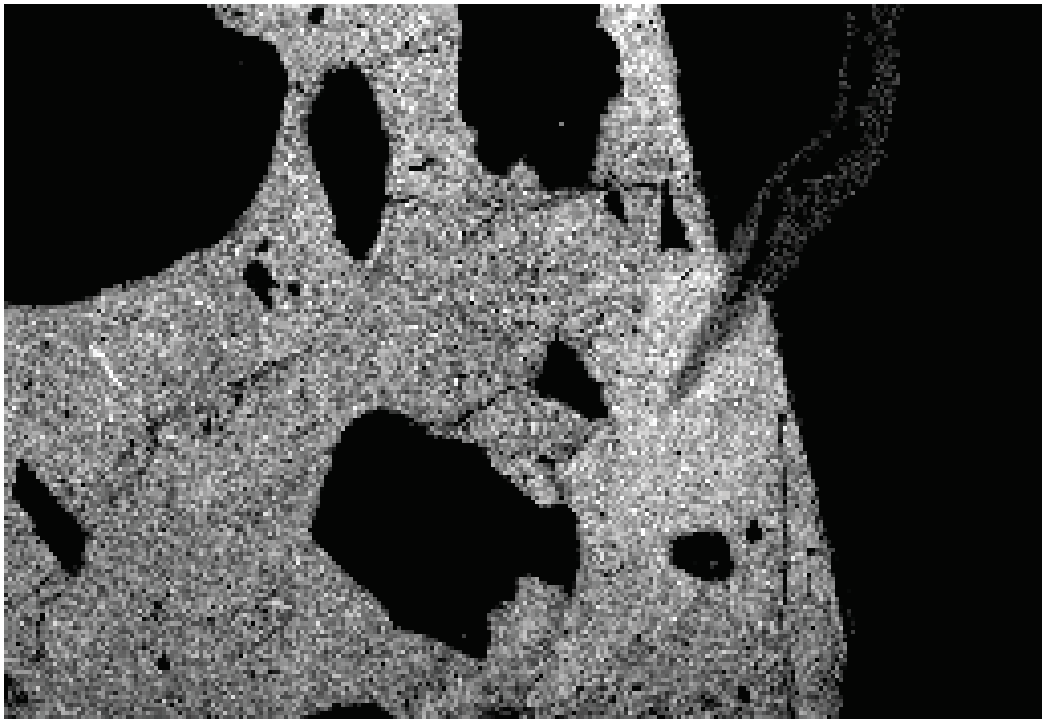

Potassium dot map illustrating K-rich ASR gel

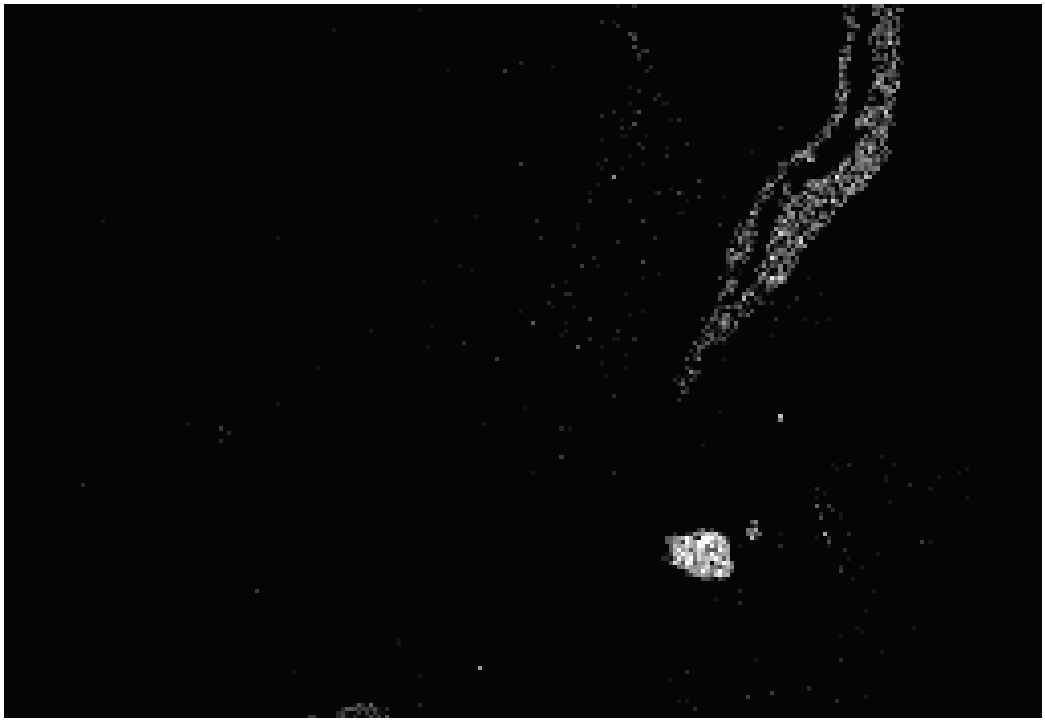

Silica dot map illustrating siliceous aggregates and silica rich gel

Sulfur dot map illustrating ettringite filled micro cracks associated with distress

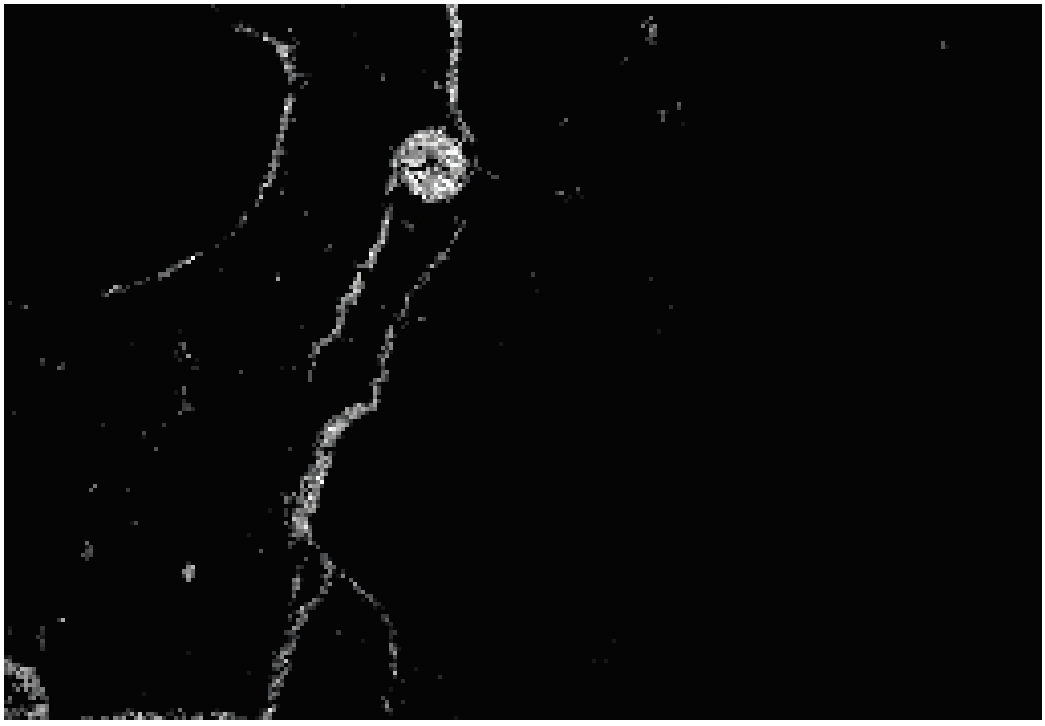

BSE image illustrating ettringite nest in the paste of core LSC12 ISF

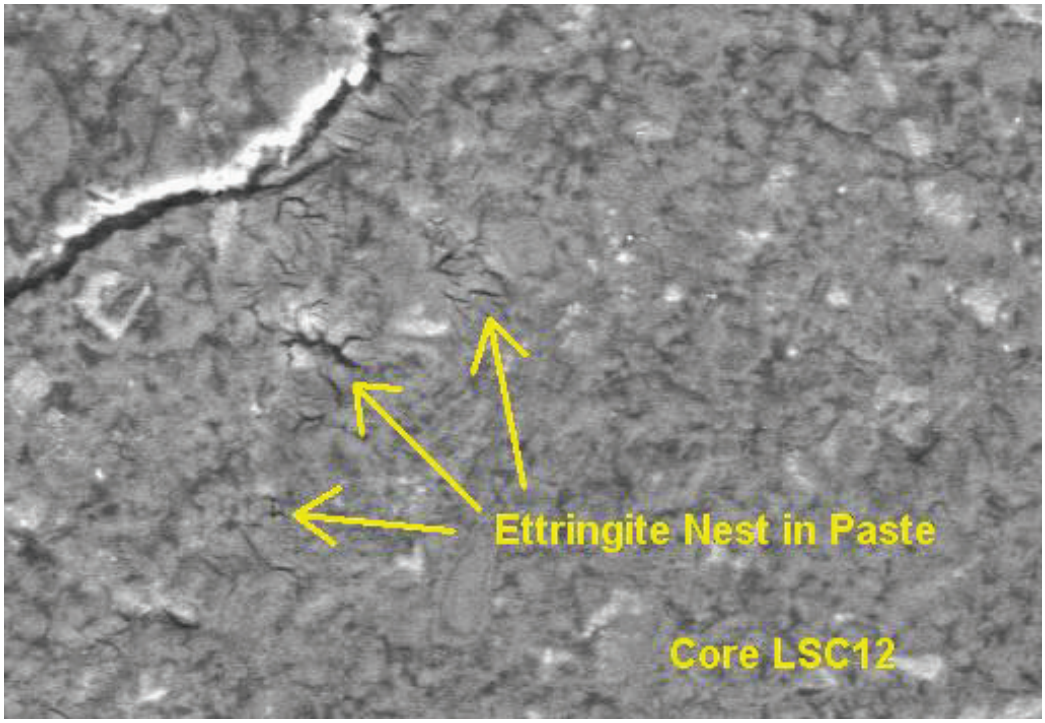

BSE image of ettringite formation/location

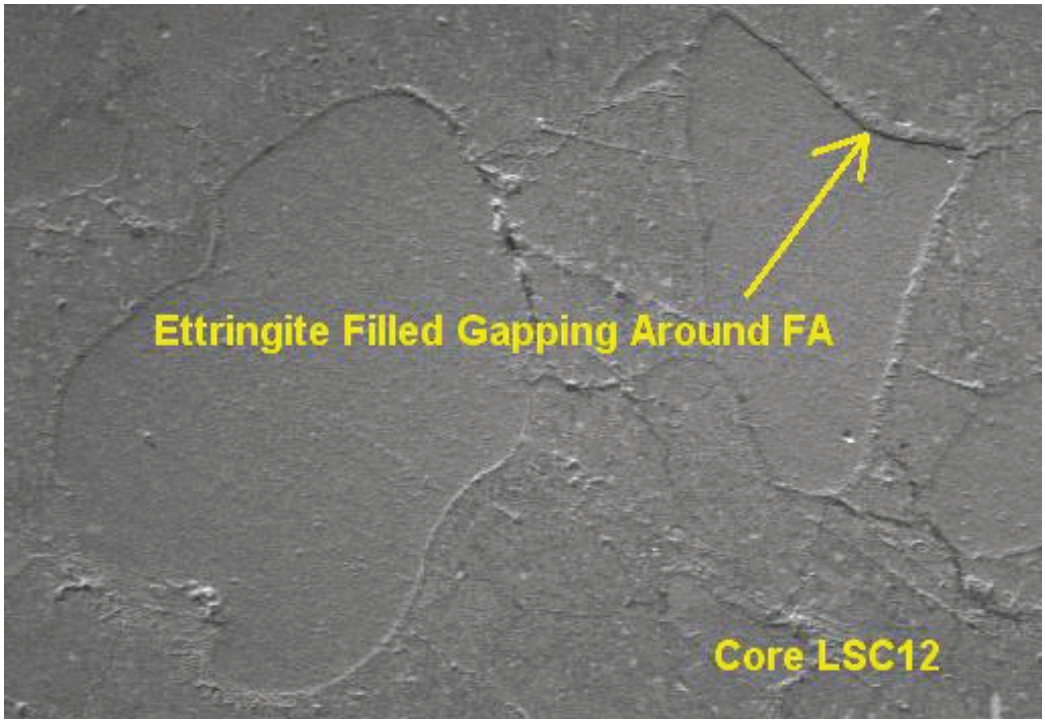

Sulfur dot map

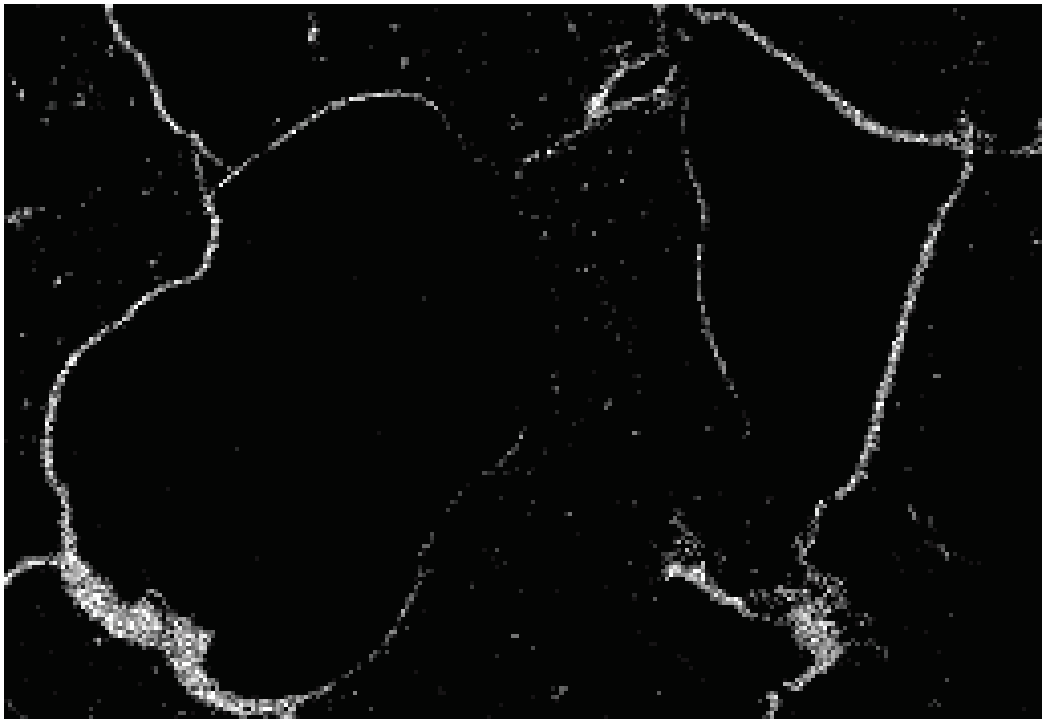

Calcium dot map

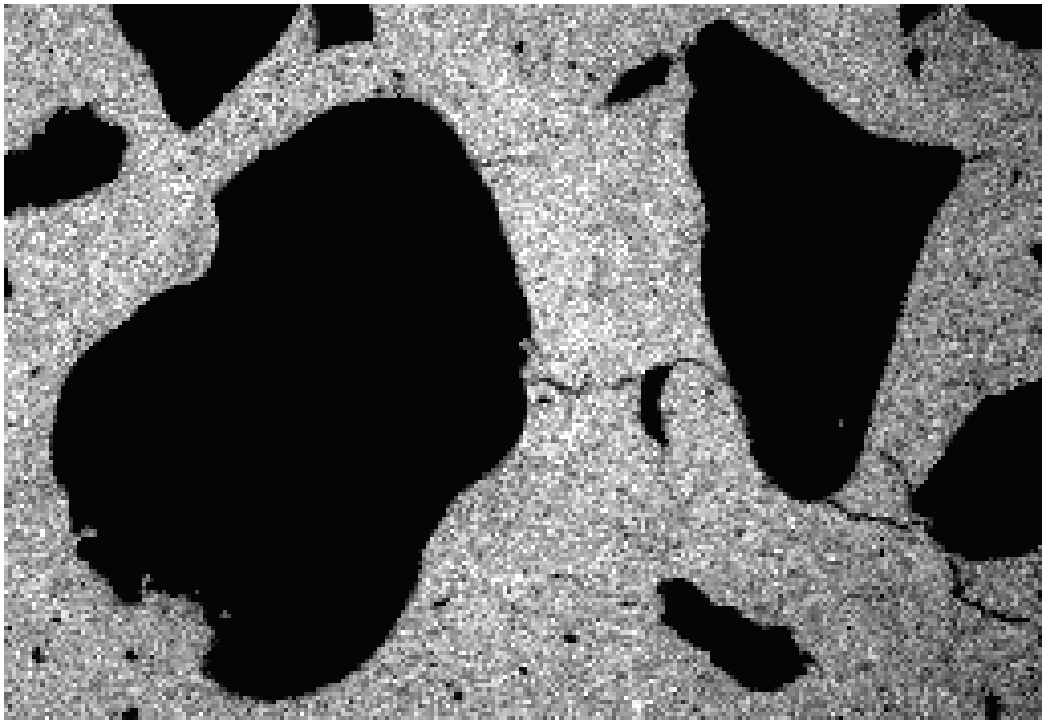

BSE image illustrating the width of the ettringite filled gap

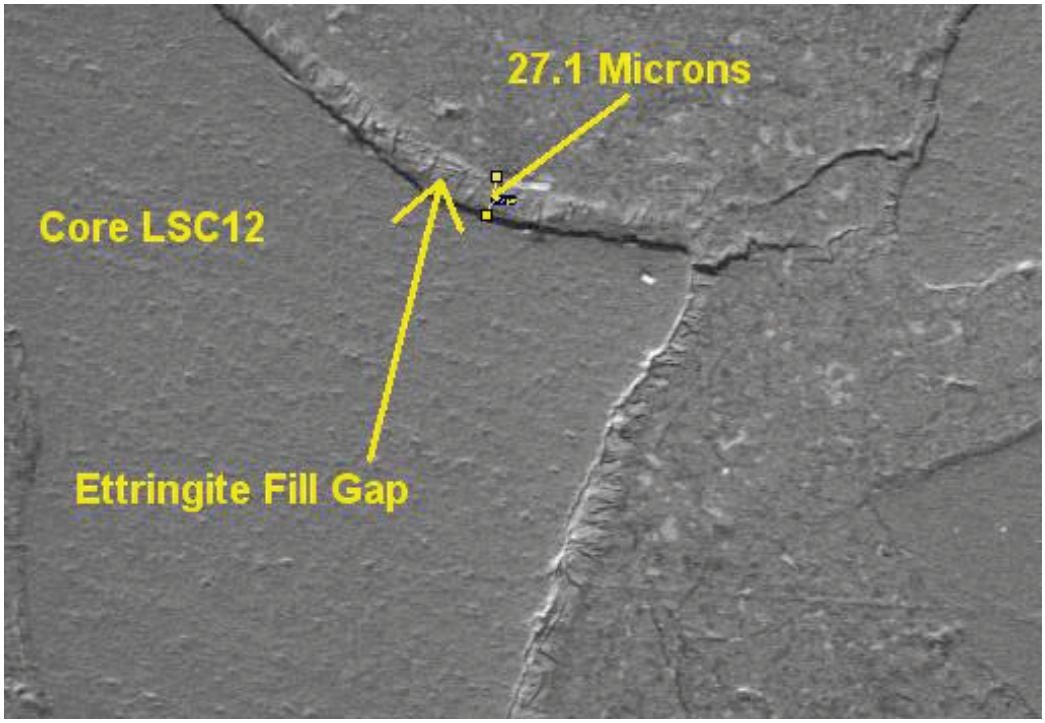

BSE image illustrating ASR reaction rim on coarse siliceous aggregate

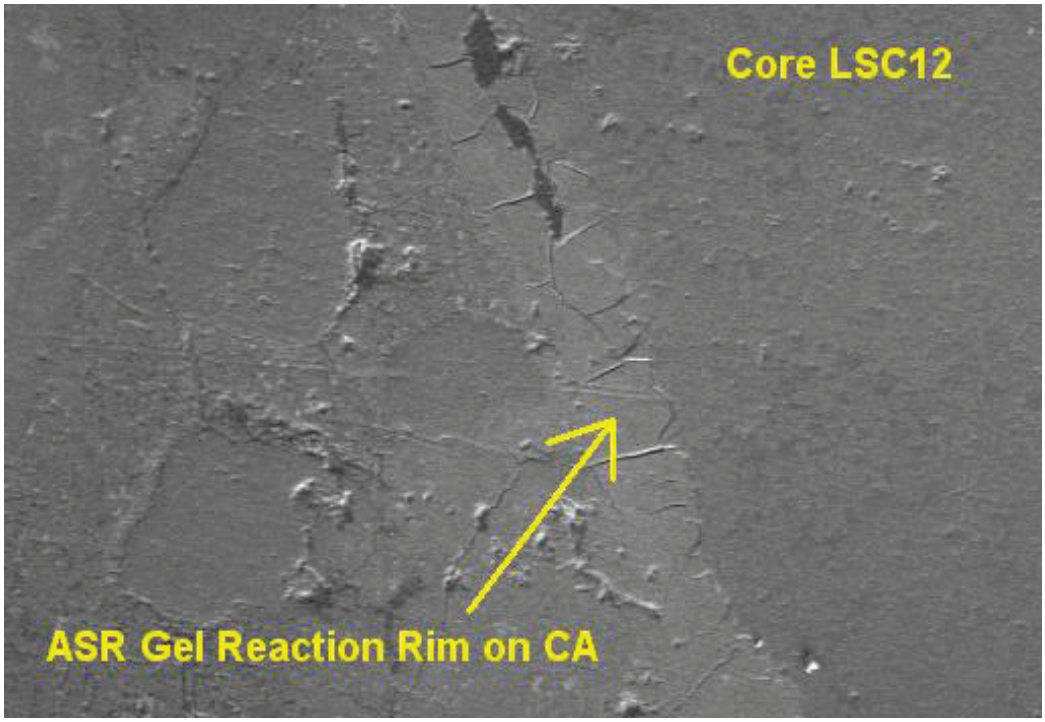

Calcium dot map

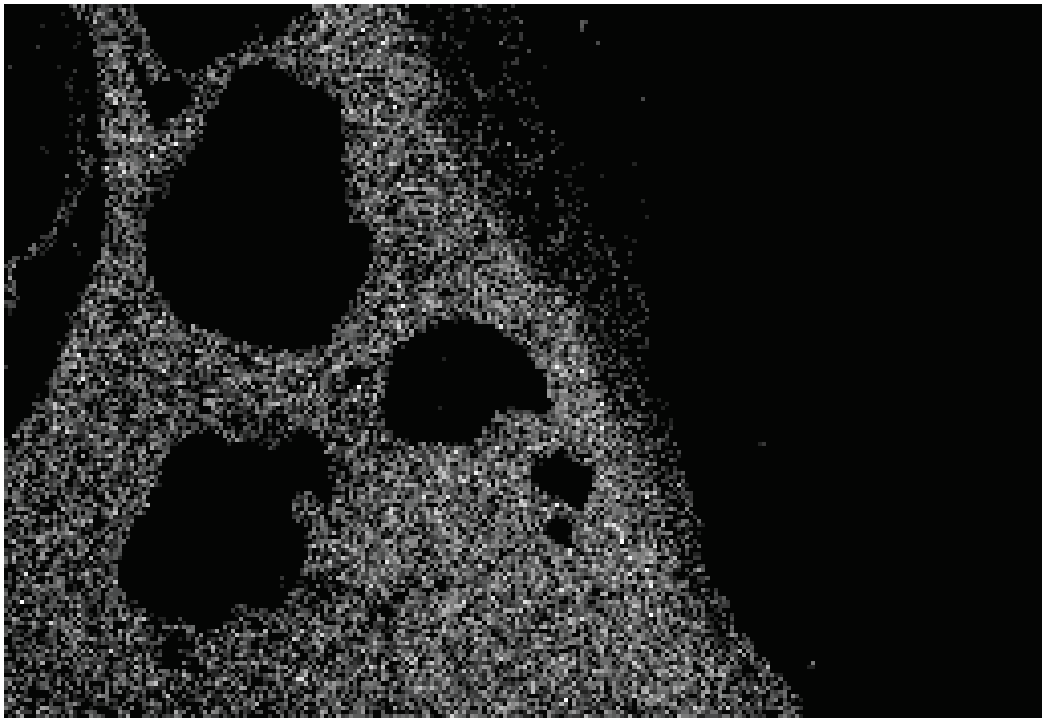

Potassium dot map

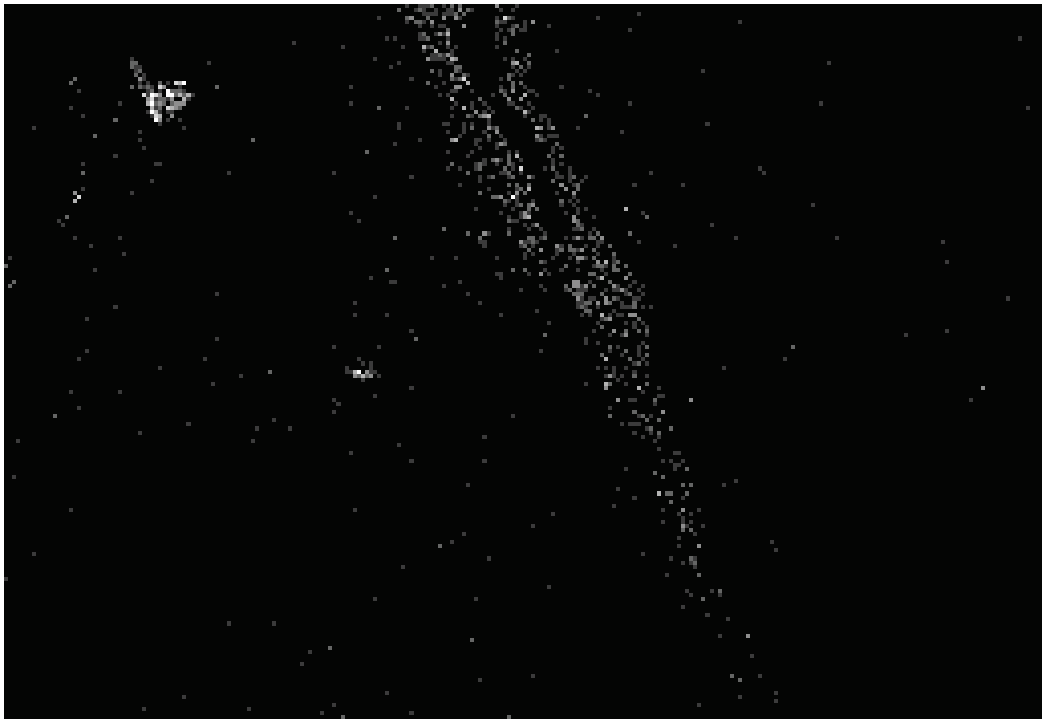

Optical image illustrating ASR gel accumulation in air void

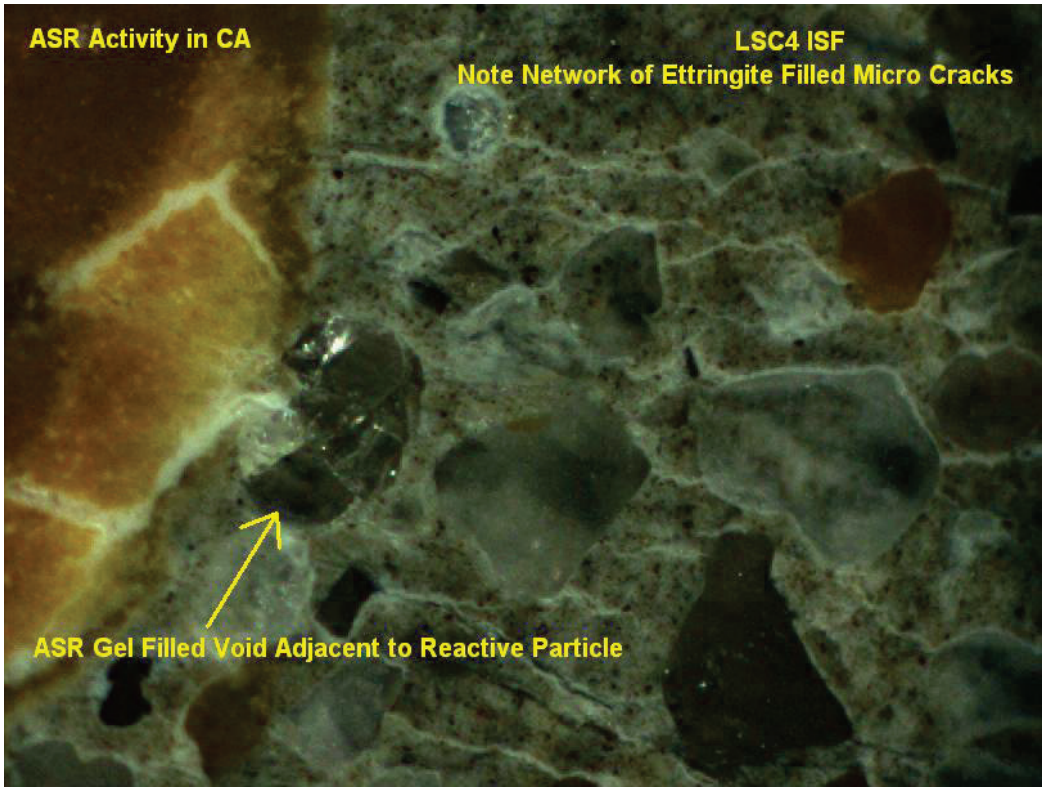

BSE image of previous optical image

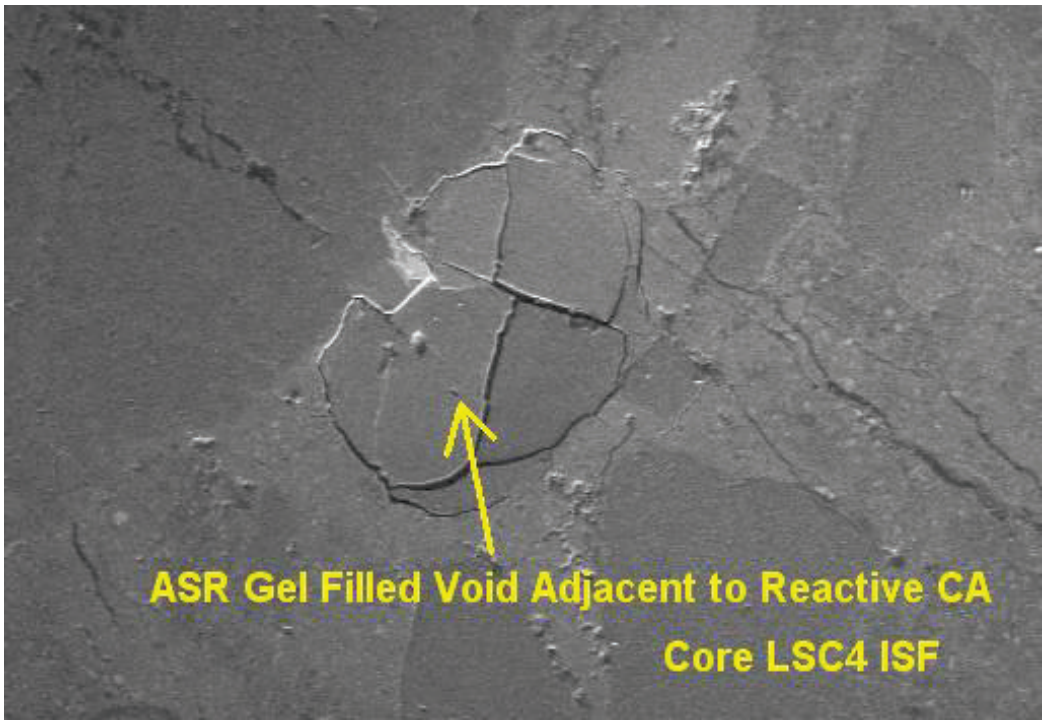

Silica dot map illustrating silica rich phases

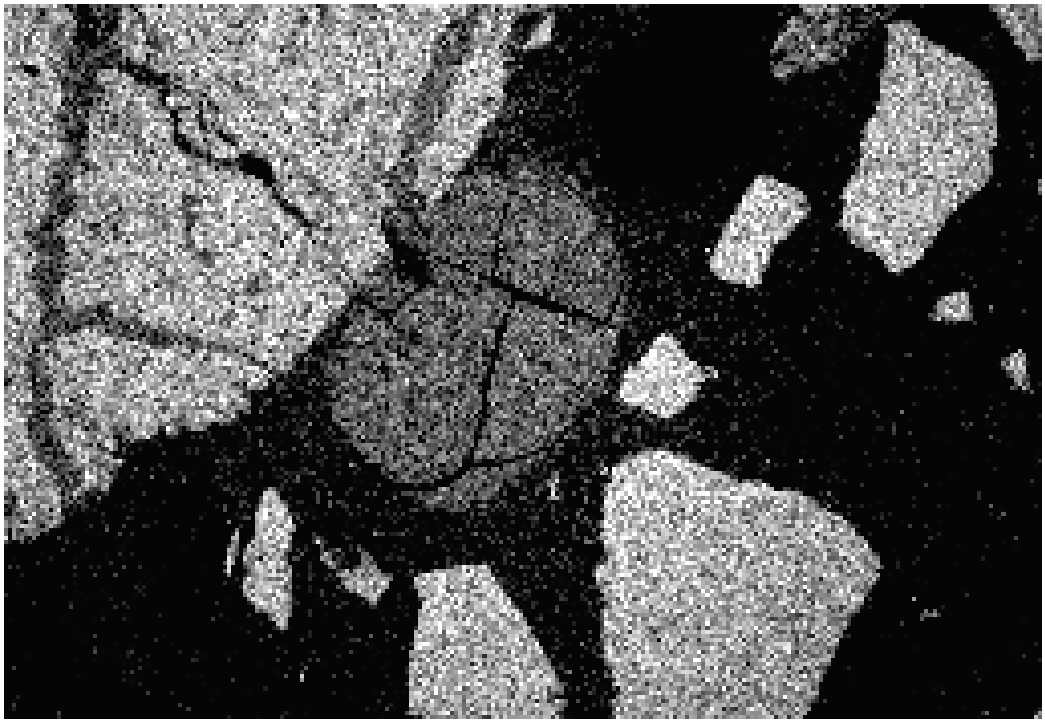

Potassium dot map illustrating K-rich gel

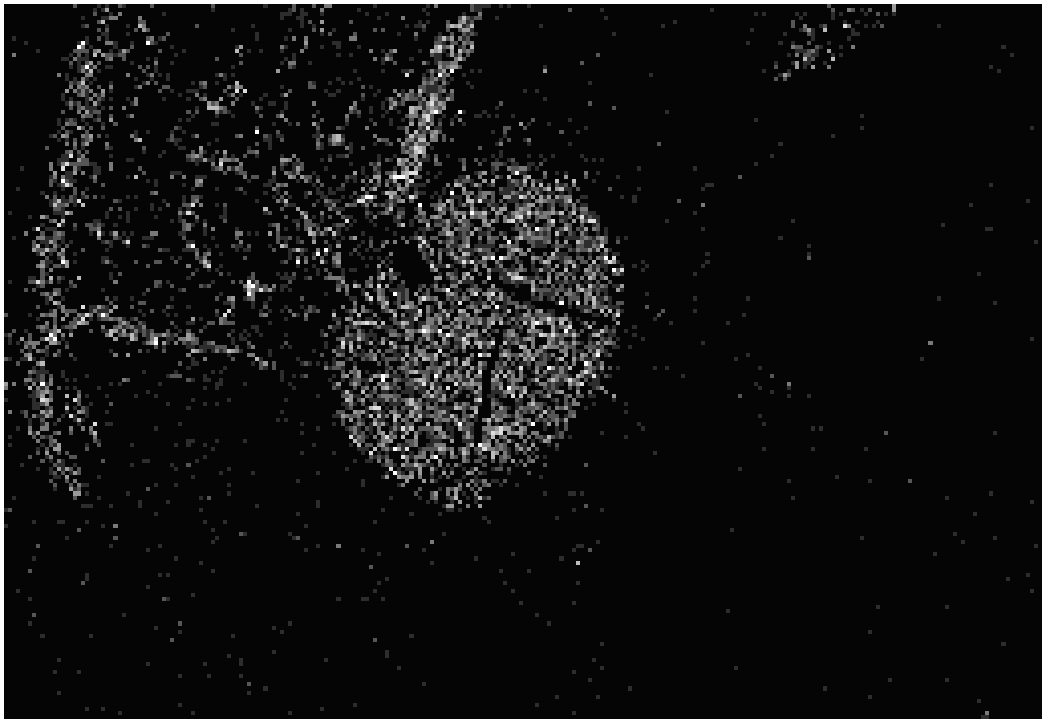

Ettringite filled network of fine micro cracks associated with ASR activity

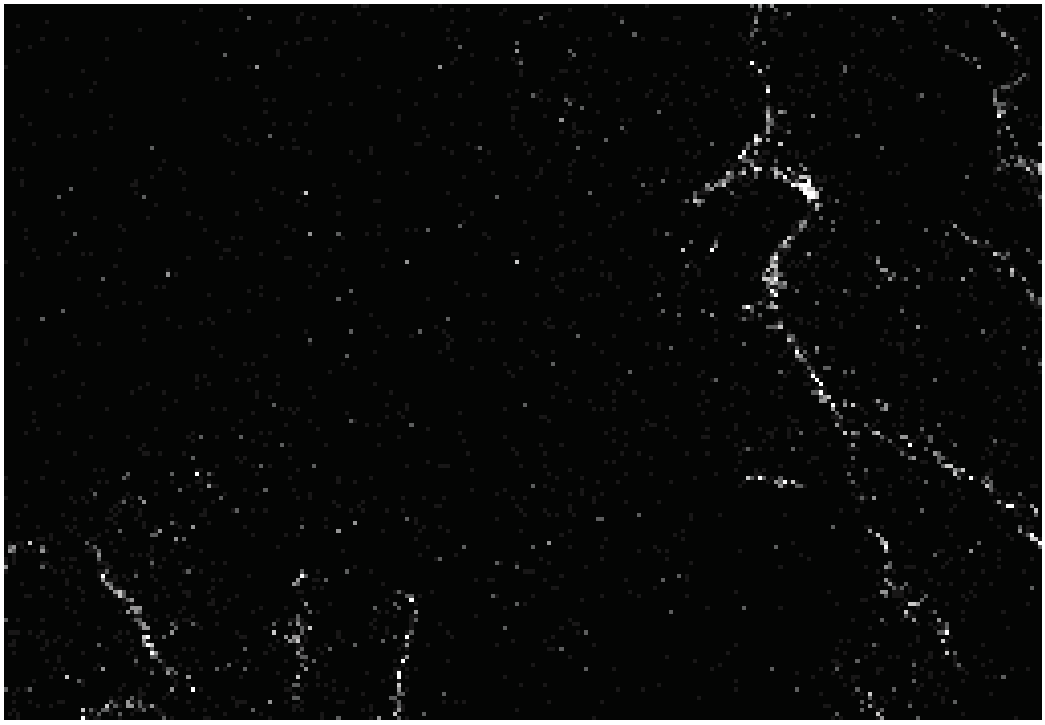

Optical image illustrating ettringite filled micro cracking

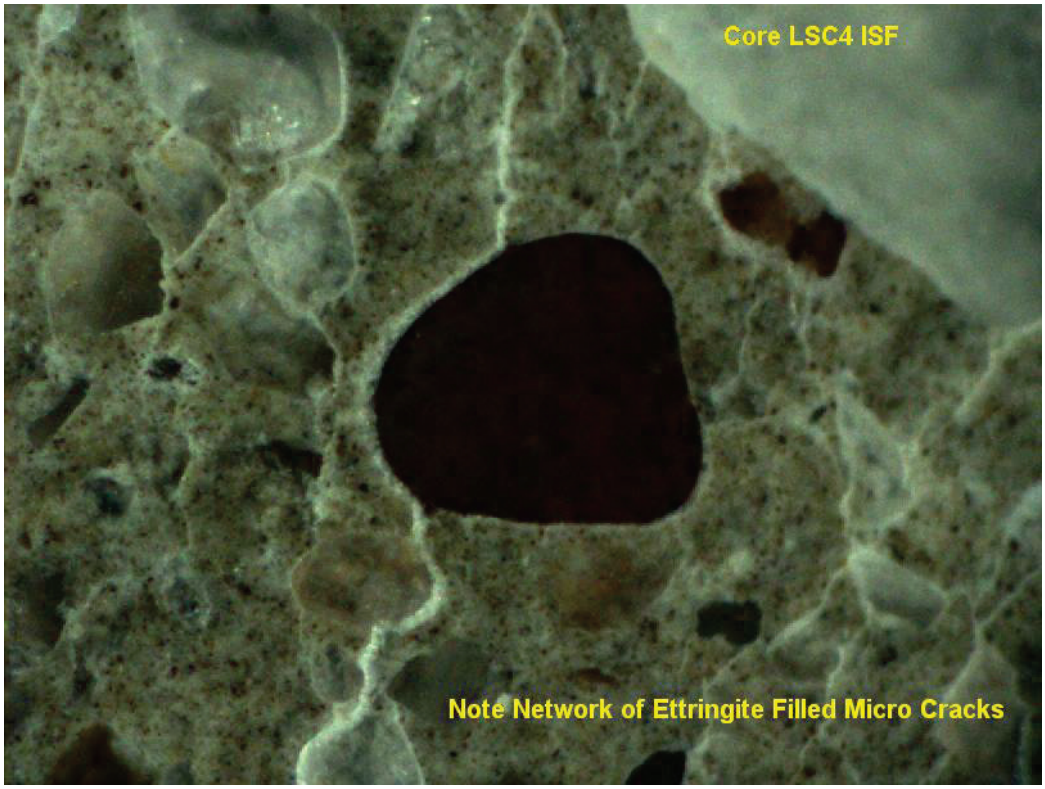

BSE image illustrating ettringite fill gap shown in previous optical image

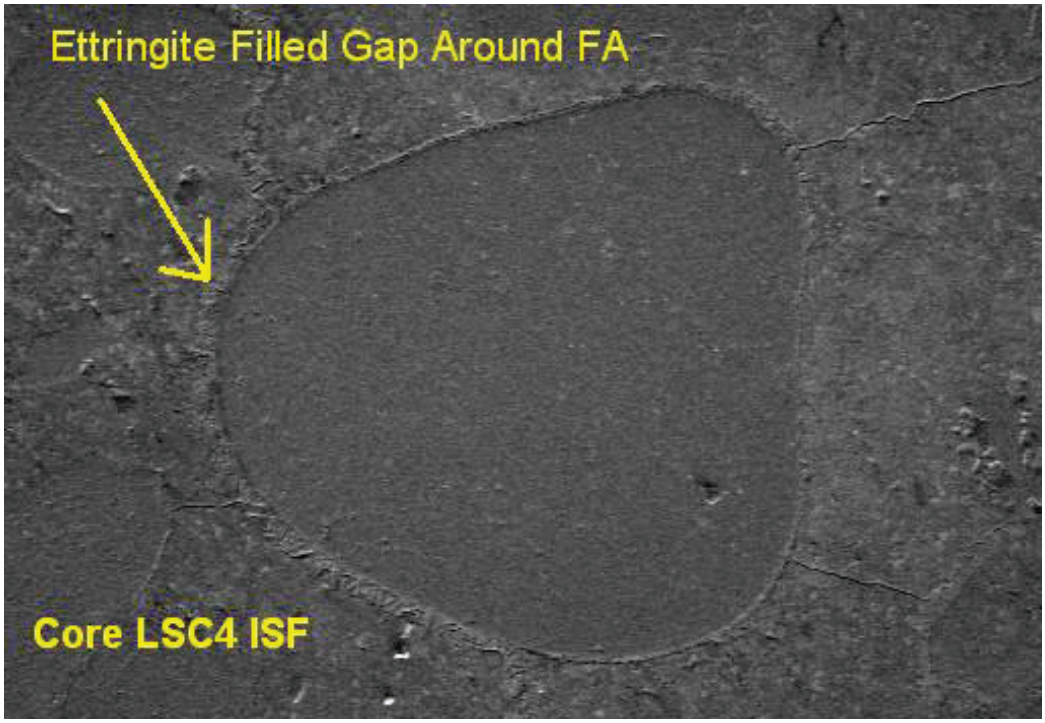

Calcium dot map

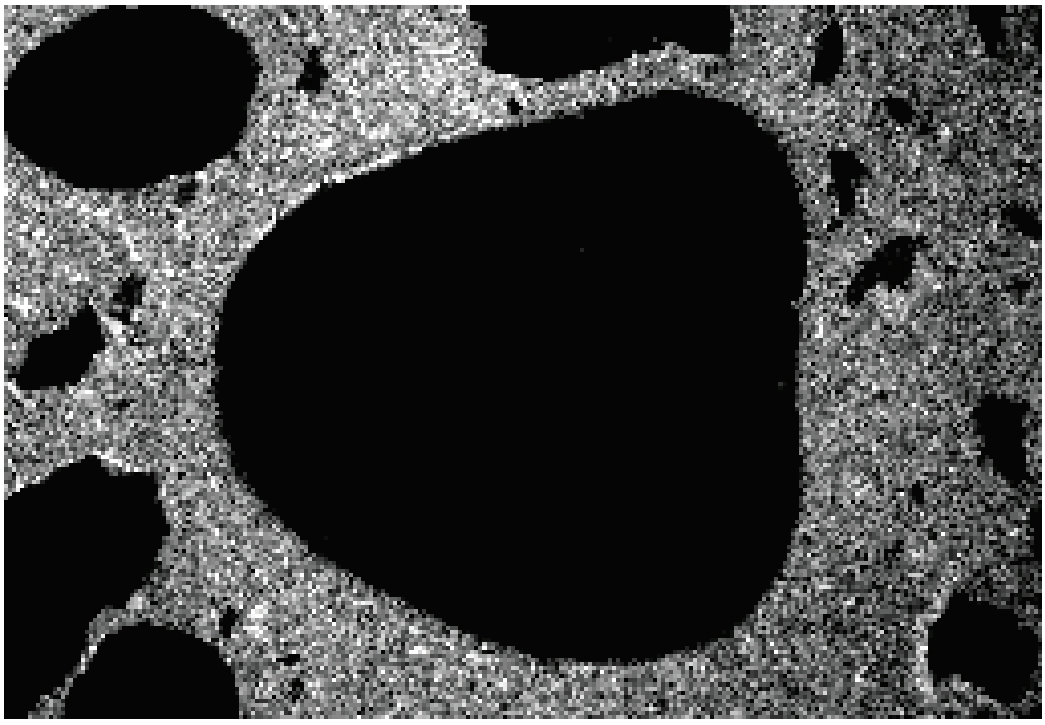

Sulfur dot map illustrating ettringite filled gap

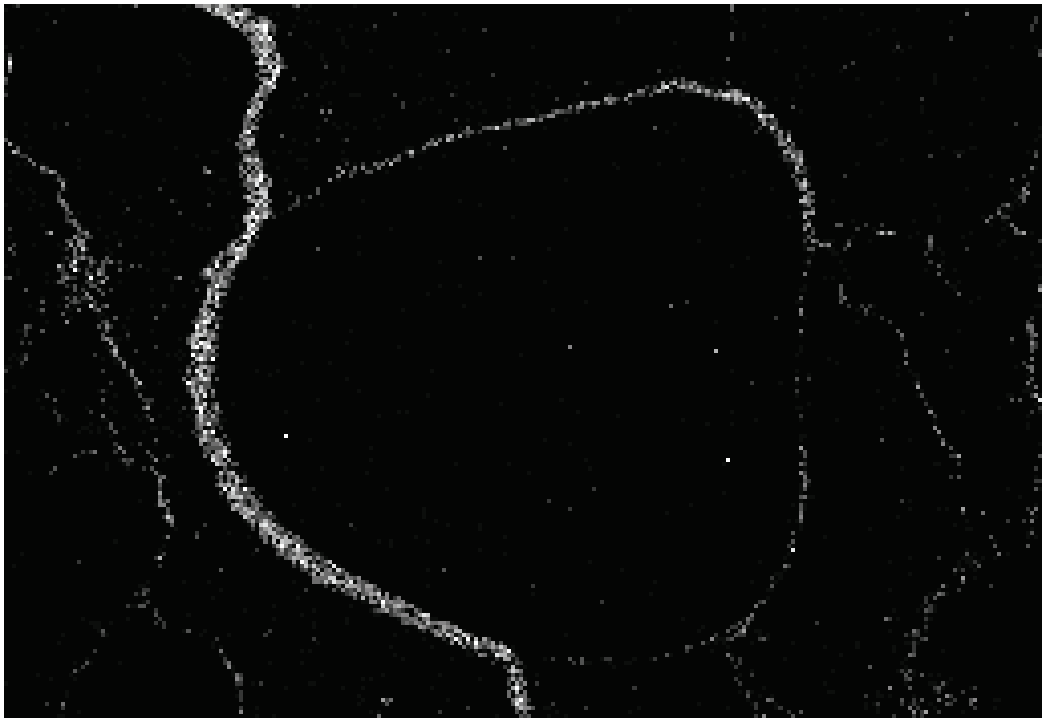

Silica dot map

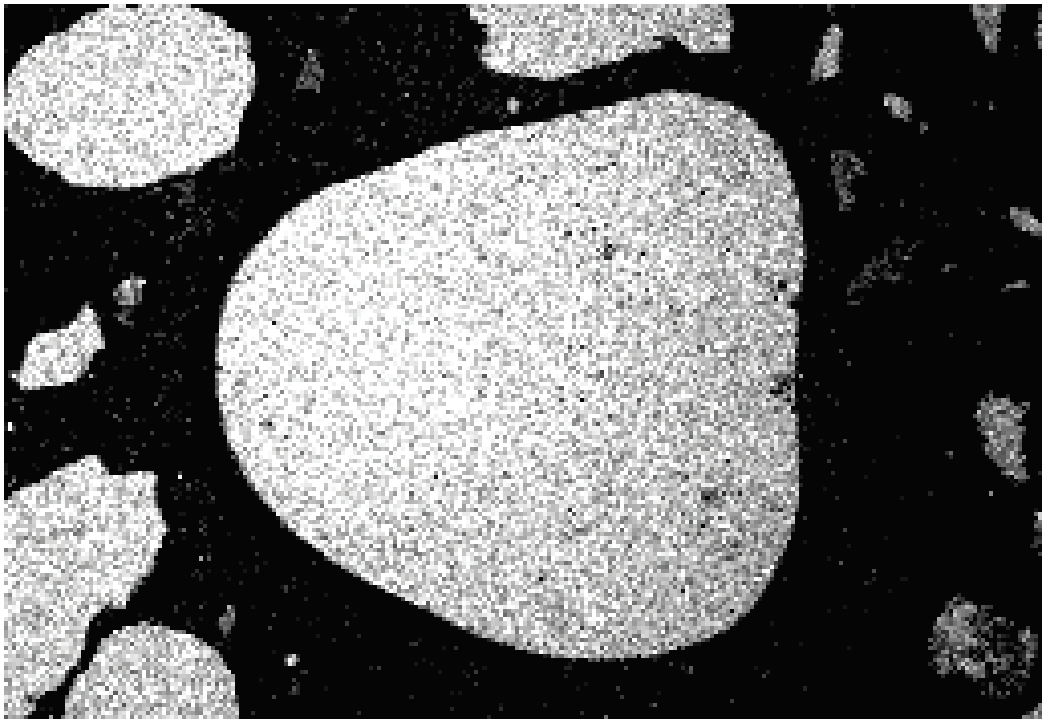

BSE image illustrating ASR activity

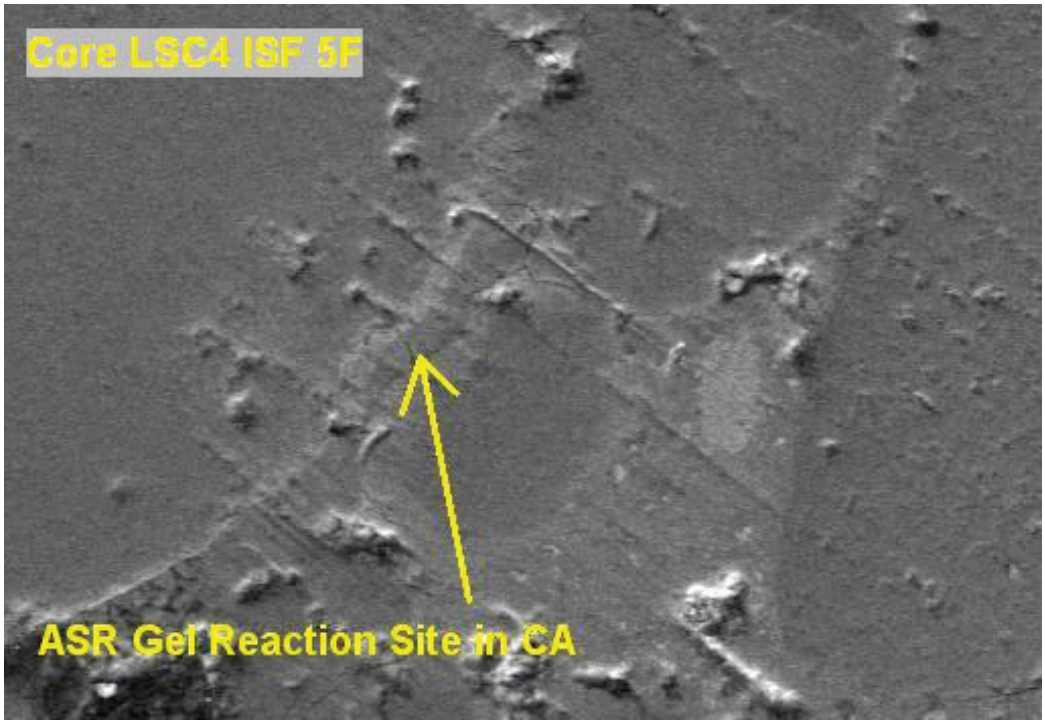

Silica dot map

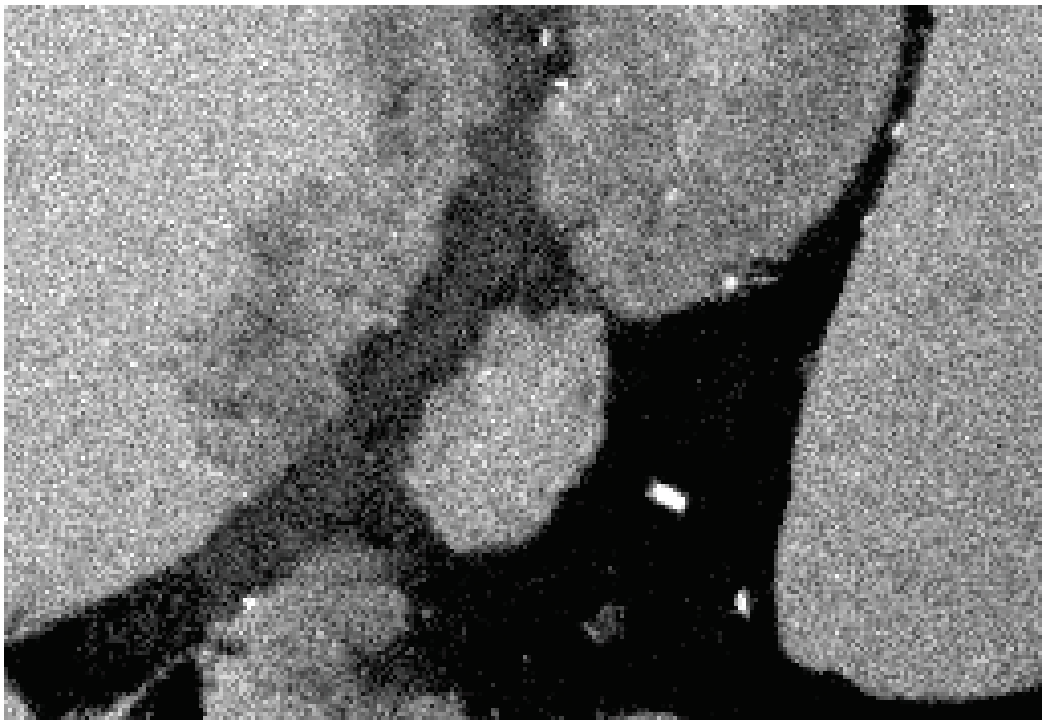

Potassium dot map illustrating k-rich ASR gel

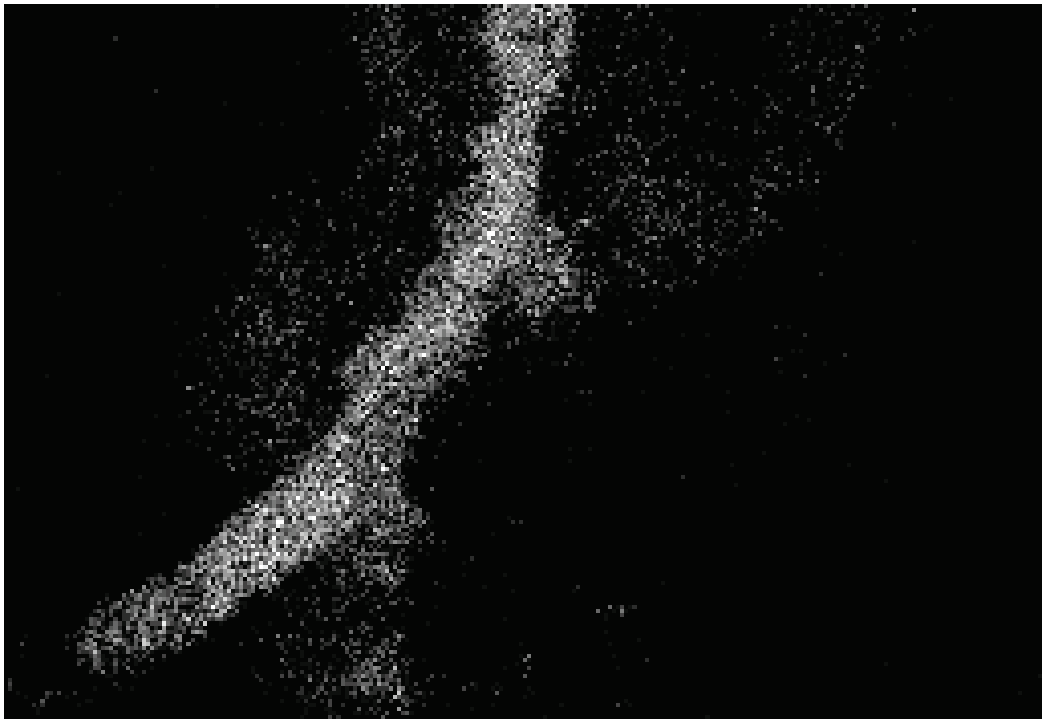

BSE image illustrating ettringite formation at paste/aggregate interface

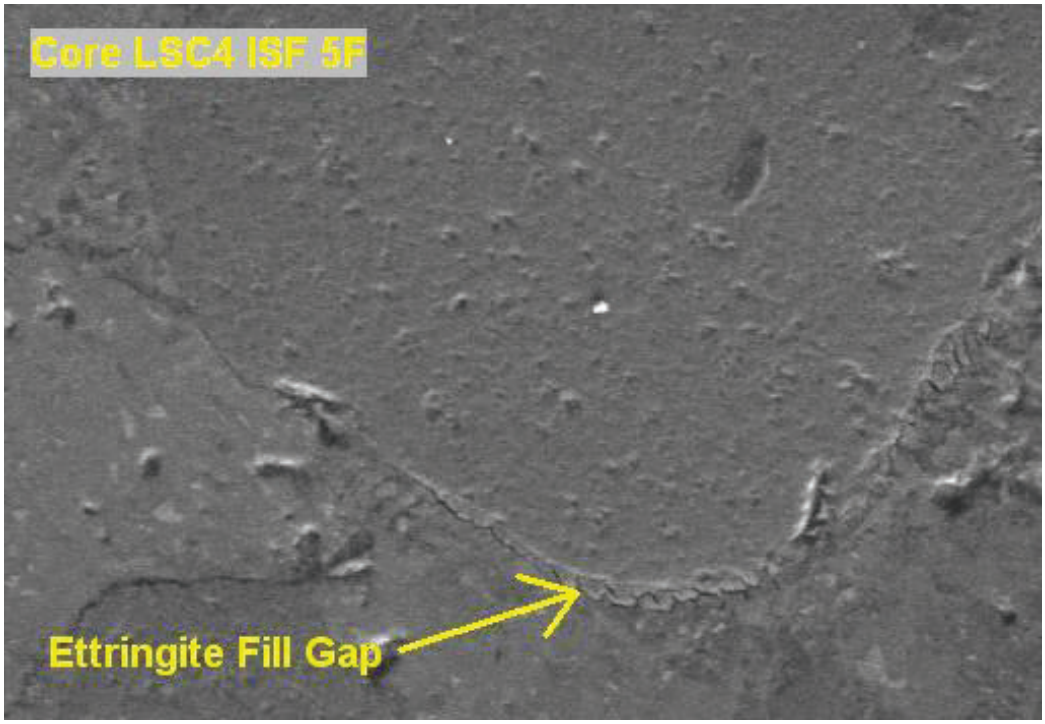

Sulfur dot map

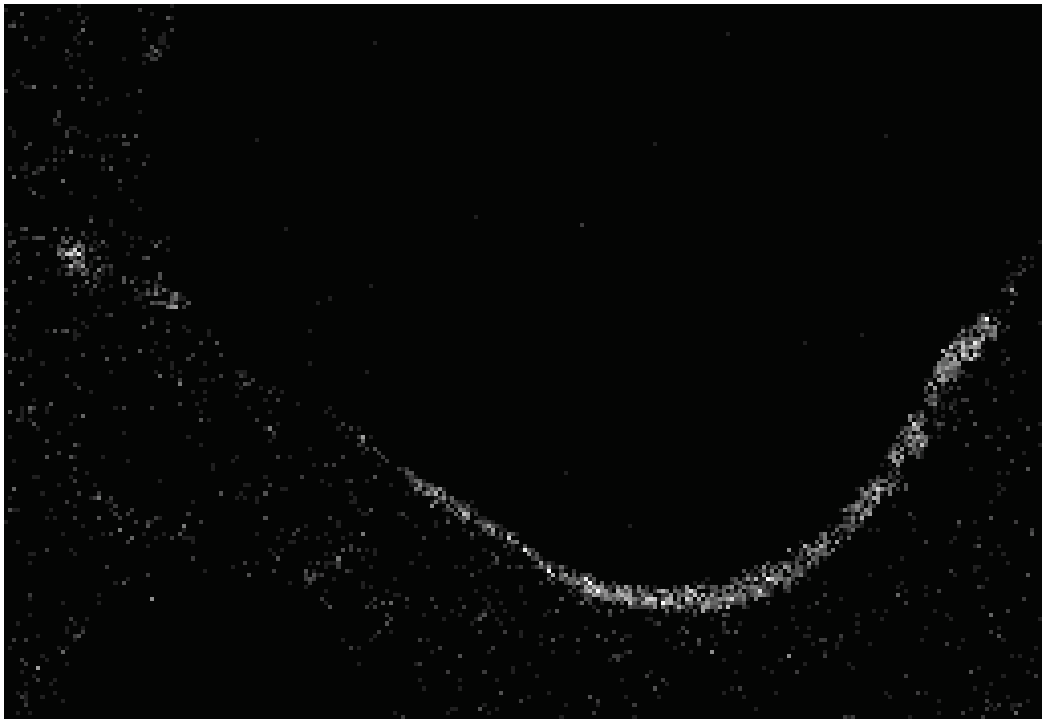

Silica dot map

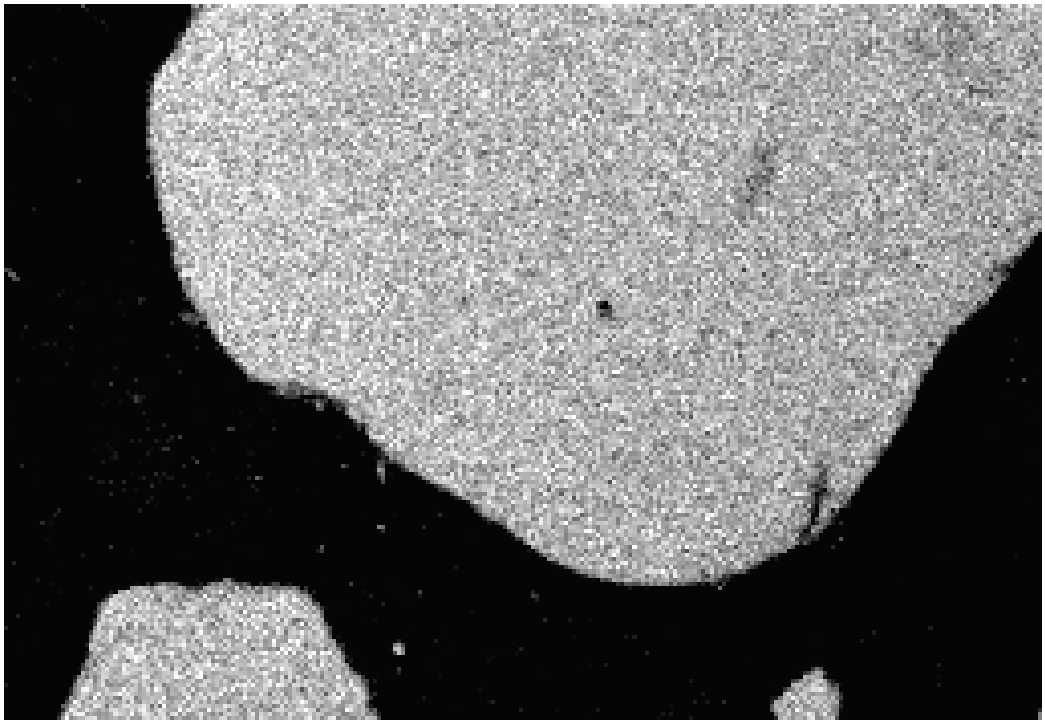

BSE image illustrating ettringite formation and location

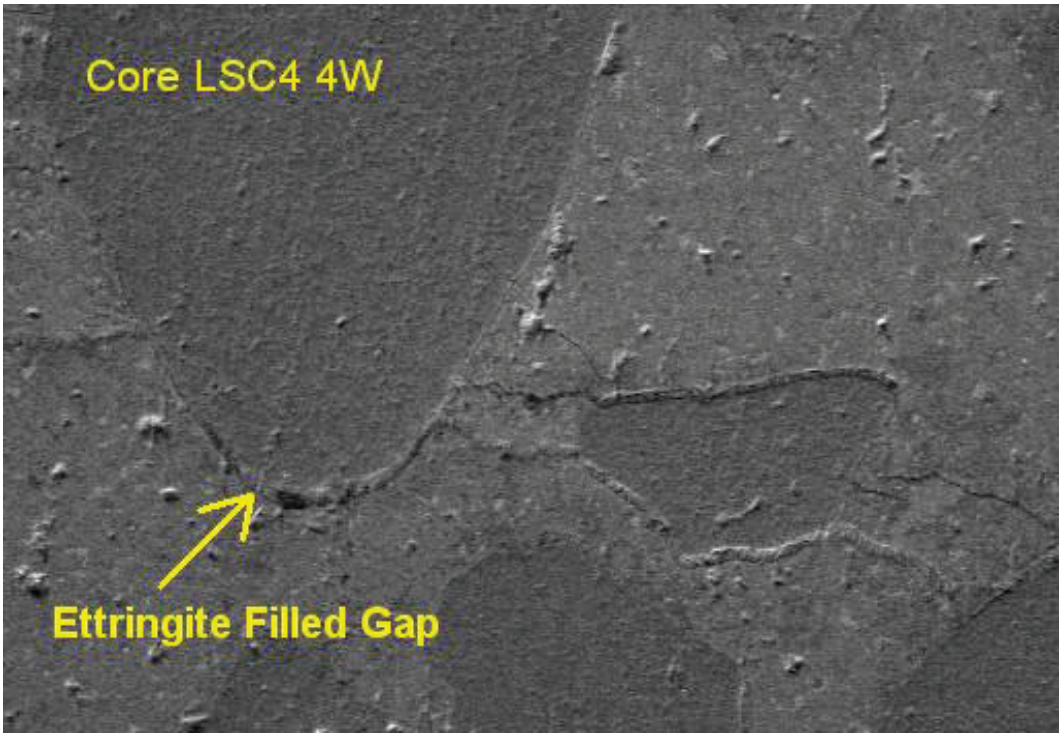

Sulfur dot map

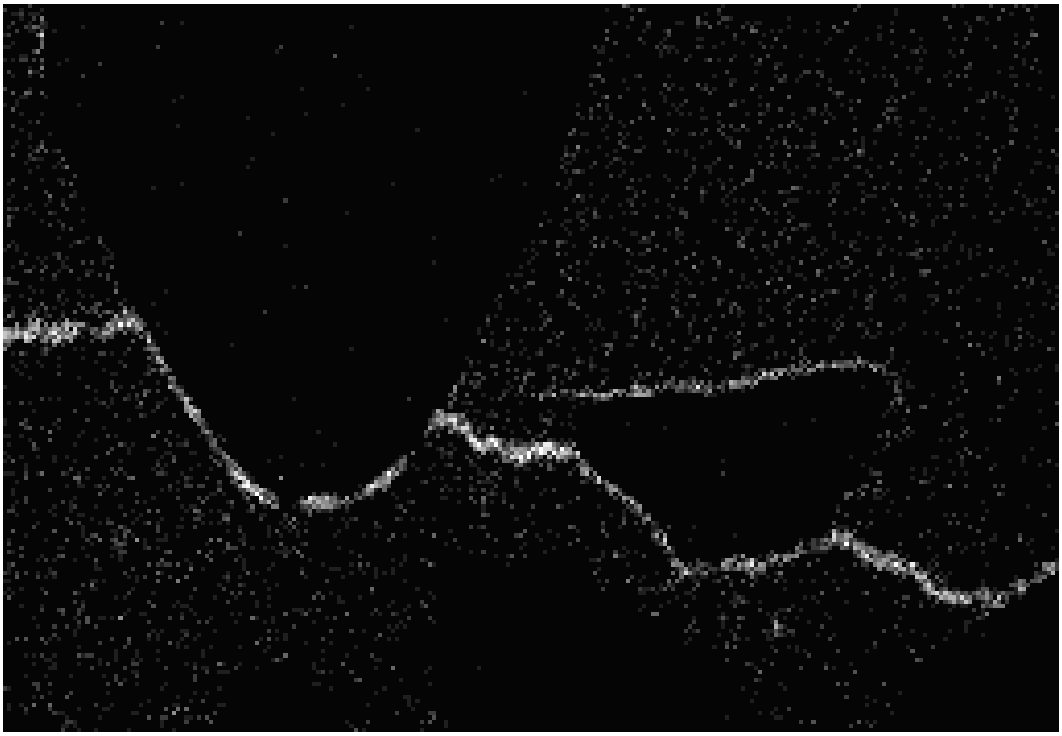

Calcium dot map

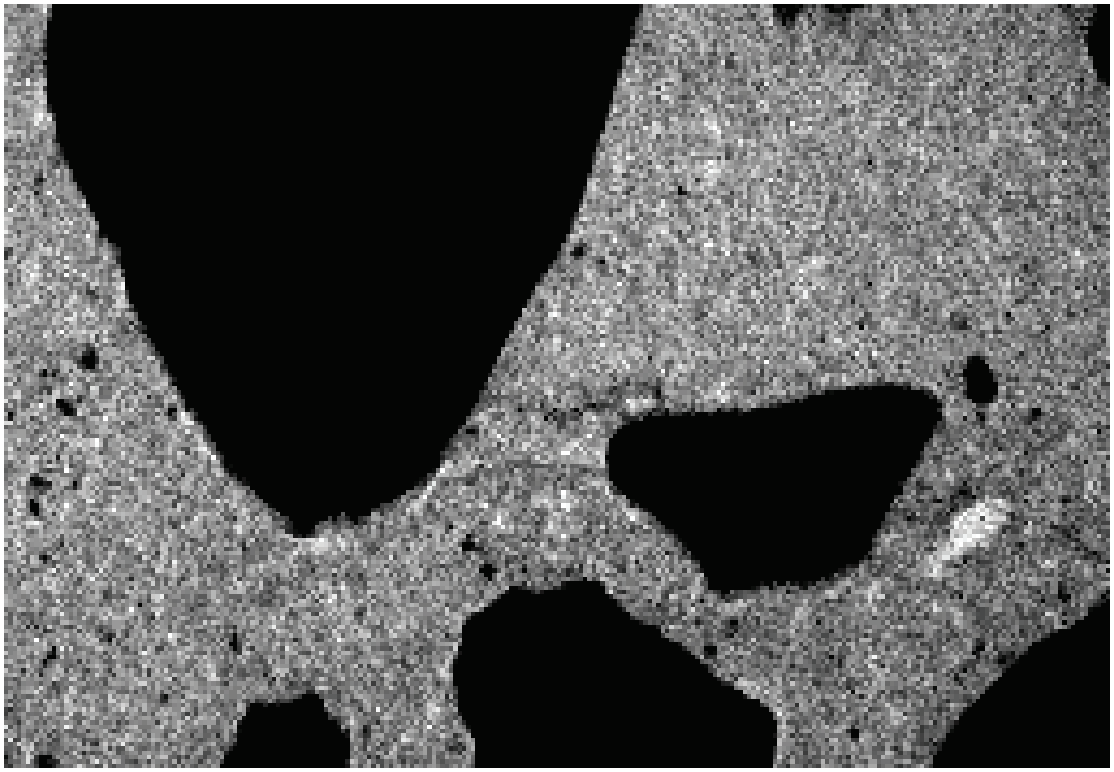

BSE image illustrating ASR gel formation

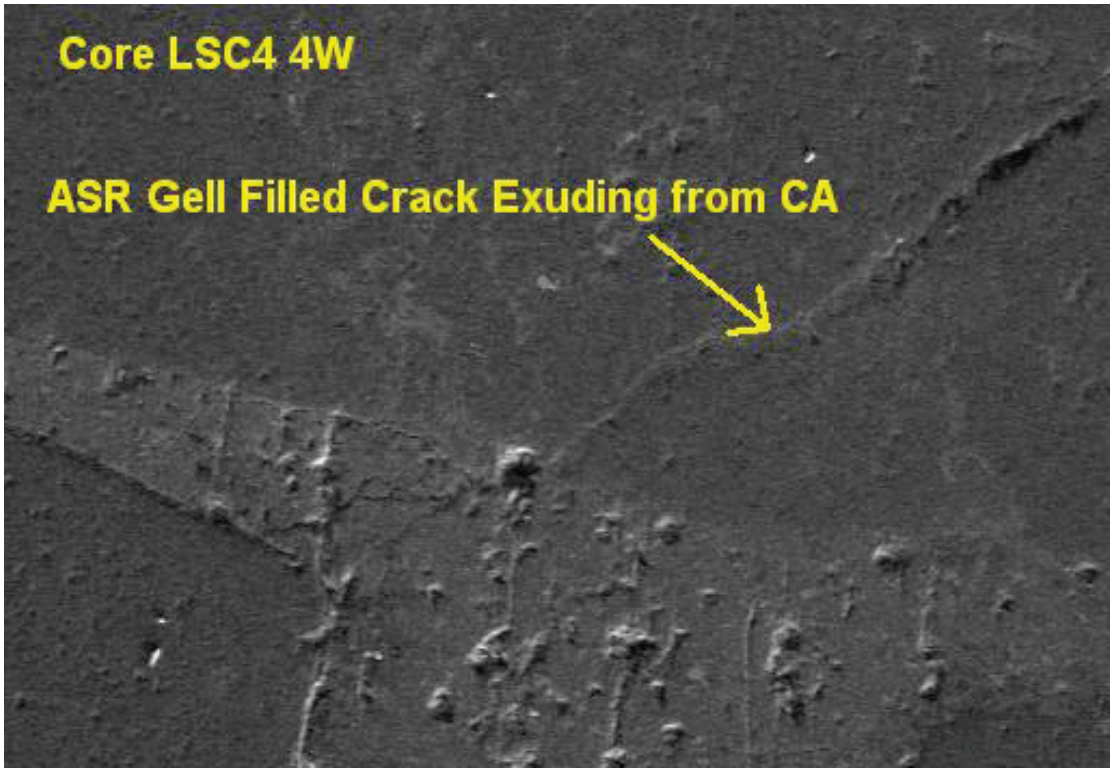

Potassium dot map

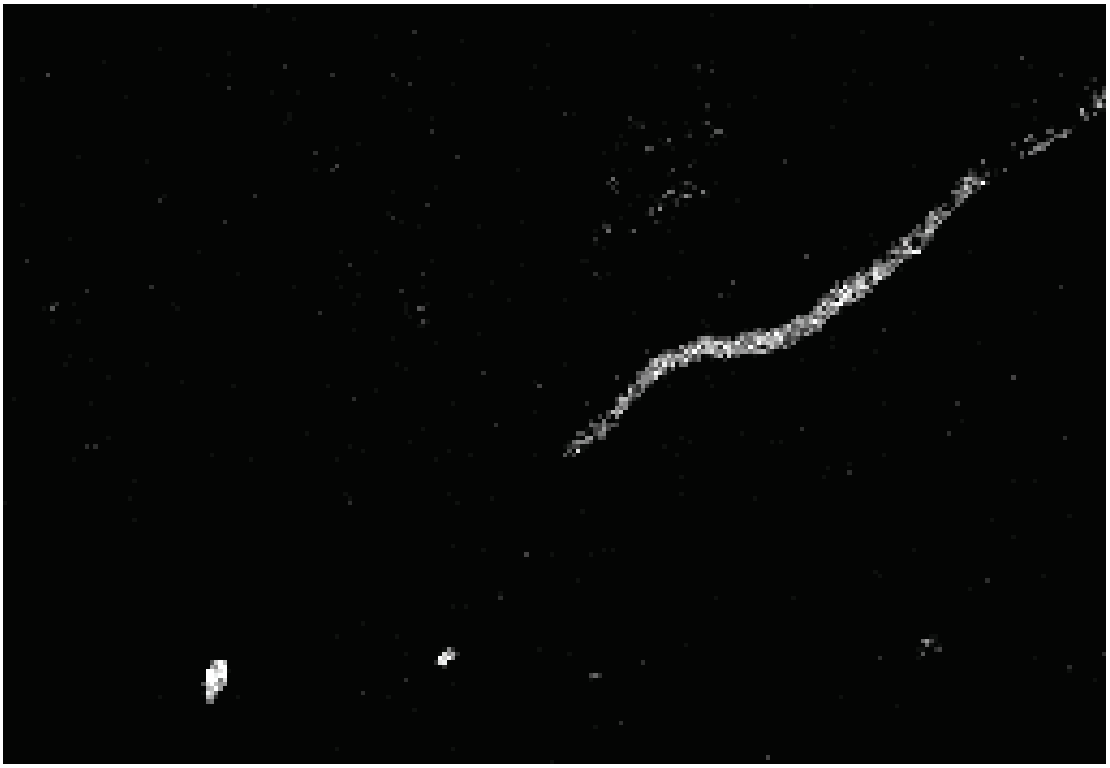

Calcium dot map

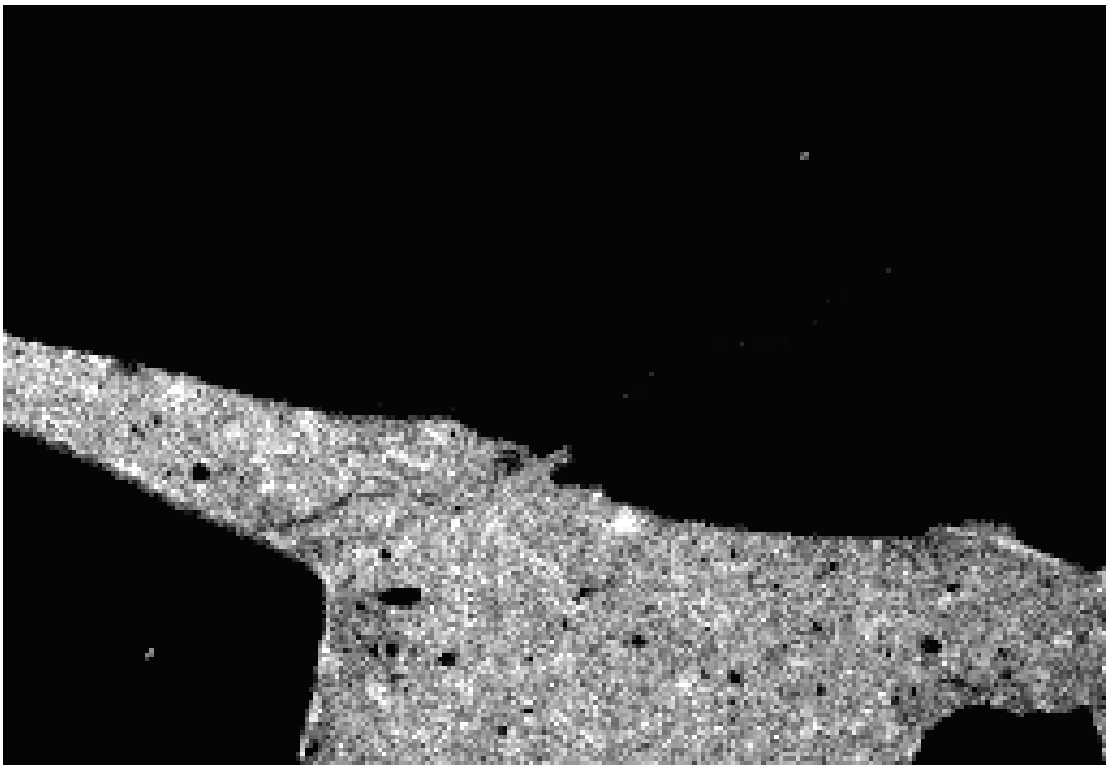

Silica dot map